

HYDRODYNAMICS OF BIVALVE
OFFSHORE AQUACULTURE

Von der Fakultät für Bauingenieurwesen und Geodäsie
der Gottfried Wilhelm Leibniz Universität Hannover

zur Erlangung des Grades
DOKTOR-INGENIEUR
Dr.-Ing.

genehmigte Dissertation

von

Jannis Landmann
geboren am 31. August 1989
in Recklinghausen

Hannover, 2022

Referent

Jun.-Prof. Dr.-Ing. Arndt Hildebrandt

Korreferent

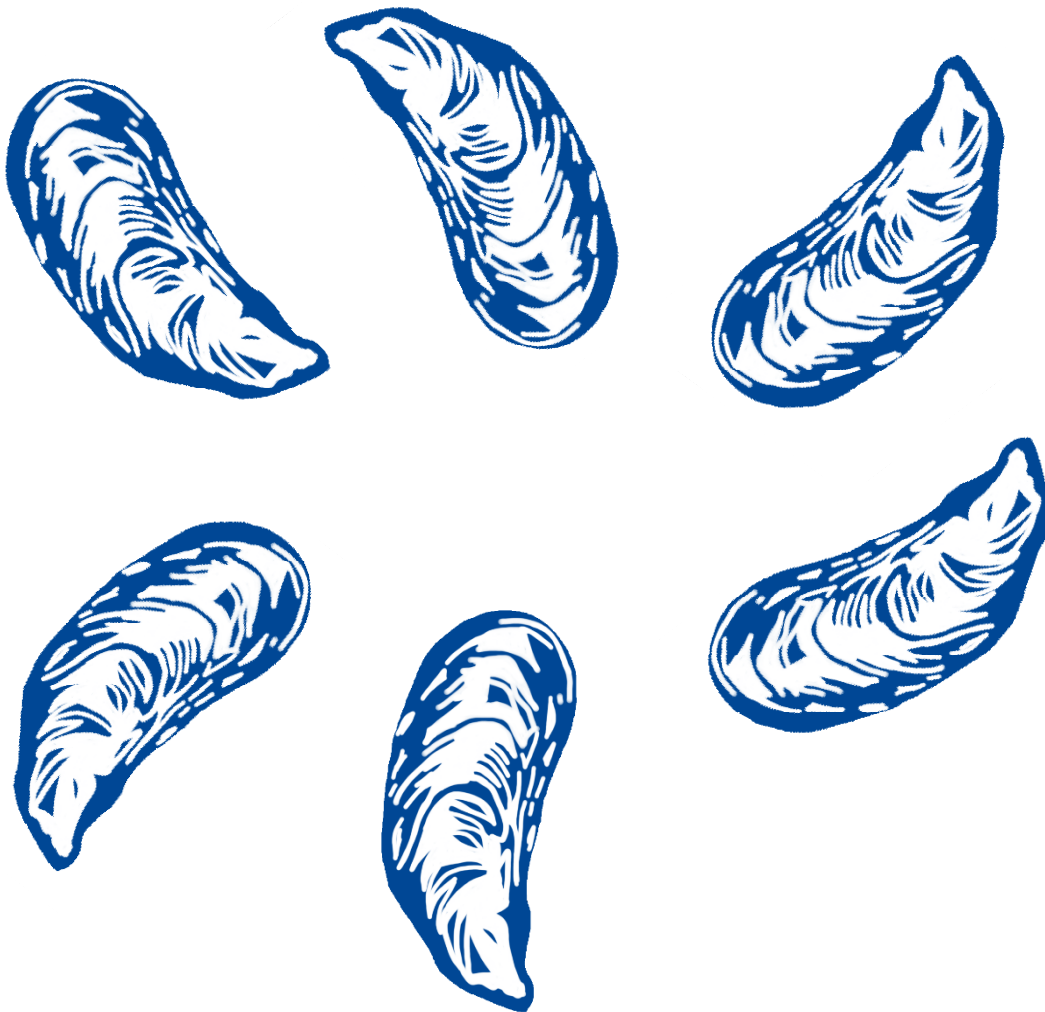
Prof. Dr.-Ing. Jacob Stolle

Tag der Promotion:

23.02.2023

HYDRODYNAMICS OF BIVALVE OFFSHORE AQUACULTURE

Jannis Landmann



Ludwig-Franzius-Institute for Hydraulic, Estuarine and Coastal Engineering
Faculty of Civil Engineering and Geodetic Science
Gottfried Wilhelm Leibniz Universität Hannover

Dissertation
23. February, 2023

Acknowledgments

Die vorliegende Arbeit ist während meiner Zeit als wissenschaftlicher Mitarbeiter am Ludwig-Franzius-Institut für Wasserbau, Ästuar- und Küsteningenieurwesen der Leibniz Universität Hannover entstanden. Die Bearbeitung verschiedener Forschungsprojekte ermöglichte es mir, die Einwirkungen auf maritime Systeme zu erforschen.

Mein besonderer Dank gilt meinem Doktorvater Herrn Prof. Dr.-Ing. Arndt Hildebrandt für seine Unterstützung und Förderung während meiner Zeit am Institut. Ich danke ihm für sein Vertrauen, das er seit meiner Studentenzeit in mich gesetzt hat, sowie für seine vielfältigen Ideen und Vorschläge, welche eine wertvolle Quelle der Motivation und Information gewesen sind. Er gab mir die Möglichkeit, meine Fähigkeiten weiterzuentwickeln und die Freiheit, interessenbasiert zu forschen. Weiterer Dank gebührt Herrn Prof.-Dr.-Ing. Jacob Stolle, der das Zweitgutachten angefertigt hat und den weiteren Mitgliedern der Prüfungskommission - Herrn Prof. Dr.-Ing. Michael Haist, der den Vorsitz übernommen hat, und Herrn Prof. Dr.-Ing. Martin Achmus. Ihnen möchte ich für Ihren Einsatz und Ihre Zeit danken.

Die wesentlichen Ergebnisse dieser kumulativen Dissertation wurden in internationalen Fachjournalen veröffentlicht. Dies wäre besonders ohne die Mithilfe meiner Co-Autoren, besonders Herrn Prof. Dr.-Ing. Nils Goseberg, Herrn Prof.-Dr. Bela H. Buck, Herrn Prof.-Dr. Henning Günther, Herrn Dr. Kevin Heasman, Frau Rebekka Kahl (geb. Gieschen), und Herrn Tim Hammer nicht möglich gewesen. Ich möchte ihnen daher für alle hilfreichen Diskussionen sowie für ihre redaktionelle und inhaltliche Unterstützung bei der Erstellung der Manuskripte danken.

Allen meinen Kolleginnen und Kollegen danke ich für die herzliche Arbeitsatmosphäre sowie für die gute und konstruktive Zusammenarbeit und Unterstützung, welche ich über die Jahre erfahren durfte. Besonders möchte ich hier meiner Arbeitsgruppe um Jannik Meyer, Lukas Fröhling, Thilo Grotebrune, und Lars Kamperdicks danken, die mir mit Körpereinsatz und ihren profunden Kenntnissen bei dem Aufbau und der Durchführung von physikalischen Modellversuchen, der Analyse von Daten, und dem Interpretieren der Ergebnisse stets geholfen haben. Ohne eure Kollegialität und Unterstützung wären die letzten fünf Jahre nicht so erfolgreich verlaufen. Weiterhin möchte ich mich bei den Mitarbeiterinnen und Mitarbeitern in der Technik und Verwaltung am Ludwig-

Franzius Institut sowie am Forschungszentrum Küste für ihre stete, aktive und verlässliche Unterstützung im Rahmen der diversen Projekte und Modellversuche bedanken. Danken möchte ich außerdem allen Studentinnen und Studenten deren teils herausragende Arbeiten ich im Laufe der Jahre betreuen durfte. Besonders möchte ich hier Tim Hammer, Rieke Santjer und Thorsten Ongsiek hervorheben, deren Abschlussarbeiten in erheblichem Maße zum Gelingen dieser Dissertation beigetragen haben.

Mein größter Dank gilt abschließend meiner gesamten Familie. Ohne eure Unterstützung hätte ich die vielen kleinen Schritte bis hier niemals geschafft. Ihr wart immer für mich da egal ob ich in Castrop-Rauxel, Adelaide, Mexiko-Stadt, Mainz, oder Hannover eure Hilfe gebraucht habe. Ich danke meinen Kindern Johan und Maja für die stets willkommene Ablenkung und das Fokussieren auf das wirklich Wichtige im Leben. Schlussendlich, danke ich Marie für ihre Liebe, Unterstützung, Vertrauen, und die Tatsache, dass sie in jeglicher Hinsicht der große Halt in meinem Leben ist.

Abstract

Without sustainable offshore aquaculture it is impossible to achieve food security for coastal communities. Growing populations in coastal zones, amounting to approximately 40% of the entire human population, exert high pressure on coastal ecosystems and natural resources, and furthermore increase the need for additional food sources. In coastal zones, marine-based nutrients offer great potential to meet this demand. With sustainability in mind, extractive species like mussels and oysters, which require no additional food, are becoming increasingly more important. Therefore, researchers, industry representatives, and policymakers alike are seeking to utilize offshore areas for shellfish aquaculture. To successfully grow shellfish in offshore areas, it is vital to understand the complex interaction of offshore aquaculture systems with waves and currents. Modelling these interactions facilitates the development of aquaculture structures that can withstand these high-energy environments. Therefore, the aim of this thesis is to increase the understanding of the complex flow around offshore shellfish aquaculture systems and their interaction with waves and currents. The literature review reports on the hydromechanic drivers with a focus on the forces, motion, and wave-structure interaction of bivalve aquaculture systems to lay a sound basis for the analysis and interpretation of the results. From there, a lack of information regarding the motions and forces of bivalve aquaculture components in steady and oscillatory flow as well as a lack of guidance as to how the complex surface of mussel dropper lines should be modelled is identified. To address these gaps of knowledge, physical experiments with live blue mussels (*Mytilus edulis*), substitute surrogate models, a newly designed aquaculture system, and naturally floating islands were conducted. The results of these experiments, published in four journal manuscripts, provide insights regarding the hydrodynamic coefficients for mussel dropper lines and its influencing parameters. Furthermore, the procedural design and creation as well as the hydrodynamic fit of a surrogate structure are shown. Wave and current tests with the novel aquaculture system and the comprehensive analysis of the hydrodynamic interaction of waves and floating natural islands in a large-scale facility provide insights regarding the motion and forces. Combined, the results enhance the understanding of the hydrodynamic processes around bivalve offshore aquaculture structures.

Keywords:

Hydrodynamics — Sustainable aquaculture — Offshore engineering —
Bivalves — Physical model tests — Forces — Motion

Zusammenfassung

Ohne nachhaltige Offshore-Aquakultur ist es nicht möglich, die Ernährungssicherheit der Weltbevölkerung zu gewährleisten. Die wachsende Bevölkerung in den Küstengebieten, die etwa 40% der menschlichen Gesamtbevölkerung ausmacht, belastet die umliegenden Ökosysteme und die vorhandenen natürlichen Ressourcen. Hunger und die damit assoziierten gesundheitlichen und sozialen Probleme sind die Folge. In den Küstengebieten bieten Nährstoffe aus dem Meer jedoch großes Potenzial zur Deckung des Nahrungsbedarfs. Im Sinne der Nachhaltigkeit gewinnen extraktive Arten wie Muscheln und Austern, die keine zusätzliche Nahrung benötigen, zunehmend an Bedeutung. Aus diesem Grund sind Wissenschaftler*innen, Industrievertreter*innen und politische Entscheidungsträger*innen gleichermaßen bemüht, ansonsten ungenutzte Offshore-Gebiete für die Muschelzucht zu nutzen. Für eine erfolgreiche Muschelaquakultur in Offshore-Gebieten ist es unerlässlich, die komplexen Wechselwirkungen der Aquakulturanlagen mit Wellen und Strömungen zu verstehen. Die Modellierung dieser Wechselwirkungen erleichtert die Entwicklung von Aquakulturstrukturen, die diesen hochenergetischen Umgebungen standhalten können. Ziel dieser Arbeit ist es daher, das Verständnis für die komplexen Strömungen um Offshore-Aquakulturanlagen und ihre Wechselwirkung mit Wellen und Strömungen zu verbessern. Die Literaturrecherche befasst sich mit den fundamentalen, hydromechanischen Einflussfaktoren auf marine Systeme. Der Fokus liegt dabei auf den Kräften, der Bewegung und der Wellen-Struktur-Interaktion von Muschelaquakulturen, um eine solide Grundlage für die Analyse und Interpretation der Ergebnisse zu schaffen. Die Literaturrecherche zeigt, dass es an Informationen über die Bewegungen und Kräfte von Muschelaquakulturen in stationärer und oszillierender Strömung mangelt. Darüber hinaus fehlt es an Anleitungen, wie die komplexe Oberfläche von Muschelkulturleinen modelliert werden sollte. Um diese Wissenslücken zu schließen, wurden physikalische Experimente mit lebenden Miesmuscheln (*Mytilus edulis*), potenziell skalierbaren Ersatzmodellen, einem neu entworfenen Aquakultur-System und schwimmenden Inseln durchgeführt. Die Ergebnisse der Experimente, die in vier Fachzeitschriften veröffentlicht wurden, geben Aufschluss über die hydrodynamischen Koeffizienten für Muschelleinen und die sie beeinflussenden Parameter. Weiterhin

werden die verfahrenstechnische Auslegung und Erstellung sowie die hydrodynamische Anpassung eines Ersatzkörpers gezeigt. Wellen- und Strömungsversuche mit dem neuartigen Aquakultur-System und die umfassende Analyse der hydrodynamischen Interaktion von Wellen und schwimmenden Inseln in einer großtechnischen Anlage liefern Erkenntnisse über die Bewegungs- und Kraftentwicklung. Zusammengefasst verbessern die Ergebnisse das Verständnis der hydrodynamischen Prozesse um Offshore-gelegene Muschelaquakulturen.

Schlüsselwörter:

Hydrodynamik – Nachhaltige Aquakultur – Offshore-Technik – Muscheln – Physikalische Modellversuche – Kräfte – Bewegung

Statement of candidate contribution

This thesis contains a series of scientific publications, which I have written as a PhD student of the Faculty of Civil Engineering and Geodetic Science of the Leibniz Universität Hannover (LUH), Germany, while simultaneously working as research associate at the Ludwig-Franzius-Institute (LuFI) of the LUH. The content of this thesis is in accordance with the faculty's regulations¹ and recommendations² for cumulative doctoral theses and represents my own work if not specified by references or acknowledgements. Publications considered for this thesis are:

- **Landmann J., Ongsiek T., Goseberg N., Heasman K., Buck B.H., Paffenholz J.-A., Hildebrandt A. (2019);** Physical Modelling of Blue Mussel Dropper Lines for the Development of Surrogates and Hydrodynamic Coefficients. *Journal of Marine Science and Engineering*; 7(3):65, <https://doi.org/10.3390/jmse7030065>

The content of this publication was originally presented at the CoastLab conference in Santander, Spain (2018). Afterwards, it was prepared as a journal publication for the Special Issue "*Selected Papers from the 7th International Conference on the Application of Physical Modelling in Coastal and Port Engineering and Science (CoastLab2018)*". The study is my own work. I conducted the physical experiments together with Thorsten Ongsiek. Thorsten Ongsiek based a student thesis on the gathered data and the MATLAB code developed by him was used in the creation of the manuscript. The student work was supervised by me. I wrote the original manuscript draft under the guidance of Arndt Hildebrandt and Nils Goseberg. Kevin Heasman and Bela H. Buck provided feedback regarding the biological and "user" perspective. Jens-André Paffenholz conducted the 3D-scanning and reviewed the final manuscript. This publication is used to

¹ see: „Verköndungsblatt der LUH vom 04.06.2020“.

² see: „Handlungsempfehlungen für das Promotionskollegium der Fakultät für Bauingenieurwesen und Geodäsie zur kumulativen Promotion vom 07.11.2019“.

describe the creation of the surrogate mussels as presented in Chapter 2.2.2 and Chapter 3.1.

- Landmann, J., Fröhling, L., Gieschen, R., Buck, B.H., Heasman, K., Scott, N., Smeaton, M., Goseberg, N., Hildebrandt, A. (2021); Drag and inertia coefficients of live and surrogate shellfish dropper lines under steady and oscillatory flow. *Ocean Engineering*; 235:109377, <https://doi.org/10.1016/j.oceaneng.2021.109377>

The study is my own work. I conducted the physical experiments. The resulting data was analyzed by me. I wrote the original manuscript draft under the guidance from Arndt Hildebrandt and Nils Goseberg. They made editorial contributions, provided feedback, and reviewed the final manuscript. Lukas Fröhling and Rebekka Gieschen provided feedback within the study. Bela H. Buck, Kevin Heasman, Nicholas Scott, and Malcolm Smeaton provided feedback regarding the biological and “user” perspective. They also reviewed the manuscript with their interdisciplinary perspective. This publication focusing on the hydrodynamics around cultivated mussel dropper lines is the basis for Chapter 3.2.

- Landmann, J., Fröhling, L., Gieschen, R., Buck, B.H., Heasman, K., Scott, N., Smeaton, M., Goseberg, N., Hildebrandt, A. (2021); New system design for the cultivation of extractive species at exposed sites - Part 2: Experimental modelling in waves and currents. *Applied Ocean Research*; 113:102749, <https://doi.org/10.1016/j.apor.2021.102749>

The research was conducted as a part of the research project “Enabling Open Ocean Aquaculture” lead by the New Zealand based Cawthron Institute. The study is primarily my own work. I conceptualized and carried out the physical model experiments in the 3D-wave and current basin in Hannover, Germany together with Rebekka Gieschen. The experiments in the inclined current flume in Braunschweig, Germany were conceptualized by Rebekka Gieschen and carried out with my support. Both experiments were performed under the supervision and guidance of Arndt Hildebrandt and

Nils Goseberg. The resulting data was analyzed by me with support by Lukas Fröhling. I wrote the original manuscript draft with feedback, editorial contributions, and review contributions by Arndt Hildebrandt and Nils Goseberg as well as Lukas Fröhling, Kevin Heasman and Bela H. Buck. Bela H. Buck, Kevin Heasman, Nicholas Scott, and Malcolm Smeaton provided feedback regarding the biological and “user” perspective. This publication detailing the experimental modelling conducted for a new aquaculture system is the basis for chapter 3.3.

- Landmann, J., Hammer, T.C., Günther, H., Hildebrandt, A. (2022); Large-scale investigation of wave dampening characteristics of organic, artificial floating islands. *Ecological Engineering*; 181:09258574, <https://doi.org/10.1016/j.ecoleng.2022.106691>

The research was conducted as a part of the research project “33496/01 - *BioSchWelle*”: *Erprobung der Wellendämpfung durch „lebende Inseln“ zur Erhöhung der Artenvielfalt in Gewässern*”³, funded by the Deutsche Bundesstiftung Umwelt (DBU) and lead by the Ludwig-Franzius Institute. The study is my own work. I conceptualized and carried out the physical model experiments in the Large Wave Flume of the Coastal Research Center in Hannover, Germany, alongside Tim Hammer under the supervision and guidance of Arndt Hildebrandt. Tim Hammer based his master’s thesis on the gathered data. The MATLAB code developed by him was used in the creation of the manuscript. The student work was supervised by me. I wrote the original manuscript draft with feedback and review contributions by Arndt Hildebrandt, Tim Hammer, and Henning Günther. This publication focusing on the impact of artificial floating islands on the wave attenuation is the basis for chapter 3.4.

³ Translation: “*BioSchWelle: testing wave attenuation by “living islands” to increase biodiversity in water bodies*”.

There is one more journal publication, I have contributed to as associated researcher at the Ludwig-Franzius-Institute, which is not further considered for this thesis:

- ④ Gieschen, R.; Schwartpaul, C.; **Landmann, J.**; Fröhling, L.; Hildebrandt, A.; Goseberg, N., 2021 Large-Scale Laboratory Experiments on Mussel Dropper Lines in Ocean Surface Waves. *J. Mar. Sci. Eng.*, 9, 29. <https://doi.org/10.3390/jmse9010029>

This contribution belongs to the Special Issue “*Selected Papers from the 8th International Conference on the Application of Physical Modelling in Coastal and Port Engineering and Science (CoastLab2020)*”. I conceptualized and carried out the physical model experiments in the Large Wave Flume of the Coastal Research Center in Hannover, Germany, alongside Rebekka Gieschen and Lukas Fröhling. Christian Schwartpaul based his bachelor’s thesis on the gathered data and the MATLAB code developed by him was used in the creation of the manuscript. The student work was supervised by Rebekka Gieschen, who wrote the main draft under the supervision of Arndt Hildebrandt and Nils Goseberg, who also contributed editorial and review contributions. Lukas Fröhling and I provided feedback within the study and editorial contributions.

All images used in this thesis are either my own or their source is labelled.

Content

Acknowledgments	i
Abstract.....	iii
Zusammenfassung.....	v
Statement of candidate contribution	vii
List of Figures	xiii
List of Tables	xvii
List of Symbols	xviii
List of Acronyms	xx
1. Introduction	1
1.1. Background	1
1.2. Motivation	3
1.3. Objectives and Outline	6
2. State-of-the-art	10
2.1. Hydrodynamic loads	12
2.2. Surface parameters.....	20
2.3. Wave-Structure interaction.....	28
2.4. Knowledge gaps	34
3. Results.....	36
3.1. Creation of surrogate mussels.....	37
3.2. Determination of drag and inertia coefficients of shellfish dropper lines under steady and oscillatory flow	42
3.3. New system design for the cultivation of extractive species at exposed aquaculture sites.....	50
3.4. Large-scale investigation of wave dampening characteristics of organic, artificial floating islands.....	59

4. Discussion	66
4.1. Synopsis	67
4.2. Limitations.....	74
4.3. Application.....	78
5. Conclusions and Outlook	82
5.1. Conclusions	82
5.2. Outlook	85
Bibliography	88
Annex.....	105
Curriculum Vitae	105
Selbständigkeitserklärung	106
Paper 1:	107
Paper 2:	108
Paper 3:	109
Paper 4:	110

List of Figures

Figure 1: Global marine aquaculture production in million tons (Mt) live weight (excluding seaweed) compared to capture fishery production and the expected rise in global population. Included is an approximation of the expected production volume till 2050 (after DNV, 2021 & UN, 2019b).3

Figure 2: (a) Principal components of a longline mussel cultivation system and (b) photograph of a dropper line ready for harvest attached to a backbone [©Goseberg, N.].....5

Figure 3: Overview of objective and scope of the thesis at hand.9

Figure 4: Working principle of the Morison equation (1950) with particle kinematics as the main driver (after Clauss et al. (1992))......13

Figure 5: Overview regarding the applicable range of various wave theories (after Le Méhauté (1976)) with all design waves used in the journal publications scattered in black, with the wave height H , the wave period T and the water depth d15

Figure 6: Common fouling organisms associated with bivalve aquaculture representing soft and hard growth with a) Vase tunicate (*Ciona intestinalis*) [©Fitridge et al., (2012)], b) Pink mouthed hydroid (*Ectopleura crocea*) [©Fitridge et al., (2012)] and c) Green algae (*Chlorophyta*) [©Goseberg, N.].....22

Figure 7: Visualization of the creation of the Abbott-Firestone Curve for cylindrical surfaces, here a mussel dropper line with $A_i(r)$, the profile's cut surface, and $A_c(r)$, the nominal surface of the cutting cylinder is displayed.27

Figure 8: Side view of the flow alteration in the presence of suspended mussel dropper lines with differentiation between three distinct flow layers [after Zhong et al. (2022)].32

Figure 9: Photograph of a specimen during the scanning process, the resulting 3D-point cloud of the scanned specimen, and the resulting exemplary solid bodies used in the section-based analysis.38

Figure 10: The Abbott-Firestone curve (AFC) of the weighted arithmetic average material distribution of all scanned sections (black) in comparison to the material distribution of the three surrogate mussels (SM 1 - 3) created.....40

Figure 11: Live mussel dropper line (LM) next to surrogate mussel dropper line 1 (SM 1), surrogate mussel dropper line 2 (SM 2) and surrogate mussel dropper lines 3 (SM 3).....	43
Figure 12: Sketch of the wave and towing tank in top and side view, highlighting the run length of the towing carriage as well as the position of the wave machine and dissipative beach.	44
Figure 13: Drag coefficient C_D of mussel dropper lines (a) and surrogates 1–3 (b) with an indication of the median drag coefficients obtained from steady flow experiments as colored crosses.	44
Figure 14: Drag C_D inertia C_M for live mussels and surrogates over Keulegan-Carpenter number KC with an indication (line) of the median value.....	47
Figure 15: Side- (A) and top (B) view of a new cultivation system for bivalve farming called “ <i>Shellfish Tower</i> ” showing the prototype dimensions [©Heasman, K.].....	51
Figure 16: Current induced drag coefficient C_D Reynolds number Re of all test cases for the single and double configuration of the <i>Shellfish Tower</i> with nonlinear fit and indication of expected Re -numbers in the Bay of Plenty (dark grey).	52
Figure 17: Empirical cumulative distribution functions of all test cases for the single configuration of the <i>Shellfish Tower</i> separated by the tested current velocity $u_{c1}= 0.0$ m/s, $u_{c2}= 1.5$ m/s and $u_{c3}= 2.2$ m/s as well as by wave 1 (H = 1.6 m, T = 5 s), wave 2 (H = 3.0 m, T = 8.0 s), wave 3 (H = 4.0 m, T = 10.0 s) and wave 4 (H =5.0 m, T = 14 s).....	54
Figure 18: Empirical cumulative distribution functions of all test cases for the double configuration of the <i>Shellfish Tower</i> separated by the tested current velocity $u_{c1}= 0.0$ m/s, $u_{c2}= 1.5$ m/s and $u_{c3}= 2.2$ m/s as well as by wave 1 (H = 1.6 m, T = 5 s), wave 2 (H = 3.0 m, T = 8.0 s), wave 3 (H = 4.0 m, T = 10.0 s) and wave 4 (H =5.0 m, T = 14 s).....	55
Figure 19: Comparison of force magnitude for an exemplary case (single configuration, H = 4.0 m, T = 10 s, Dir = 90°) with ($u_c= 2.2$ m/s) in comparison to the no current case ($u_c= 0.0$ m/s) to exemplify occurring snap loads in the <i>Shellfish Tower</i> system. The x-, y- and z-force components forming the magnitude force are displayed.....	56

Figure 20: (a) Sketch of a single reed gabion with added XPS foam sheet as used in the experiments and the fundamental mechanisms responsible for buoyant behavior and (b) cultivated reed gabions floating in a canal.60

Figure 21: Large Wave Flume (GWK) with wave paddle to the right, test field with artificial floating islands in the middle and dissipative beach to the right (not to scale). The location of the wave gauges (WGs) needed for the determination of incident and transmitted wave heights is also indicated alongside the instrumentation in the test field consisting of ultra-sonic sensors (USS), Acoustic Doppler Velocimeters (ADV), and motion tracking cameras.60

Figure 22: (a) The transmission coefficient is displayed as a scatter over wave frequency for a composite of configuration 1 (4x3 m AFIs) and configuration 2 (3x4 m AFIs). (b) The same data set with medians for tests with varying wave heights is displayed for the measured and ideal wave period. (c) A subpanel representation of the distribution for a single wave height, i.e., $H = 0.1$ m, is given together with the corresponding probability density distribution.....61

Figure 23: The reflection coefficient is displayed for a composite of configuration 1 (4x3 m AFIs) and configuration 2 (3x4 m AFIs) with the combined medians for tests with varying wave heights displayed for the ideal wave period.62

Figure 24: Motion behavior in heave (z-direction) and surge (x-direction) over time for a single reed gabion in the center of the AFIs. Every subplot (a - i) describes the motion under varying wave periods $T = 1.5$ s - 8.0 s and a constant wave height ($H = 0.15$ m) for the full test duration.63

Figure 25: (a - f) Depiction of a single wave ($H = 0.8$ m, $T = 6$ s) passing two blue mussel (*Mytilus edulis*) specimen and the SM 1 surrogate. The wave peak (d) passes the live blue mussel dropper lines, and the surrogate, with a length of 2.0 m each, which were mounted to stainless steel wires connected to a concrete block at the bottom and a steel beam at the top of the flume (g) in a distance of approximately 97 m from the wave machine.68

Figure 26: Schematic view of soft and hard biofouling on a dropper line (a) with real-life examples of green-lipped mussels (*Perna canaliculus*) [©Goseberg, N.] (b) and blue mussels (*Mytilus edulis*).....70

Figure 27: Images from the set-up, deployment, and operation of the *Shellfish Tower* at the Ōpōtiki site in New Zealand. (a) Shellfish Tower loaded on the service vessel just prior to deployment, (b) construction of the Shellfish Tower and conducting a weight test, (c) underwater image after deployment, (d) response test during deployment, (e) inspection after 4 months and horizontal test mode including a fouling inspection (f) [©Heasman. K.].....80

List of Tables

Table 1: Relevant non-dimensional quantities.....	10
Table 2: Reported values of drag C_D and inertia C_M coefficients for mussel dropper lines. Ranges of tested Reynolds Re numbers and Keulegan-Carpenter KC numbers are indicated.	18
Table 3: Absolute surface roughness height k_r for various engineering materials.	20
Table 4: Reported values of roughness height for mussel dropper lines as well as surrogate structures are shown. The ranges of the tested diameter and relative roughness are indicated (sources are indicated in Table).....	24
Table 5: Approximated values for reflection coefficients C_R of fixed and floating structures (sources are indicated in Table).....	29

List of Symbols

Symbol	Dimension		
$\Sigma A_i(r)$ Profile's cut surface	[m ²]	R_K / S_K Medial roughness	[-]
$A_c(r)$ Cylindrical surface	[m ²]	R_{PK} / S_{PK} Reduced peak roughness	[-]
$A_c(r)$ Surface of cutting cylinder	[m ²]	R_{VK} / S_{VK} Reduced valley roughness	[-]
C_D Drag coefficient	[-]	c_{depth} Cut depth	[m]
C_{Diss} Dissipation coefficient	[-]	k_r Surface roughness height	[m]
C_M Inertia coefficient	[-]	l_i Length of material cut	[m]
C_R Reflection coefficient	[-]	l_n Length of section	[m]
C_T Transmission coefficient	[-]	$\frac{u}{f_s D}$ Reduced velocity	[-]
D_{cyl} Cylinder diameter	[m]	\dot{u} Water particle acceleration	[m/s ²]
F_D Drag force	[N]	u_c Current velocity	[m/s]
F_M Inertia force	[N]	$\frac{\pi D}{L}$ Diffraction parameter	[-]
H_i Initial wave height	[m]	Δ Relative roughness parameter	[-]
H_r Reflected wave height	[m]	F Total horizontal force	[N]
H_t Transmitted wave height	[m]		
P_t Unfiltered profile depth	[m]		

<i>A</i>		<i>z</i>	
Referential area	[m ²]	Wave amplitude	[m]
<i>D</i>		<i>ν</i>	
Characteristic diameter	[m]	Kinematic viscosity	[m ² /s]
<i>H</i>		<i>ρ</i>	
Wave height	[m]	Density	[kg/m ³]
<i>KC</i>		<i>ω</i>	
Keulegan-Carpenter number	[-]	Angular frequency	[rad/s]
<i>L</i>			
Wavelength	[m]		
<i>Re</i>			
Reynolds number	[-]		
<i>T</i>			
Wave period	[s]		
<i>V</i>			
Referential volume	[m ³]		
<i>c</i>			
Wave propagation speed	[m/s]		
<i>d</i>			
Overall water depth	[m]		
<i>f</i>			
Frequency	[1/s]		
<i>k</i>			
Wave number	[m ⁻¹]		
<i>r</i>			
Cutting cylinder's radius	[m]		
<i>t</i>			
Position in time	[s]		
<i>u</i>			
Water particle velocity	[m/s]		
<i>x</i>			
Position in space	[m]		

List of Acronyms

2D

Two-dimensional

3D

Three-dimensional

ADV

Acoustic Doppler Velocimetry

AFC

Abbott-Firestone-Curve

AFI

Artificial floating islands

BAC

Bearing area curve

DNV

Det Norske Veritas

DOI

Digital Object Identifier

ECDF

Empirical cumulative distribution functions

FAO

Food and Agriculture Organization of the United Nations

GWK

Großer Wellenkanal (The Large Wave Flume)

IMTA

Integrated multitrophic aquaculture

LuFI

Ludwig-Franzius-Institute

LUH

Leibniz Universität Hannover

SDG

Sustainable Development Goal

SM 1

Surrogate Mussel 1

SM 2

Surrogate Mussel 2

SM 3

Surrogate Mussel 3

UN

United Nations

USD

United States Dollar

USS

Ultra-sonic sensor

WG

Wave gauge

XPS

Extruded polystyrene



1. Introduction

1.1. Background

Coastal zones are exhibiting high rates of population growth and continued urbanization. Currently, around 40% of the global population, 2.85 billion people, live within 100 kilometers of the coast (UN, 2019a). This number is expected to rise in the future. The coastal population is projected to increase by 13% (3.21 billion) till 2035 (Maul and Duedall, 2019). Furthermore, 90% of urban areas are situated on coastlines (Elmqvist et al., 2019) and the population densities in these coastal zones are approximately three times greater than the global average (Small and Nicholls, 2003). The reasons for such a concentration are a combination of economic, geographic, and societal drivers (de Sherbinin et al., 2012; Hugo, 2011; Neumann et al., 2015; Seto, 2011). Coastal cities provide numerous incentives for coastward migration and urbanization. They are perceived as more advantageous in terms of employment, education and economic benefits when compared to inland settlements and cities (Dwarakish and Salim, 2015; Gallup et al., 1999; Sekovski et al., 2012). The increasing population and urbanization are main drivers of change in coastal zones and generate high pressure on coastal ecosystems, natural resources, and increase the demand for food products.

As illustrated by the UNs Sustainable Development Goal⁴ (SDG) number 2 (zero hunger), achieving food security and fighting hunger for a growing global population is one of the 17 major tasks for the future. To this end, an improved nutrition, and especially a steady supply of proteins, is needed. Proteins are a component in almost all biological processes (Cozzone, 2002) and, in general, they can be obtained from animal- or plant-based sources. Coastal zones are home to a large variety of animals and plants and marine based proteins harvested in coastal

⁴ By adopting the 2030 Agenda, with its 17 Sustainable Development Goals, the 193 member states of the United Nations have created a framework for national action and global cooperation on sustainable development. The initiative aims to end poverty and other deprivations and recognizes the need for strategies that improve health and education, reduce inequality, and spur economic growth on a global level while preserving and protection the natural resources.

zones offer a great potential to sustainably increase the protein supply for a growing world population. Fish products are a major global protein source, and they are a rich source of essential fatty and amino acids, vitamins, and minerals. Additional benefits include replacement scenarios where land-based meats are substituted by aquaculture proteins. This has the potential to reduce terrestrial land use, as less space is needed for the cultivation of land-based livestock if it is partly replaced by aquaculture. This, in turn, could allow cutting greenhouse gas emissions through afforestation (Röös et al., 2017). The global production of fish⁵ is estimated to have reached 179 million tons in 2018, from which 156 million tons were used for human consumption and the remaining 22 million tons for non-food uses (FAO, 2020). In 2017, aquatic produce accounted for 17% of the global consumption of animal proteins, and 7% of all proteins consumed (FAO, 2020). Capture fisheries are responsible for 54% of all produce (97 million tons), while marine and inland aquaculture are responsible for the remaining 46% (82 million tons) (FAO, 2020). An assessment of global fish stocks suggests that nearly 35% of all fish stocks are currently overfished, 55% are fished in a sustainable manner with the remaining 10% not being fully exploited (Noakes, 2014). Thus, increasing the catch rate from commercial fisheries for human alimentation is likely not an option and any increased demand must be met by aquaculture production (Osmond and Colombo, 2019). This is supported by the fact, that the volume of capture fishery has been near constant since the late-1980s, as all species in question have been caught at maximum sustainable yield (Costello et al., 2020). Since then, aquaculture production has risen proportionately with global demand. It is needed to fulfill the future demand for marine based proteins.

Against the background of an increasing global population, aquaculture and its products can increase the global supply of foods while also possessing great potential to address malnutrition and diet-related diseases in line with the SDGs of the UN.

⁵ In this context, the term “fish” includes fish, crustaceans, mollusks, and other aquatic animals, but excludes aquatic mammals, reptiles, seaweeds, and other aquatic plants.

1.2. Motivation

Currently, aquaculture is mainly focused on coastal areas. This is causing conflicts with various inshore and nearshore stakeholders, regarding the required space as well as environmental concerns (Buck, 2004; Froehlich et al., 2017; Naylor and Burke, 2005; Naylor et al., 2000). To reduce the conflict potential and ease pressure on nearshore ecosystems, marine aquaculture⁶ is one step towards the large-scale expansion of marine food production. Against this background, researchers, policy makers and industry officials are currently promoting a focused effort towards marine aquaculture (DNV, 2021; European Commission, 2021; Mascorda Cabre et al., 2021; NOAA, 2011). Figure 1 highlights the importance of marine aquaculture regarding the stagnating volume of capture fisheries, as well as the expected rise in production until 2050 when considering a growing food and protein demand due to an increasing global population.

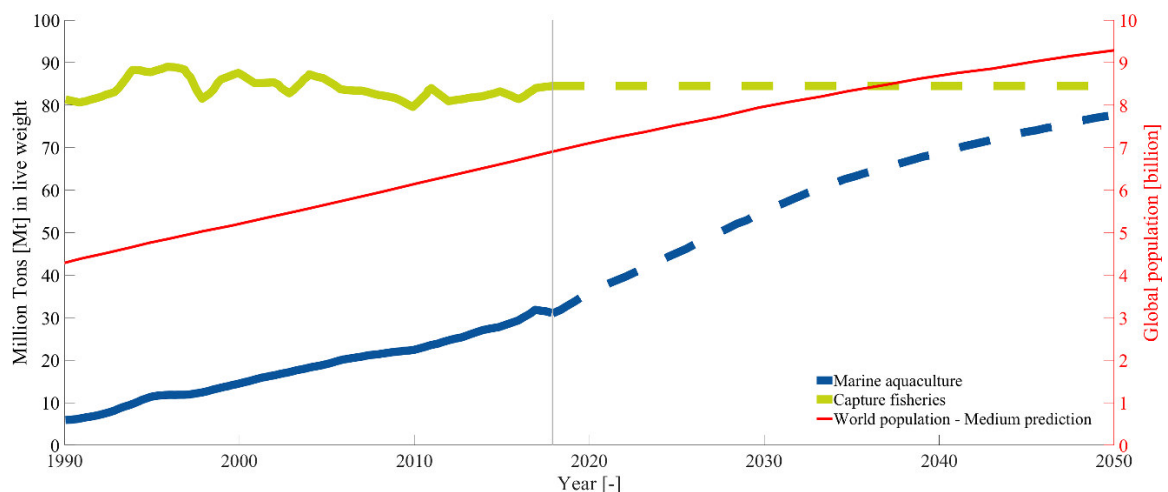


Figure 1: Global marine aquaculture production in million tons (Mt) live weight (excluding seaweed) compared to capture fishery production and the expected rise in global population. Included is an approximation of the expected production volume till 2050 (after DNV, 2021 & UN, 2019b).

Currently, the aquaculture industry focusses on high-value, mostly carnivorous, species like salmon, trout, tilapia or marine finfish (Tacon, 2020). Producing one kilogram of these high value species requires to feed them with up to five

⁶ Despite growing interest, the terms “marine-” or “offshore aquaculture” are not well defined (Froehlich et al., 2017). In the context of this thesis, the terms “marine-” or “offshore aquaculture” comprise aquaculture conducted an undefined distance off the coast with varying aquatic species.

kilograms of wild fish (Naylor et al., 2000). Consequently, the long-term sustainability of such an industry remains questionable until the dependence of capture fisheries on caught fish is reduced. A more sustainable solution regarding increasing demands for aquatic foods are filter feeders, such as bivalves, who extract organic matter from the water for their growth. That means that there is no need to provide filter feeders with an external source of food, as they directly feed on the nutrients in the water. This results in a relatively cost-effective harvestable crop if a suitable habitat is provided (Stevens et al., 2008). Bivalves also provide important ecosystem services by influencing water filtration, nutrient cycling, habitat structure, species diversity, and food web dynamics (Mascorda Cabre et al., 2021).

Thus, the focus of this study is set on offshore bivalve aquaculture. In 2018, 17.7 million tons of mollusks, mainly comprised of bivalves, with an estimated value of USD 34.6 billion were farmed (FAO, 2020). Globally, over 1.5 million km² could potentially be developed for marine bivalve aquaculture according to Gentry et al. (2017). This prediction is based on the relative productivity potential of ocean areas for marine aquaculture and site-selection criteria such as temperature tolerance, location-specific growth potential and constraints such as allowable depth or other relevant environmental conditions. Currently, bivalves are cultivated mainly in suspended cultures. Raft cultures, mainly used in Spain, consist of metal, wooden or plastic lattices supported by floats (Duarte et al., 2014). Mussel dropper lines are suspended from the rafts, which are normally floating on the sea's surface. Rafts are mainly used near shore, while systems for more exposed sites exist (Dewhurst, 2016). Longline farming is considered the most promising system in regard to offshore expansion (Buck and Langan, 2017; Cheney et al., 2010). Longline farms consist of rows made from vertically oriented dropper lines, which are suspended from a main line, called backbone. The dropper lines consist of a polyester rope at the core to which the mussels are attached via their byssus fiber, the bundled filaments secreted by bivalves. The mussels attach themselves to the fibrous material during their larvae or spat state and then bind to the polyester rope as they grow. Floats attached to the backbone provide buoyancy. Mooring lines ensure the entire system stays in place and fix the structure to the ground via screws or ballast anchors. In Figure 2, the principal parts of a longline system are displayed alongside photographs from real life locations.

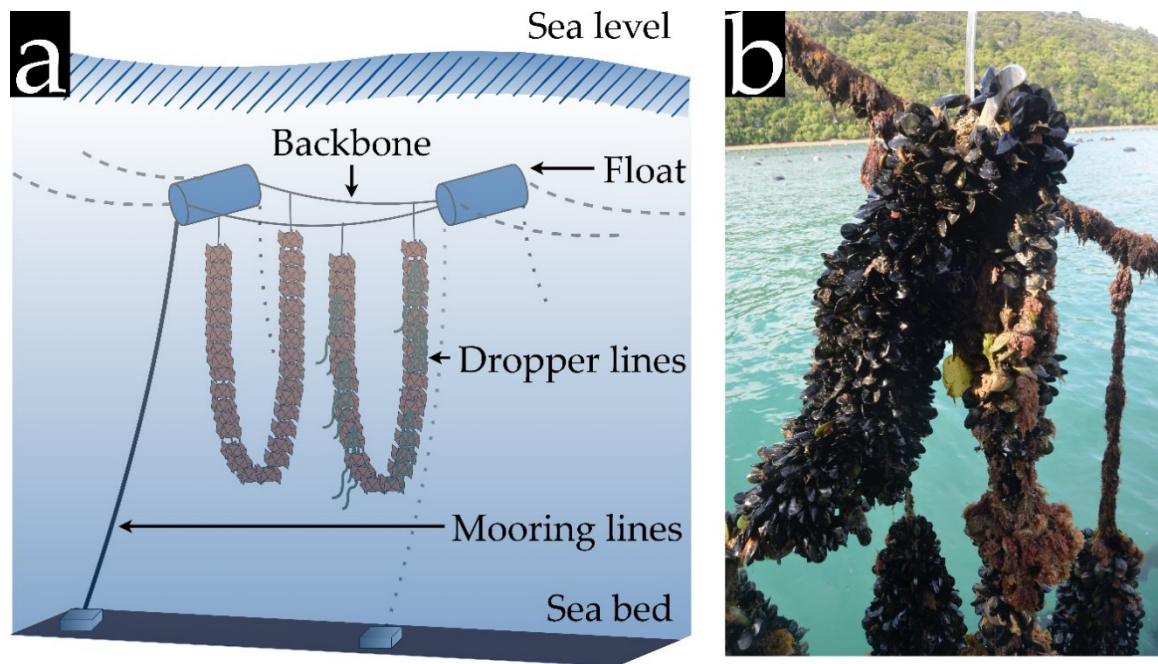


Figure 2: (a) Principal components of a longline mussel cultivation system and (b) photograph of a dropper line ready for harvest attached to a backbone [©Goseberg, N.].

Contrary to the mainly observational and numerical approaches used to estimate the forces on bivalve aquaculture systems up to date, this thesis focuses on the hydrodynamic loads of mussel dropper lines and a cultivation system under laboratory conditions to gain a better understanding of the processes around bivalve offshore aquaculture systems. The greater motivation for this thesis is to address hydrodynamic uncertainties to enable researchers, policy makers and industry officials alike to make informed, fact-based choices regarding bivalve offshore aquaculture.

1.3. Objectives and Outline

This thesis consists of several studies scrutinizing the complex flow around bivalve aquaculture structures as well as the structures' interaction with waves and currents. The studies comprise physical experiments with live blue mussels (*Mytilus edulis*), potentially scalable, substitute surrogate models, a newly designed aquaculture system, and naturally floating islands. Incorporating the results from all experiments, the general objective of this thesis is to:

- separate, detail and discuss the dominant hydromechanic drivers in bivalve offshore aquaculture systems to improve predictions of motion and forces within these systems.

To achieve this, the specific objectives addressed in this thesis are to:

- gain insight into the complex hydrodynamics in the vicinity of mussel dropper lines in open ocean environments to then separate the interdependent loads they are subject to.
- create and evaluate surrogate structures that can be used for live blue mussels (*Mytilus edulis*).
- evaluate and assess drag C_D and inertia C_M coefficients of live and surrogate dropper lines under steady as well as oscillatory flow conditions, including surface gravity waves.
- prove the feasibility and functionality of an aquaculture system usable for the collection and cultivation of mussel spat as well as farming of oysters, scallops, and seaweed in marine environments.
- determine and discuss the governing wave and structure parameters regarding wave dampening and structure movement as well as the main dissipation mechanisms of natural, floating structures.

The thesis' state-of-the-art (see Chapter 2) summarizes the general hydromechanic drivers in marine systems while focusing on forces, motion, and wave-structure interaction. With this, the state-of-the-art-chapter lays a basis for the analysis and interpretation of the experiments. Knowledge of hydrodynamic loads on any floating structure is paramount in determining the necessary mooring and anchoring mechanisms. The individual and combined influence of steady and oscillatory flows on the loading of slender structures, such as the mussel dropper

lines, are detailed (see Chapter 2.1). Furthermore, the influence of roughness on the force evolution of marine structures is presented. The mussel dropper lines can be assumed to be highly rough. Furthermore, the surface descriptor as an important parameter to create mussel surrogates mimicking real-life organisms in laboratory experiments is introduced (see Chapter 2.2). An overview of the wave-structure interactions regarding mainly aquaculture systems is presented. It highlights the influence of these systems on the flow and their potential to attenuate waves in high-energy environments (see Chapter 2.3). Connecting all these information facilitates identifying the current gaps of knowledge regarding offshore aquaculture (see Chapter 2.4).

The principal results of this thesis are subject of several international journal publications (see Chapter 3). The first publication focuses on the creation of surrogate mussel dropper lines suitable for physical experimentation (see Chapter 3.1). In this study, the processes involved in 3D-scanning live blue mussel (*Mytilus edulis*) specimen are detailed. Based on the scanned data, three distinctly different surrogate with a common surface descriptor are created. The second publication focuses on the determination of the drag and inertia coefficients of mussel dropper lines under steady and oscillatory flow (see Chapter 3.2). In this study, the loads, a mussel dropper is subjected to in offshore environments, are separated and studied using physical model tests. The methodology for the creation of the hydrodynamic coefficients and the respective results are detailed. This study emphasizes that the choice of the characteristic diameter for a natural structure such as the mussel dropper lines must be considered regarding the hydrodynamic coefficients. The third publication focuses on the experimental modelling of a new system design to cultivate extractive species at exposed sites (see Chapter 3.3). The experiments serve to determine mooring loads, inclination angles, and drag coefficients of the structure. Observed snapping loads during the model and prototype tests are critical for the longevity of the structure and the results show that they must be considered during the mooring design. The fourth publication within this thesis focuses on the wave attenuation capacity of artificial floating islands (see Chapter 3.4). Physical model tests in a large-scale facility determine the motion of the structure as well as the structure's capacity to dampen waves. While not being used in aquaculture, the suspended canopies, and islands themselves dampen waves in the same manner as floating aquaculture systems.

In this sense, the published manuscripts presented in this thesis give an overview of different contemporary features of offshore aquaculture, dealing with both traditional engineering, sustainability, and biology-related aspects, as well as the potential for wave attenuation and thus shore protection. The outcomes of the publications within this thesis are reflected in a discussion on the gathered insights elucidated against the identified gaps of knowledge (see Chapter 4.1). This section also highlights the limitations of the presented research and shows its applicability to real-world scenarios (see Chapter 4.2 and 4.3). A graphical overview regarding the objectives and scope of this thesis can be seen in Figure 3.

Chapter summary 1:

*Against the background of a growing global population, the expected demographic changes in coastal communities resulting in increased urbanization are highlighted. The resulting need for **sustainable food sources**, especially proteins, is emphasized. In coastal communities, one such source could be aquaculture, of which the societal, ecologic, and economic impact is shown.*

*The motivation of this thesis is based on an effort to extend **sustainable bivalve aquaculture** into offshore locations. The challenges and possible benefits, as recorded in literature, are highlighted to show the potential contribution of bivalve aquaculture to the sustainable protein supply.*

*The general **objective of the thesis** to separate, detail and discuss the influencing, hydromechanic drivers in bivalve offshore aquaculture systems is introduced. To achieve this aim the approach of combining a comprehensive state of art, the results which have been published in manuscripts, and a resulting discussion is established.*

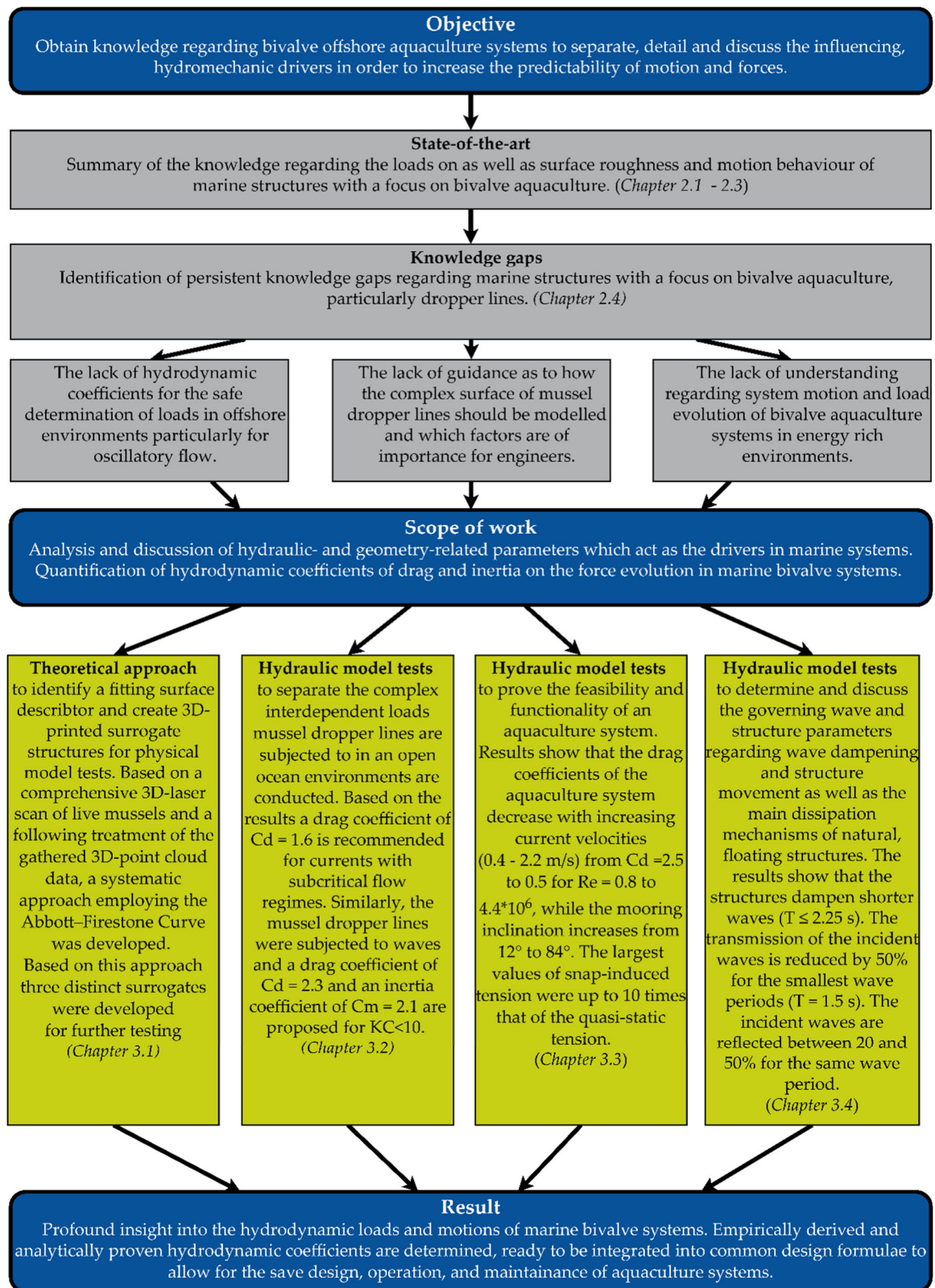


Figure 3: Overview of objective and scope of the thesis at hand.



2. State-of-the-art

To allow for a comprehensive analysis and interpretation of the experimental results and as groundwork for the analysis, this chapter provides an overview regarding the fundamental as well as recent developments on the topics of hydrodynamic loads, relevant surface parameters, and wave-structure interaction in connection with the broader topic of aquaculture. Finally, the resulting knowledge gaps are presented in detail. The scope of this chapter encompasses fully turbulent, high-energy flow conditions, which typically prevail in offshore environments.

For the successful design, installation, operation, and maintenance of offshore industries, in these conditions, a solid understanding of the hydrodynamics and its influencing parameters is necessary. To enable a comparison of the flow processes for various scales and fluid characteristics, the geometric similarity of the object in flow and their boundary limits need to be established. Furthermore, the acting forces in the flow system must be in a fixed relationship to one another at any point in time. To understand the effect of the marine environment on the object and especially the resulting forces experienced by the structure, certain non-dimensional parameters⁷ (see Table 1) play an important role.

Table 1: Relevant non-dimensional quantities.

Parameter	Equation
Reynolds number	$Re = \frac{u * D}{\nu}$ (2.1)
Keulegan-Carpenter number	$KC = \frac{u * T}{D}$ (2.2)
Relative roughness	$\Delta = k_r / D$ (2.3)

⁷ Further non-dimensional quantities (e.g. diffraction parameter $\frac{\pi D}{L}$ and reduced velocity $\frac{u}{f_s D}$) exist, but only the most relevant for this thesis are listed here. For further information on these, as well as the topic of dimensional analysis, see exemplary Chakrabarti (2005).

In the equations given in Table 1, Re is the Reynolds number, u is the water particle velocity, D is the characteristic diameter of the observed object, ν is the kinematic viscosity of the fluid, KC is the Keulegan-Carpenter number, T is the wave period, Δ is the relative roughness parameter, and k_r is the surface roughness height. The Reynolds number (1883) is the ratio of inertial forces to viscous forces within a fluid which is subjected to relative internal movement due to different fluid velocities in a steady flow. The Keulegan-Carpenter number (1958) describes the relative importance of the drag forces over inertia forces in an oscillatory flow. The surface roughness influences the forces on slender objects and especially the values of the hydrodynamic drag and inertia coefficients differ significantly with the roughness of the objects surface.

2.1. Hydrodynamic loads

The hydrodynamic loads consist of inertial and viscous forces. The loads hydrodynamic phenomena can transfer to offshore structures are mainly dependent on the water particle kinematics. These are induced by oscillating and steady flows and are influenced by a myriad of interdependent parameters stretching over local (wave height, wave period, water depth, structure parameters) to global (ocean currents, tides, storm events) scales. The appropriate engineering approach⁸ for the determination of the hydrodynamic loads themselves is dependent on the relationship between the characteristic diameter of the observed object D and the present wavelength L . For slender members of marine systems, where the presence of the structure is assumed to have a negligible effect on the passing flow, the Morison equation (1950) is commonly used to determine the horizontally acting forces. It can be used when the ratio of relative size of the structure's diameter D to the wavelength L is $\frac{D}{L} < 0.2$. For larger marine objects, i.e. $\frac{D}{L} \geq 0.2$, where the effect of the structure on the incident wave field must be taken into account, the linear diffraction theory introduced by MacCamy and Fuchs (1954) can be used to approximate the diffracted surface elevation as well as the occurring loads. In the context of this thesis, a ratio of $\frac{D}{L} < 0.2$ applies for the investigated objects and the Morison approach is applied.

2.1.1. Morison equation

Morison et al. (1950) proposed an empirical method to determine the horizontal wave force on a slender body ($\frac{D}{L} < 0.2$). In that approach, the hydrodynamic pressure field and horizontal components of water particle velocity and acceleration for a specific wave theory, which is dependent on the site-specific wave parameters, are identified and incorporated into the Morison equation (1950) where nonlinear drag forces F_D and inertia forces F_M are superimposed.

⁸ More complex methods for the determination of fluid forces that include various nonlinearities exist. These are mainly based on high-fidelity numerical methods like CFD (Donea and Huerta, 2003; Ferziger and Perić, 2002).

This can be depicted as:

$$F = F_D + F_M = \frac{1}{2}\rho C_D u^2 A + \rho C_M V \dot{u} \quad (2.4)$$

where F is the total horizontal force, ρ is the density of the water, C_D is the drag coefficient, u is the horizontal particle velocity, A is the referential area in flow, C_M is the inertia coefficient, V is the volume of the structure and \dot{u} is the horizontal particle acceleration. The hydromechanic drag and inertia coefficients found in equation (2.4) are empirical values used to quantify various parameters related to the shape of the investigated structure, its surface roughness, and the site-specific wave properties. They are usually determined experimentally. A sketch of the working principle of the Morison equation (1950) is shown in Figure 4.

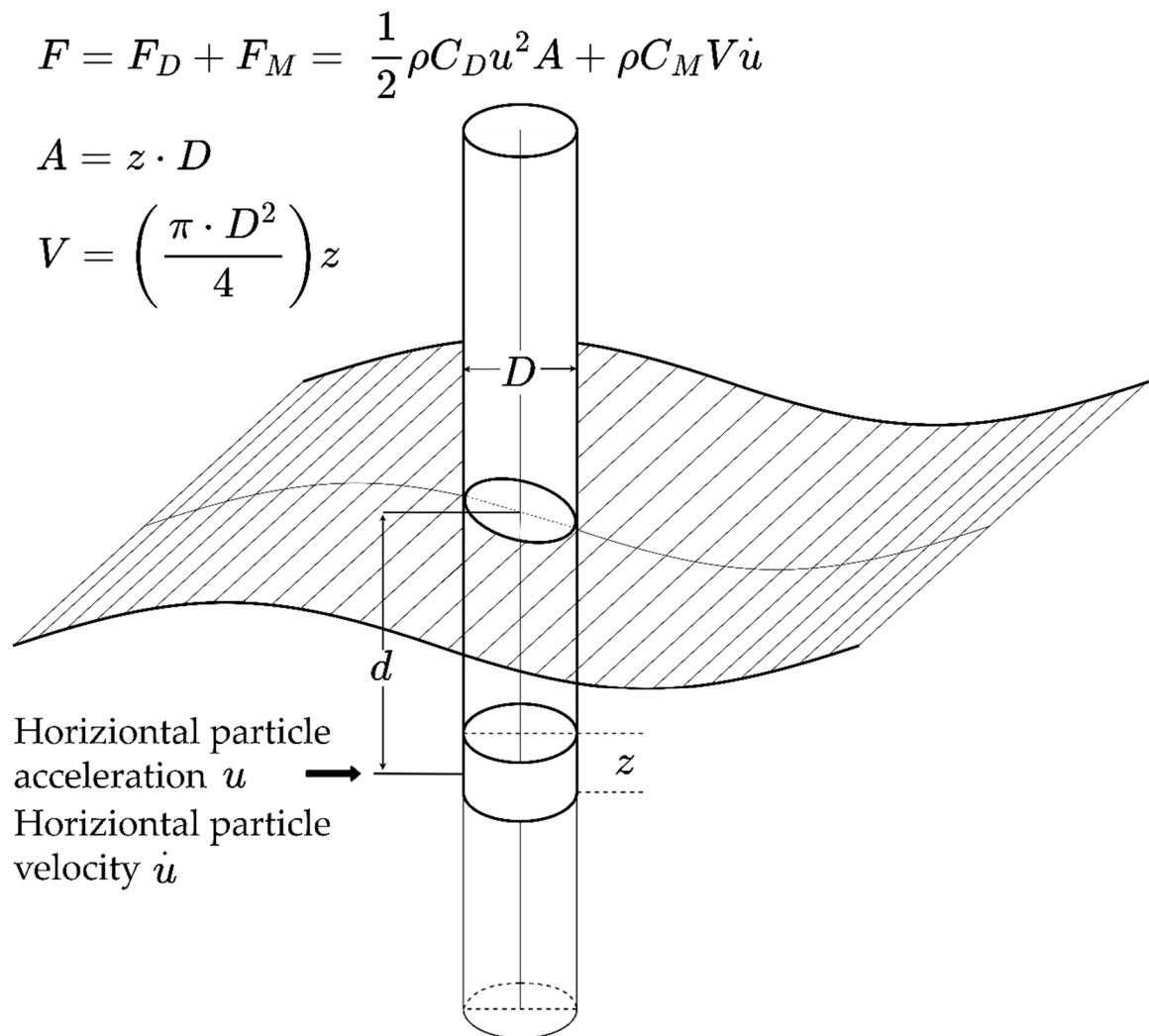


Figure 4: Working principle of the Morison equation (1950) with particle kinematics as the main driver (after Clauss et al. (1992)).

2.1.2. Wave kinematics

The water particle velocity and acceleration needed to solve the Morison equation (1950) are determined according to their explicit wave theories (e.g. Airy, Stokes, stream function or cnoidal theory), which are dependent on site-specific metocean data. These wave theories are based on different idealized boundary conditions and provide approximations of varying accuracy. Nevertheless, these theories provide good results, particularly for two-dimensional case studies. These monochromatic wave parameters are commonly used for practical engineering questions. More information regarding the fundamental formulations as well as the presented wave theories is gathered, compiled and available from several textbooks, providing further information and covering a broader scope than this chapter (Clauss et al., 1994, 1992; Dean and Dalrymple, 1991; Holthuijsen, 2007; Méhauté, 1976; Oertel et al., 2015; Sarpkaya, 2010).

In the case of this thesis, the wave theories covered by the experiments in the journal manuscripts (see Chapter 3.2, 3.3, and 3.4) are shown in Figure 5. There, the Le Méhauté (1976) diagram, which provides an overview regarding the applicable range of various wave theories, is superimposed with all input wave combinations used in the different wave flumes. As can be seen, mainly the linear Airy wave theory (1845) and Stokes 2nd order wave theory (1847) were applied for intermediate⁹ to deep water waves in this thesis.

⁹ Due to size limitations in the used flumes regarding the water depth, no deep-water waves for all scenarios could be recreated. The equations shown for Airy wave theory cover intermediate-water waves. The formulations regarding deep- and shallow-water waves can be found exemplary in Clauss et al. (1992) or Malcherek (2010).

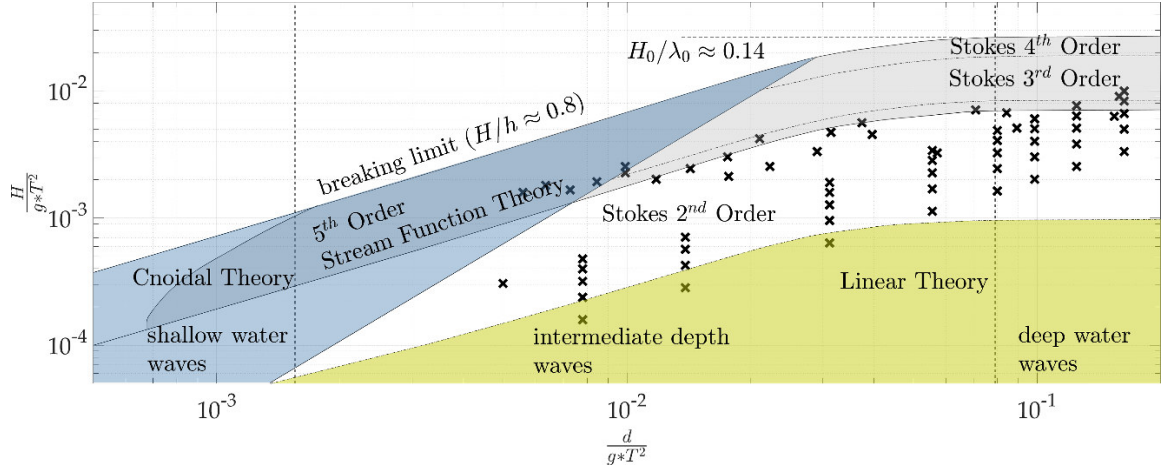


Figure 5: Overview regarding the applicable range of various wave theories (after Le Méhauté (1976)) with all design waves used in the journal publications scattered in black, with the wave height H , the wave period T and the water depth d .

Although Airy (1845) developed his theory for tidal waves, it is the standard formulation for fundamentally describing waves at sea. These waves are expressed by the water particle motion, which describes a transport in closed elliptical orbits where both axes decrease with increasing water depth. The complex derivation is not shown here, only the result is presented. The water elevation of a linear wave, running in x -direction, can be depicted as:

$$\eta_{Airy} = \frac{H}{2} * \cos(kx - \omega t) \quad (2.5)$$

where H is the wave height, $k = \frac{2\pi}{L}$ is the wave number with the wavelength L , x is the position in space, $\omega = \frac{2\pi}{T}$ is the angular frequency, with the wave period T , and t is the position in time. The amplitudes of horizontal wave acceleration and velocity according to the linear Airy wave theory (1845) are given as:

$$|u_{Airy}| = \frac{H}{2} \omega \frac{\cosh[k(z+d)]}{\sinh(kd)} * \cos(kx - \omega t) \quad (2.6)$$

$$|\dot{u}_{Airy}| = \frac{H}{2} \omega^2 \frac{\cosh[k(z+d)]}{\sinh(kd)} \sin(kx - \omega t) \quad (2.7)$$

where $z = 0$ is the distance from the still water line and d is the overall water depth from the still water level.

Airy wave theory (1845) has been proven to provide best results for small amplitudes in comparison to the overall water depth. Furthermore, it disregards the more accurate trochoid-shaped water elevation under waves in favor of a symmetric, sinusoidal wave profile. However, the waves occurring in nature are predominantly quite steep, even if the amplitude remains small. Therefore, a more accurate depiction can be achieved by utilizing more advanced theories, like the Stokes wave theories (1847). Here, non-linearities are considered, so that for deep water conditions and waves in the transition region, the motion processes are more accurately captured. In this thesis, mainly the 2nd order wave theory is used. The expression for the water elevation in the Stokes 2nd order wave theory (1847) is:

$$\eta_{Stokes_{II}} = \frac{H}{2} * \cos(kx - \omega t) + \frac{\pi H}{4L} \left(1 + \frac{3}{2 \sinh^2 kd} \right) \coth kd * \cos 2(kx - \omega t) \quad (2.8)$$

The amplitudes of horizontal wave acceleration and velocity are given as:

$$\begin{aligned} |u_{Stokes_{II}}| &= \frac{\pi H}{T} \frac{\cosh[k(z+d)]}{\sinh(kd)} \cos(kx - \omega t) \\ &+ \frac{3}{4c} \left(\frac{\pi H}{T} \right)^2 \frac{\cosh 2[k(z+d)]}{\sinh^4(kd)} \cos 2(kx - \omega t) \end{aligned} \quad (2.9)$$

$$\begin{aligned} |\dot{u}_{Stokes_{II}}| &= \frac{2\pi^2 H}{T^2} \frac{\cosh[k(z+d)]}{\sinh kd} \sin(kx - \omega t) \\ &+ \frac{3\pi}{2L} \left(\frac{\pi H}{T} \right)^2 \frac{\cosh 2[k(z+d)]}{\sinh^4 kd} \cos 2(kx - \omega t) \end{aligned} \quad (2.10)$$

where $c = \frac{L}{T}$ is the wave propagation speed.

2.1.3. Hydrodynamic coefficients

The Morison equation (1950) supplemented by the correct wave theory provides a practical method to determine the incident wave loads on a marine structure if the empirical constants of the hydrodynamic coefficients are known. These are generally determined experimentally by solving Equation (2.4), provided that the water particle kinematics and inline loads are established. Two methods to evaluate the hydrodynamic coefficients, a least-squared error approach and a min-max approach, were used by Heideman et al. (1979). They concluded that the Morison equation (1950) with constant coefficients can be adjusted to fit measured local forces and kinematics satisfactorily. Especially regarding cylinders, many

experiments have been conducted and accepted values of the drag and inertia coefficient for various cases are available. For further information in this regard see Sarpkaya (2010), who presents a brief summary of the literature giving explicit C_D and C_M values for cylinders alongside suggested values for the hydrodynamic coefficients.

In the context of this thesis, the Morison equation (1950) is an often-used approach to determine the hydrodynamic loads on aquaculture systems. In the absence of experimental data, engineering judgment is necessary to determine the hydrodynamic coefficients. In numerical studies by Raman-Nair and Colbourne (2003) and Raman-Nair et al. (2008) mussel dropper lines are modelled as slender cylinders to which the Morison equation is applied. In their studies, the drag coefficients have been assumed as $C_D = 1.5$ and $C_D = 1.2$, respectively. The authors stress the necessity of physical experiments or field tests to obtain realistic values as no basis for their assumptions is given. A more recent numerical investigation assumes $C_D = 1.1 - 1.7$ as realistic values for the modelling of submerged shellfish longlines (Knysh et al., 2020). Their numerical model of a longline aquaculture system showed little sensitivity to the exact choice of drag coefficients regarding the predictions for mooring line tensions and longline dynamics. Detailing the overall physics of offshore shellfish aquaculture, Stevens et al. (2008) suggest values of $C_D = 1.5$, linked to research regarding ultra-rough cylinders. They concluded that further research within this highly interdisciplinary topic needs to be conducted in a multi-scale approach, e.g. as feeding and spat retention take place in an individual scale while load dynamics need to be conducted for parts of the system or the system as a whole. Xu et al. (2020) assumed the drag coefficient of mussel dropper lines to range from $C_D = 1.1$ to 1.2 based on a computational fluid dynamics approach through a 3D-Large Eddy Simulation. None of these assumptions are based on validated physical experiments and should be considered as an estimate.

In a study regarding the hydrodynamic implications of offshore shellfish systems, a provisional drag coefficient was determined using towing tank tests on a length of dropper line (Plew et al., 2005). A resulting drag coefficient of $C_D = 0.89$ was determined. In a later investigation, a drag coefficient of $C_D = 1.27$ was determined through further physical model experiments (Plew et al., 2009) where mussel shells

(*P. canalicus*) were glued onto 10 mm polythene hoses to imitate dropper lines. Gagnon and Bergeron (2011) report on tests conducted with four 4 m long dropper lines where a drag coefficient of $C_D = 1.25$ was determined. The dropper lines were cut by divers and dragged behind a boat where a load cell was located. The influence of waves and current was not included in the results, which likely affects the outcome. Gieschen et al. (2021) conducted large-scale experiments on mussel dropper lines under oscillatory flow covering a wide KC-range from 10 to 380. They reported drag coefficients of $C_D = 3.4 - 3.9$. However, due to relative horizontal motion of the dropper lines, further enhancement of the evaluation method is required for a more precise estimation. The inertia coefficients C_M was not covered.

The results presented above are compiled into Table 2 to show the large uncertainties regarding the hydrodynamic coefficients as well as the absence of research on mussel dropper lines in oscillatory flow.

Table 2: Reported values of drag C_D and inertia C_M coefficients for mussel dropper lines. Ranges of tested Reynolds Re numbers and Keulegan-Carpenter KC numbers are indicated.

Source	Steady flow		Oscillatory flow		
	C_D	$Re [x10^4]$	C_D	C_M	$KC [-]$
Raman-Nair and Colbourne (2003)	1.5	-	-	-	-
Plew et al. (2005)	0.89	0.4 – 1.2	-	-	-
Raman-Nair et al. (2008)	1.2	-	-	-	-
Stevens et al. (2008)	1.5	-	-	-	-
Plew et al. (2009)	1.3	1.0 – 7.0	-	-	-
Gagnon and Bergeron (2011)	1.25	3.5 - 10	-	-	-
Knysh et al. (2020)	1.1 – 1.7	>4.0	-	-	-
Xu et al. (2020)	1.1 -1.2	0.39 - 10	-	-	-
Landmann et al. (2021a)	1.6	2.3 - 14	2.3	2.1	1.9 – 8.8
Gieschen et al. (2021)	-	-	3.9	-	10 - 380

Chapter summary 2.1:

The Morison equation (1950), as an empirical method to determine the wave force on a slender body ($\frac{D}{L} < 0.2$) is introduced and the importance of choosing the corresponding, correct wave kinematics according to their explicit wave theories is highlighted. While a multitude of accepted values of the hydrodynamic coefficients for various cases is available, the research regarding bivalve aquaculture, and mussel dropper lines, is scarce.

The available investigations are based on assumptions or conducted under very idealized boundary conditions with a limited number of tests. Almost all research focuses on steady flow while also stating that different results are expected for oscillatory flow. The currently available research does not allow for a generally valid statement regarding the correct hydrodynamic coefficients used regarding bivalve aquaculture.

2.2. Surface parameters

2.2.1. Surface Roughness in marine environments

As mentioned in Chapter 2.1, the hydrodynamic loads a marine object is subjected to are greatly influenced by the surface roughness of the object itself. Surface roughness can be defined as a homogeneous or heterogeneous deviation from the mean level of a surface (see Eq. (2.3)). In Table 3, values for the surface roughness height k_r for various engineering materials are listed.

Table 3: Absolute surface roughness height k_r for various engineering materials.

Material [-]	Surface roughness height k_r [m]
Concrete	0.003 – 0.005
Rusted steel (corrosion)	0.0015 – 0.004
Steel	0.0001 – 0.0009
Stainless steel	0.000001 - 0.00006
PVC, PE, etc.	0.000015 - 0.00007

As shown in Table 3, a surface roughness height of $k_r = 0.000001$ corresponds to the surface of steel (e.g. newly installed monopiles). This is considered as smooth in marine environments. However, the surfaces of many marine structures are not smooth. The roughness of the structural surface may originate from multiple sources. The appendages attached to a structural component of a marine system can cause irregularities that lead to changes in the flow. Another source of roughness is marine growth, attaching itself to any surface in contact with marine waters. The hydrodynamic loads as well as the structural response on a roughened structure can differ significantly from those that occur on a clean structure under identical flow conditions. This is due to the parts protruding into the flow as well as an increase in the effective diameter and the effective mass, which affects the natural frequency and damping of structure.

Generally, the loads on a slender structure in marine conditions increase with greater roughness. If the surface of the structure is not smooth, the roughness shifts the point of flow separation at the structure and the corresponding wake behind the structure, causing a change in the drag coefficient. The roughness of the

structural surface breaks up the flow earlier in the velocity field, reducing the overall velocity and creating a larger wake. In this case, the flow around a rough surface separates from the surface earlier than would be the case with a smooth object. This shift triggers a premature and less distinct drag crisis for objects with a higher roughness. The higher the roughness, the earlier this separation occurs. This causes the development of a pressure gradient between the up- and downstream areas of the object.

Considering the Morison equation (1950) (see Chapter 2.1.1), increased roughness results in a larger drag coefficient C_D and larger drag force. The inertia coefficient C_M is affected to a lesser extent by roughness. It increases rapidly and reaches a maximum at a Reynolds number corresponding to that at which C_D falls to a minimum. At higher Reynolds numbers, C_M decreases to near-constant values that are lower than a comparable smooth structure. Experiments conducted by Sarpkaya (1976a, 1976b) and a comparative review by the same author (Sarpkaya, 1990) showed the influence of surface roughness on the hydrodynamic coefficients of circular cylinders. It has also been demonstrated that the Morison equation is applicable for ultra-rough cylinders (Wolfram and Naghipour, 1999), to which mussel dropper lines can be compared when they grow in suspended cultures. For more general information regarding the influence of surface roughness on the force evolution along slender bodies consider the work by Sarpkaya (2010).

In the context of this study, desired (e.g. aquaculture) as well as undesired (e.g. fouling) marine growth is treated from an engineering point of view. From the moment of submergence, all marine objects are settled by marine micro-organisms which initiate the settlement of more complex entities (Cooksey and Wigglesworth-Cooksey, 1995; Jonsson et al., 2004; Railkin, 2003; Schoefs et al., 2022). This marine growth alters the offshore structure itself and the flow conditions around it, affecting its performance (Heaf, 1979). The projected area of the structure is increased as well as the surface roughness, which in turn affects drag and inertia coefficients and thereby the loads. Consequently, marine growth is a technical, economic, and environmental challenge affecting most sea-based activities. It has been the focus of study by oil and gas industries (Houghton, 1978), naval industries (Woods Hole Oceanographic Institution, 1952), and more recently aquaculture (Dürr and Watson, 2009; Fitridge et al., 2012), and marine renewable

energy industries (Gill, 2005; Langhamer et al., 2009; Schoefs and Tran, 2022; Shi et al., 2012; Soares and Garbatov, 2017). Examples for marine growth associated with bivalve aquaculture are shown in Figure 6.

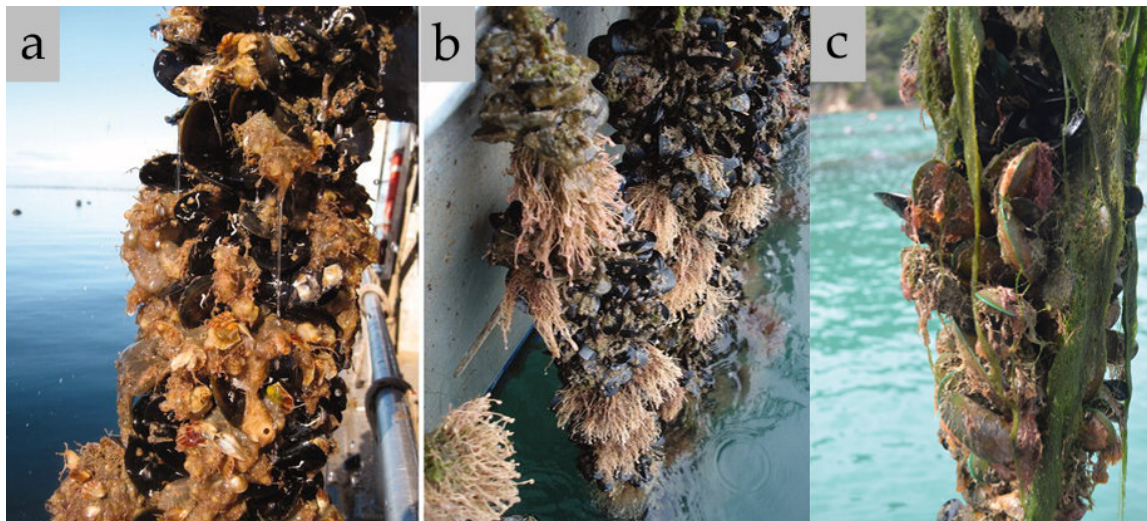


Figure 6: Common fouling organisms associated with bivalve aquaculture representing soft and hard growth with a) Vase tunicate (*Ciona intestinalis*) [©Fitridge et al., (2012)], b) Pink mouthed hydroid (*Ectopleura crocea*) [©Fitridge et al., (2012)] and c) Green algae (*Chlorophyta*) [©Goseberg, N.].

Regarding marine growth, Heaf (1979) examined the potential extent and importance in regard to the performance of fixed offshore platforms in the North Sea. He showed that an increased tube diameter due to marine fouling, leads to an increased projected area and displaced volume and hence to increased hydrodynamic loads. Furthermore, with an increase in marine growth, the mass increases, which leads to a decrease in its natural frequency.

Nath et al. (1984) conducted physical experiments in a wave tank with artificially as well as marine roughened cylinders ($k = 0.023$ m). The results show that the maximum force coefficients for a heavily roughened vertical cylinder are tightly arranged according to the Keulegan-Carpenter number. Furthermore, the phase angle is similarly much more organized than for the smooth cylinder.

In an extensive study by Theophahatos (1988), horizontally oriented, artificially roughened cylinders with diameters from $D = 0.15 - 0.40$ m and roughness heights from $k = 0.0015 - 0.01$ m as well as partially roughened cylinders with diameters of $D = 0.40$ m and roughness heights from $k = 0.008 - 1.0$ m and marine roughened cylinders with diameters from $D = 0.31 - 0.40$ m and

roughness heights from $k = 0.008 - 1.0$ m were tested. The results show that marine growth significantly increases hydrodynamic loads. This increase varies with the type of marine growth. The most severe increase in drag forces is caused by kelp growth which may amount to more than 100% compared to that of a smooth cylinder. The author concluded that marine growth cannot be adequately characterized by a single parameter such as relative roughness and that further parameters such as surface cover, species type, and thickness need to be considered. Similarly, ISO (2019) guidelines recommend that site-specific studies need to be conducted to establish the likely type, thickness, and depth dependence of marine growth before a construction is begun.

Wolfram and Naghipour (1999) analyzed data obtained with artificially roughened circular cylinders ($k = 0.023$ m) and concluded that a weighted least square method generally gave the best predictive accuracy.

Henry et al. (2016) visualized and discussed the effect of different types of marine growth in the wake of a cylinder. Their study highlights the changes on the cylinder hydrodynamics induced by a developing fouling community, going from small hard roughness ($k = 0.003$ m) to fully developed soft fouling ($k \sim 1$).

Marty et al. (2021) developed a model to represent the hard growth on marine objects and used it to determine the impact of roughness on drag and inertia coefficients. The effect of roughness on the drag coefficient for low KC numbers (~ 3) in oscillating flow was shown to lead to a 62% increase of drag forces with increased roughness. The results show a constant difference between the inertia coefficient of 0.3 between the two rough cylinders with a higher value for the higher roughness ($k = 0.091$ m and $k = 0.136$ m). Moreover, they concluded that most hydrodynamic tests over-simplify the shape of marine growth, and when it is more realistic, the exact shape is not well documented. Therefore, they recommend that future research needs to precisely document the relative roughness, shape, organization, and areal density.

The tested roughness of marine growth as recorded in literature is listed in Table 4 to show the large variations in marine roughness. This shows that the term itself is not sufficiently defined as it encompasses hard as well as soft growth which has a high dependency on location as well as biological parameters. The specific effect

of the roughness of mussel dropper lines and the importance of the corresponding characteristic diameters are extensively discussed in Chapter 3.2.

Table 4: Reported values of roughness height for mussel dropper lines as well as surrogate structures are shown. The ranges of the tested diameter and relative roughness are indicated (sources are indicated in Table).

Source	Description	Roughness height k [m]	Diameter D [m]	Relative roughness $\Delta = k/D$ [-]
Nath et al., (1984)	Artificially/ marine roughened cylinder	0.0047	0.203	0.023
Theophahatos, (1988)	Artificial roughened cylinders	0.0015 – 0.01	0.15 – 0.40	0.005 – 0.01
	Partially roughened cylinders	0.008 – 1.0	0.40	0.02 – 2.5
	Marine roughened cylinders	0.008 – 1.0	0.31 – 0.40	0.016 – 2.5
Wolfram and Naghipour, (1999)	Artificial roughened cylinders	0.008	0.21 – 0.51	0.038
Henry et al., (2016)	Artificial roughened cylinders	0.0 – 0.003	0.042	0.0 – 0.07
Marty et al., (2021)	Artificial roughened cylinders	0.0 – 0.03	0.16 – 0.28	0.0 – 0.136

2.2.2. Surface descriptor and surrogate creation

Based on the importance of surface roughness in regard to marine environments, a surface descriptor, used in the physical experiments presented in the journal publications (see Chapters 3.1 and 3.2), is introduced. Surface descriptors are a numeric representation of chosen surface characteristics of an arbitrary object. Proceeding from the assumption that drag and inertia coefficients are significantly influenced by surface geometry and roughness, a precise description of the original surface is necessary for the design of a surrogate model.

As a common surface descriptor, the Abbott-Firestone curve (AFC) is selected. The AFC or bearing area curve (BAC) used as a statistical curve comprising rough peaks is considered an important tool for describing surface profiles in mechanical engineering (Gadelmawla et al., 2002; He et al., 2022). With this method, a thorough quantification of an arbitrary surface geometry and porosity in a two-dimensional plane is possible (Abbott and Firestone, 1933). The AFC displays the material distribution M_r [%] as a function of the fluctuation in material surface c_{depth} [m]. This can be described as:

$$M_r(c_{depth}) = \frac{100\%}{l_n} * \sum_{i=1}^n l_i(c) \quad (2.11)$$

where l_n is the total length of the recorded section and l_i is the length of material cut at the depth c_{depth} . The AFC separates its roughness profile into peak, medial and valley portions (Abbott and Firestone, 1933). These separate planes differ in depth and main function, e.g. the peak portion has a major influence on a surface's run-in characteristics whereas the valley area defines the amount of water that may be dragged along when interacting with the flow around an object. The depth of peak, medial, and valley portion is expressed by the parameters reduced peak roughness R_{PK} , medial roughness R_K , and reduced valley roughness R_{VK} (DIN, 1998). In order to achieve an averaging effect, unrepresentative peaks and valleys which make up less than two percent are disregarded (Abbott and Firestone, 1933).

The AFC enables the separate evaluation of a surface regarding run-in characteristics, load-bearing capacity, roughness, and absorption of liquids. Since the AFC has originally been designed as a descriptor for two-dimensional roughness profiles, a transfer into three-dimensional space is necessary to analyze the data obtained from the laser scanning of the live mussel specimen. Like the two-dimensional case, the 3D-AFC is based on an imaginary cutting-plane being steadily moved downwards from the profiles highest peak to the lowest valley. This procedure is mathematically described by:

$$SM_r(c_{depth}) = \frac{100\%}{A} * \iint_{x,y} dx dy \quad (2.12)$$

where A is the regarded surface within the coordinate system x, y (Lemke et al., 2003). The 2D-parameters reduced peak roughness R_{PK} , medial roughness R_K , and reduced valley roughness R_{VK} can be transferred to 3D and are renamed to reduced peak roughness S_{PK} , medial roughness S_K , and reduced valley roughness S_{VK} (DIN, 2012). In 3D, the material portions of peaks and valleys are named SM_{r1} and SM_{r2} . After having recorded a three-dimensional surface's AFC, a comparison with others is possible.

In the context of this work, the AFC is used as the primary surface descriptor and basis for all surrogate models. As part of this thesis deals with cylinder-roughness featuring a large unfiltered profile depth P_t to cylinder diameter D_{cyl} ratio of: $\frac{P_t}{D_{cyl}} \approx 0.5$, a definition of the AFC for cylindrical geometries is introduced. Instead of filtering out the cylinder's cylindricity and determining the material portion SM_r as a function of height c of a cutting plane, the cylindricity stays untouched allowing for the profile to be cut with a cylindrical surface $A_c(r)$ providing the material portion as a function of the cutting cylinder's radius r . Accordingly, the AFC for cylindrical bodies with a large unfiltered profile depth to cylinder diameter ratio is defined as:

$$SM_{r,cylindrical}(r) = 100\% * \frac{\sum A_i(r)}{A_c(r)} \quad (2.13)$$

where $\sum A_i(r)$ is the profile's cut surface and $A_c(r)$ is the nominal surface of the cutting cylinder. This is depicted exemplary for a mussel dropper line in Figure 7. Due to its promising characteristics regarding surface description, the cylindrical AFC is applied in the creation of the mussel dropper lines. The application of this process and the created surrogates are presented in Chapter 3.1.

$$SM_{r,cylindrical}(r) = 100\% * \frac{\sum A_i(r)}{A_c(r)}$$

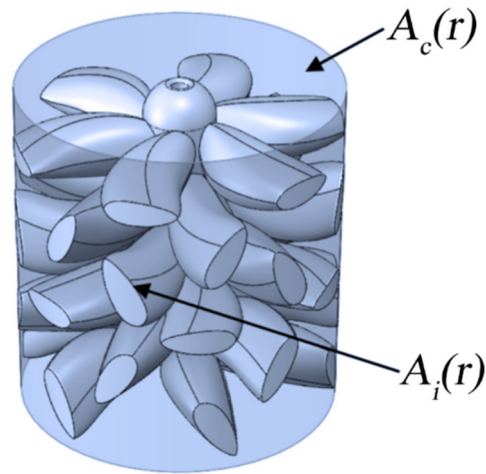


Figure 7: Visualization of the creation of the Abbott-Firestone Curve for cylindrical surfaces, here a mussel dropper line with $A_i(r)$, the profile's cut surface, and $A_c(r)$, the nominal surface of the cutting cylinder is displayed.

Chapter summary 2.2:

The influence of the **surface roughness** on the force evolution of marine objects is known for a wide range of materials and system types. The associated processes leading to an increase in loads are highlighted. Regarding bivalve aquaculture, the research so far shows that **marine roughness** encompasses hard as well as soft growth which has a high dependency on location as well as biological parameters.

Furthermore, the **Abbott-Firestone curve** as concise tool for describing surface profiles is introduced. The surface descriptor enables the separate evaluation of a surface regarding run-in characteristics, load-bearing capacity, roughness, and absorption of liquids. The application towards the creation of mussel dropper surrogates is highlighted.

2.3. Wave-Structure interaction

Wave-structure interaction is a key consideration for the safe and cost-effective design and operation of any marine systems. It refers to the interactions between waves and any structure in their way. These interactions are visible in front of the structures as reflections, on the structures themselves as run-up and dissipation, and behind the structures as overtopping, refraction, diffraction, scattering, and transmission. Accurate design methods are required to estimate the influence of these effects, as well as the system response in marine environments.

In the context of this thesis, the protection of marine resources against wave action is highly important. Breakwaters are often used for the necessary wave attenuation. These are commonly investigated coastal engineering structures that reduce the wave action in inshore waters, minimize coastal erosion, and increase the safety for anchoring or passing marine vessels. Conventionally, these are built on rubble-mound foundations with quarried rocks, concrete caissons, or rock armor resting on the slope. However, in the light of growing offshore activities floating breakwaters are becoming increasingly more important to protect installations in deeper waters. They are seen as more beneficial with increasing water depth, as the cost and work required for conventional breakwaters at the same location drastically increases. As most wave energy is located near the free surface, as the water particle motion and associated fluid velocity decreases with the depth, no conventional foundations are needed.

When an incident wave passes a floating structure, the wave energy can be attenuated by a number of phenomena such as reflection, wave breaking, friction, vortex formation, vortex shedding, jet mixing, as well as resonance (Sawaragi, 1995). The magnitude of this attenuation is dependent on hydraulic parameters (e.g. wavelength, wave steepness, obliqueness of incoming waves) and geometry-related parameters (e.g. length, width, height, mass, and roughness of structure). For the determination of the overall effectiveness of floating systems, dimensionless coefficients can be used. In this regard, wave transmission describes the phenomenon in which the incident wave energy approaches a floating breakwater at the front, is dissipated to an extent, and a reduced wave is transmitted at the rear. The resulting transmission coefficient C_T is determined as:

$$C_T = \frac{H_t}{H_i} \quad (2.14)$$

with H_t being the transmitted wave height and H_i being the initial wave height in meters. The initial wave height is commonly determined using a reflection analysis in the frequency domain based on a method developed by Mansard and Funke (1980), which also provides the reflection coefficient C_R of the structure. For regular waves the reflection coefficient C_R is calculated as:

$$C_R = \frac{H_r}{H_i} \quad (2.15)$$

with H_r being the reflected wave height. When combining equations (2.14) and (2.15), the determination of the energy dissipation by the structure is possible. A dissipation coefficient C_{Diss} can be calculated as:

$$C_{Diss} = \sqrt{1 - C_R^2 - C_T^2} \quad (2.16)$$

An overview regarding approximated values for the reflection coefficient of floating and fixed structures is given in Table 5.

Table 5: Approximated values for reflection coefficients C_R of fixed and floating structures (sources are indicated in Table).

Structure	Reflection coefficient C_R [-]
Vertical wall with crest above water (Goda, 2010)	0.7 – 1.0
Cylindrical floating breakwater (Ji et al., 2016)	0.15 – 0.65
Artificial floating islands (Landmann et al., 2022)	0.1 – 0.6
Rubble-mound breakwater (Seelig and Ahrens, 1981)	0.1 – 0.6
Concrete armored breakwater (Goda, 2010)	0.3 – 0.5
Porous floating breakwater (Wang and Sun, 2010)	0.05 – 0.35
Natural beach (Goda, 2010)	0.05 – 0.2

The interaction between waves and a floating system regarding reflection, transmission and dissipation is described in Chapter 3.4. Floating breakwaters are

specially designed to attenuate waves. Their construction and operation are scarcely affected by increasing water depth and they interfere with the overall water circulation in a negligible manner. However, natural structures consisting of a variety of wetland plants, aquatic vegetation, kelp beds and oyster reefs can also serve as breakwaters. As part of a “living shoreline” they can contribute to the protection of coastal areas (Davis et al., 2015; Palinkas et al., 2022; Saleh and Weinstein, 2016). These “living shorelines” are defined as natural, shallow water, shoreline stabilization and habitat restoration techniques that have the potential to increase the living space for estuarine and coastal organisms (Bilkovic et al., 2016; Gittman et al., 2016; Moosavi, 2017; Scyphers et al., 2011). Many aquaculture systems such as those comprised of kelp and mussels (Mascorda Cabre et al., 2021) can also be considered as nature-based breakwaters with the ability to attenuate wave energy as well as provide ecosystem service.

Since wave energy attenuates with depth, crop cultivated near the surface like kelp or mussels is expected to have a larger impact on wave attenuation than beds growing on the bottom. To this end, several field studies are available, focusing on the hydrodynamic and environmental impacts of aquaculture installations. In those, Gibbs et al. (1991) observed flow attenuation of up to 70% in local circulation patterns around longline systems. Boyd and Heasman (1998) investigated the effects of the dropper line density on the flow pattern. They observed flow reductions of 86% and 75% for dropper lines spaced 0.6 m and 0.9 m apart, respectively. Pilditch et al. (2001) observed a 40% flow speed reduction within an 80 × 50 m² suspended scallop culture system. Similarly, Plew et al. (2005) demonstrated flow speed reductions within longline systems. They observed that a 650 m × 2450 m mussel farm with suspended dropper lines attenuates the wave energy by approximately 5% (0.1 Hz), 10% (0.2 Hz), and 17% (0.25 Hz) depending on the wave frequency. In an observational study by Stevens and Petersen (2011) the complex flow conditions around shellfish farms are described. Three farm units with three sections of 32 longlines each were considered. They concluded that the response of the flow affected by the canopy is complex and highly variable. Newell and Richardson (2014) reported flow attenuations of 75 – 80% arising from drag due to culture ropes and supporting infrastructure. Zhao et al. (2019) investigated the wave attenuation characteristics of suspended kelp farms. Their results indicate that 20 longlines with 100 plants/m could reduce up to 23% of the wave

energy. Liu and Huguenard (2020) investigated the impact of a floating oyster aquaculture farm on the intratidal dynamics of a low inflow estuary using field observations and an idealized numerical model. They observed a streamwise flow reduction, which affects streamwise advection and hinders development of lateral circulation near the farm. Zhong et al. (2022) observed that the presence of suspended mussel farms reduces the flow by more than 79%, 55%, and 34% in the upper, middle, and bottom layers of the farm center based on a numerical model and observational results. A work by Shi et al. (2011) concentrated on a three-dimensional model modified by including two types of drag to study the dynamic coupling between physical and biological processes of an area used for suspended aquaculture. The authors showed the vertical structure of currents in a suspended aquaculture site and determined a 40% reduction in average flow speed. Plew (2011) conducted flume experiments of suspended canopy configurations and divided velocity and turbulence profiles into three layers: bottom-boundary, canopy-shear, and internal-canopy layers. Based on a work by James et al. (2016), James and O'Donncha (2019) numerically modeled the flow conditions in and around suspended canopies. An increasing average drag coefficient was observed with decreasing canopy blockage ratio, and an empirical relationship for the vertical variation of the drag coefficient was developed. Qiao et al. (2016) investigated the interactions between suspended canopies and the surrounding flow in comprehensive physical experiments with varying ratios of canopy to water column depths. They concluded that the suspended canopy influences the mean flow structure, the turbulence behavior, and the momentum transport.

This multitude of studies shows that the highly ordered and heterogeneous canopies created through aquaculture affect the flow, but non-linear effects lead to highly variable results. The flow alteration in the presence of suspended mussel dropper lines as recorded in literature is shown in Figure 8.

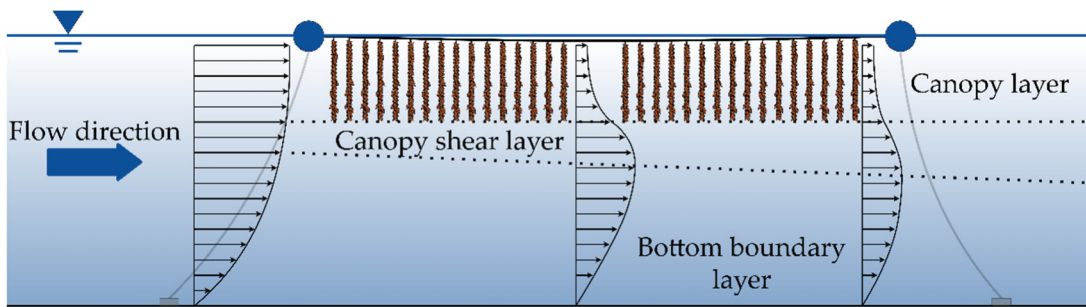


Figure 8: Side view of the flow alteration in the presence of suspended mussel dropper lines with differentiation between three distinct flow layers [after Zhong et al. (2022)].

These interactions describe mostly the effect of the structure on the flow. However, the motion of the structure itself cannot be neglected. For the safe cultivation of products, spontaneous motion, which induces high accelerations, needs to be avoided. The potentially hazardous force peaks on mooring systems introduced by snap loads must be considered as well. The phenomenon of snap loads has been investigated in physical (Bardestani and Faltinsen, 2013) as well as numerical model tests (Hsu et al., 2018; Palm et al., 2017, 2013; Palm and Eskilsson, 2020). Hsu et al. (2017) conducted physical model tests on a semi-submersible floating offshore wind platform under currents, waves, and wind. These authors suggest that an inclusion of snap-induced tension maxima in ultimate limit state evaluations could be beneficial. Qiao et al. (2020) investigated the occurrence and conditions for snap loads in mooring lines through the calculation of dynamic tension under different excitation parameters and influence factors. They concluded that higher pre-tension provides a benefit for avoiding snap loads in mooring lines. Observational studies in bivalve aquaculture farms with a focus on the hydrodynamics, stresses, motion of whole farms of mussel longlines as well as growth behavior and stock density of the bivalves in exposed environments are also available (Díaz et al., 2011; Drapeau et al., 2006; Gagnon and Bergeron, 2011; Garen et al., 2004; Plew et al., 2005). Gagnon and Bergeron (2017) showed that the tension in and acceleration of submerged mussel longline farms is significantly smaller compared to surface systems. Stevens et al. (2007) identified tidal loading as a main contributor to the overall force acting on a surface longline farm and assumed that oscillating wave forces contribute significantly.

This shows that an understanding of the interactions between marine aquaculture systems and the marine environment is essential for predicting the sustainability

in exposed conditions. A large bivalve farm system, including a myriad of mussel dropper lines, is affected by the flow and itself has an impact on the flow. Further research is necessary to quantify that impact.

Chapter summary 2.3:

Wave-structure interactions are introduced regarding the wave attenuation potential of floating structures. As they are a key consideration for the safe and cost-effective design and operation of any marine system, the main parameters (transmission-, reflection-, and dissipation coefficient) for the determination of the overall effectiveness are established.

Based on this, the research regarding the effect of bivalve aquaculture systems on the surround flow is shown. Here the *wake effects, system motion and mooring considerations* are highlighted.

2.4. Knowledge gaps

The literature review presented in the previous chapters provides fundamental knowledge and reports on the recent advances regarding the hydrodynamics around bivalve aquaculture. It shows that complex flow situations are still seldomly considered for the prediction of the hydrodynamic loads of offshore bivalve aquaculture. Evidently, there is a lack of knowledge regarding the effects of realistic marine flow conditions on bivalve offshore aquaculture systems, despite the increasing availability of more and more sophisticated laboratories and numerical models that would allow investigations into such processes. Several knowledge gaps, relating to the objectives of this thesis, are summarized, and described in the following:

- Commonly, the force coefficients of mussel dropper lines are inferred from limited towing tests (Plew et al., 2009), or in few cases, by using observational data from farms (Gagnon and Bergeron, 2017). The determination of the hydrodynamic coefficients of mussel dropper lines or their surrogates through physical or numerical experiments has also not been conducted for oscillatory flow regimes (see Table 2). As summarized by Gagnon (2019) the hydrodynamic coefficients of mussel suspensions in waves are unknown. However, it is assumed that their influence is significant (Stevens et al., 2007).
- There is no clear guidance as to how the complex surface of mussel dropper lines should be modelled. Most experiments over-simplify the shape of marine growth (Gagnon, 2019), and when it is more realistic, the exact shape is not well documented (Plew et al., 2009). As stated by Marty et al. (2021) future research needs to precisely document the relative roughness, shape, organization, and areal density. It remains unclear to date how appropriate surrogate dropper lines are with respect to the forces exerted on them as well as to which parameters influence their behavior.
- The influence of bivalve aquaculture structures on the flow is largely well understood (Zhong et al., 2022). However, the influence of the structure motion on the force evolution in a prospected move to open ocean environments is not. In this environment, the maximum forces generated by waves can be more than one order of magnitude larger than in coastal

sites (Gagnon, 2019). Novel approaches are scarce (Heasman et al., 2021) and the exact adaptation and implementation into existing systems is not well understood.

Based on the literature review, there is clear need for developing a deeper understanding of the hydrodynamics around bivalve aquaculture systems to allow for the development of offshore farming systems. Leveraging the results from the studies presented in Chapter 3, this thesis aims to support this desired development of actual systems and design approaches by principally investigating the hydrodynamic forces and resulting force coefficients of mussel dropper lines and aquaculture systems in steady and oscillatory flows.

Chapter summary 2.4:

*In this chapter, three **knowledge gaps** identified through the literature review are summarized*

First, the lack of hydrodynamic coefficients for the safe determination of loads in offshore environments particularly for oscillatory flow is shown. Second, the lack of guidance as to how the complex surface of mussel dropper lines should be modelled and which factors are of importance for engineers is shown. Third, there is a lack of understanding regarding system motion and load evolution.

Based on this, the need for developing a deeper understanding of the hydrodynamics around bivalve aquaculture systems is empathized.



3. Results

Based on the gaps of knowledge identified above (see Chapter 2.4) physical experiments were conducted in a variety of laboratories to identify and reliably predict the hydromechanic drivers in bivalve offshore aquaculture systems. The findings of these experiments, which were submitted as a collection of international journal publications, are presented below. The sections contain a shortened and adapted version of the manuscripts abstracts, results, and conclusions, which are complemented by a selection of the main articles' figures.

All articles have been published under open access licenses and are freely available for every interested party from the publishers. They can be found by their citation or Digital Object Identifier (DOI), provided at the beginning of each section in this chapter.

3.1. Creation of surrogate mussels

Landmann J., Ongsiek T., Goseberg N., Heasman K., Buck B.H., Paffenholz J.-A., Hildebrandt A. (2019); Physical Modelling of Blue Mussel Dropper Lines for the Development of Surrogates and Hydrodynamic Coefficients. *Journal of Marine Science and Engineering*; 7(3):65. <https://doi.org/10.3390/jmse7030065>

3.1.1. Abstract

In this work, laboratory tests with live bivalves as well as the conceptual design of additively manufactured surrogate models are presented. The overall task of this work is to develop a surrogate best fitting to the live mussels based on the identified surface descriptor. To derive geometrical models of the mussel dropper lines, 3D-point clouds were prepared by means of multidimensional laser scanning to obtain a realistic surface model. Centered on the 3D-point cloud, a suitable descriptor for the mass distribution over the surface was identified and three 3D-printed surrogates of the blue mussel were developed for further testing. These were evaluated regarding their fit to the original 3D-point cloud of the live blue mussels (*Mytilus edulis*) via the chosen surface descriptor.

3.1.2. Results

The overall aim of the study is to develop artificial surrogates that feature similar characteristics as compared to the live specimen regarding their hydrodynamic behavior in currents and waves. To this end, a terrestrial laser scanner was used to acquire a 3D-point cloud as a digital copy of live in-situ specimen. The acquisition of the 3D-point cloud was carried out without immersing the specimen into the wave flume as subaquatic scanning is less accurate and difficult to achieve (Wozniak and Dera, 2007). Three tripods were pre-mounted to allow for an exact positioning of the 3D laser scanner. Furthermore, reference points for the spatial registration were added in the vicinity of the scanning area. The 3D-point clouds from the differently positioned tripods were combined to a single 3D-point cloud, with every single point containing information about global x-, y- and z-positions as well as the intensity. Due to the 3D-point cloud's quality affected by challenging scan conditions, e.g. moving live mussels and aquatic animals, wet and black

surfaces to be scanned, and shifts caused by moving air, the data needed to be treated. For this and regarding limited computational resources, the 3D-point cloud was divided into ten separately analyzed sections. A statistical outlier removal filter was applied to each section to remove unwanted data points. As the cylindrical AFC assumes a solid body the 3D-point clouds of all generated surfaces were closed. In total, 4,368,790 single points for all ten sections within 0.915 m long blue mussel dropper line were considered. A live blue mussel specimen during the scanning process, the resulting 3D-point cloud, and resulting exemplary solid bodies used in the section-based analysis are shown in Figure 9.

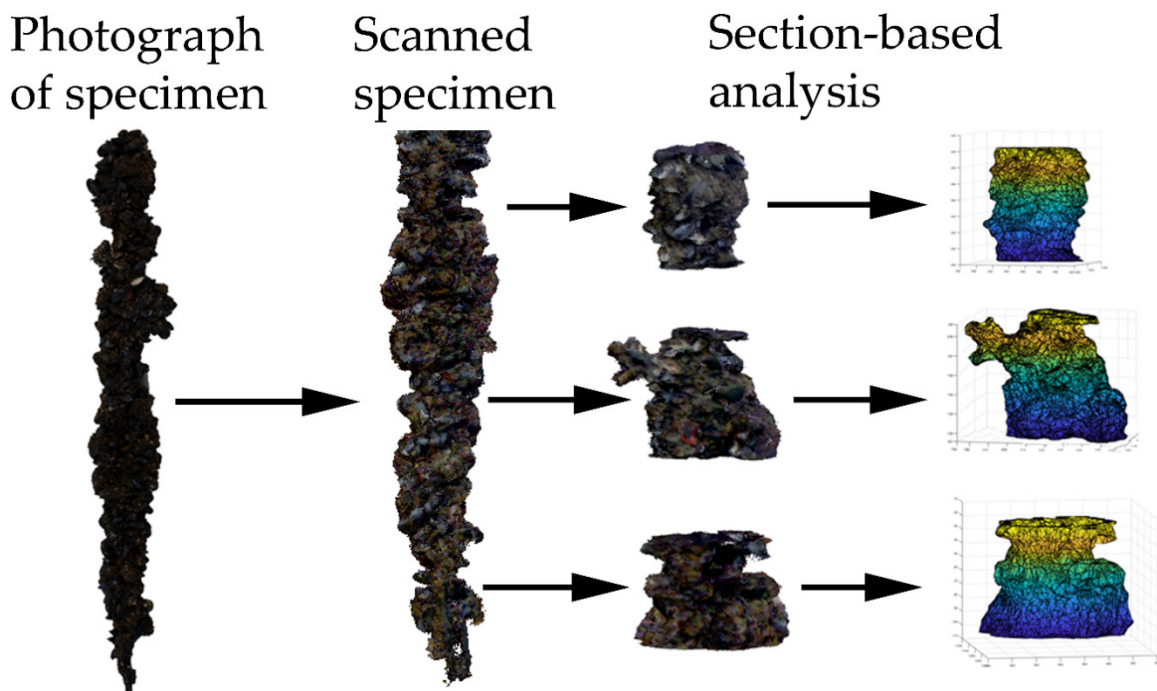


Figure 9: Photograph of a specimen during the scanning process, the resulting 3D-point cloud of the scanned specimen, and the resulting exemplary solid bodies used in the section-based analysis.

The solid bodies were analyzed regarding the AFC with the procedure introduced in Chapter 2.2.2. This resulted in the weighted arithmetic average material distribution (see Figure 10). Generally, the mean specimen had a maximum diameter of 13.6 cm and a minimum diameter 3.3 cm at the 2- and 98-percentile. The average diameter of the analyzed sections was determined as 10.3 cm. Three surrogate models were created centered on the distribution curve.

The first concept (SM 1) was based on a singular mussel, placed multiple times around a central cylinder. To that end, the length, volume, weight, and width of a

representative number of sample blue mussel shells were recorded, and a digital representation was developed with computer-aided design. The average model of the blue mussel shells was then arranged around a core cylinder (depicting a mussel crop rope in size/diameter), by varying each shell's rotation. The mean weight per unit length was chosen as a metric, and to match the surrogate's overall geometry with varying angles as compared to the live blue mussels (*Mytilus edulis*).

The second concept (SM 2) for a surrogate model was based on the closest fitting 3D-point cloud section to the weighted arithmetic average material distribution. This is selected because its mass distribution features the most similarity to the original. The triangulated section estimated the facets not covered by the 3D-scan due to a blocked field of view.

The third surrogate (SM 3) was based on a reproduction of the weighted arithmetic average material distribution combined with a simplified geometry. This was achieved by choosing a slender cylinder with 10 leave-shaped outcrops, and it was proposed as a more simple, potentially easier to build and scale surrogate, providing a novel geometric approach to future testing. The combined weighted arithmetic average material distribution of all sections is depicted in Figure 10 together with the created models.

The three different surrogates have been put forward to investigate their behavior under steady and oscillatory flows.

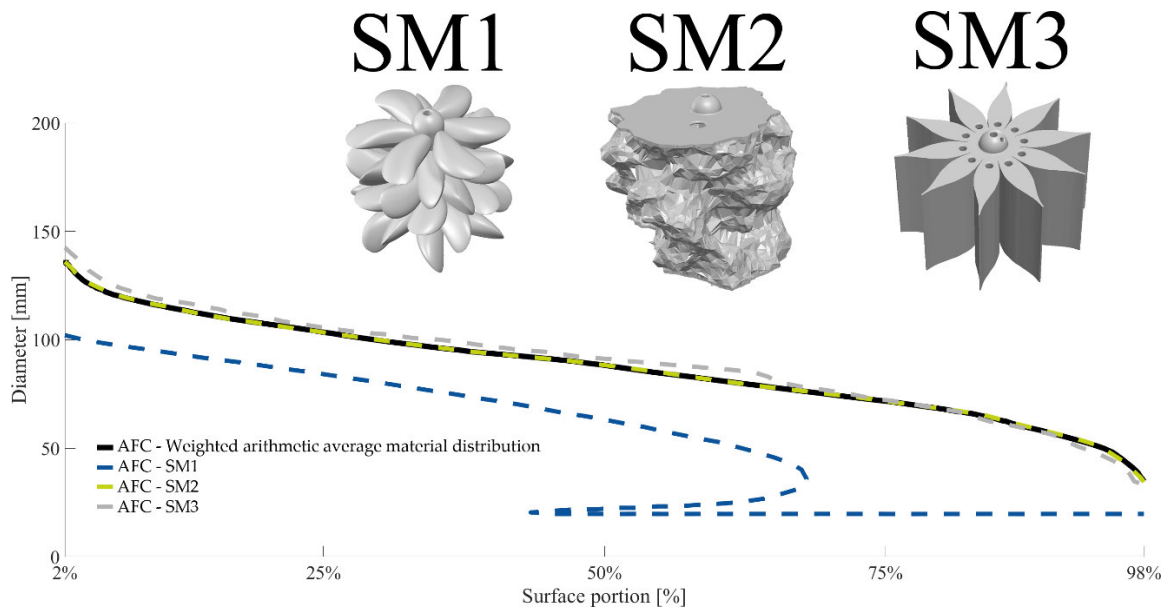


Figure 10: The Abbott-Firestone curve (AFC) of the weighted arithmetic average material distribution of all scanned sections (black) in comparison to the material distribution of the three surrogate mussels (SM 1 - 3) created.

3.1.3. Conclusion

A 3D-laser scan of live mussels was conducted, which resulted in the generation of a 3D-point cloud of 5.4 million data points. A systematic approach employing the Abbott–Firestone Curve was developed that allows an analysis regarding the material distribution as a function of the fluctuation in the material surface. With this approach, three concepts for surrogate models were developed:

- ❶ Concept 1 (SM 1) was based on single, uniform mussels. These were added to a slender cylinder at different angles of incidence until the mean weight per unit length was equal to the original live mussel data recorded.
- ❷ Concept 2 (SM 2) was based on the closest fitting 3D-point cloud section of the live mussels regarding the weighted arithmetic average material distribution.
- ❸ Concept 3 (SM 3) was a reproduction of the weighted arithmetic average material distribution through a much simpler geometry.

The developed surrogates featured similar characteristics to the live mussels regarding the chosen surface descriptor. In the future, a validation of the hydrodynamic characteristics is necessary to provide a scalable surrogate dropper line that can be used in a variety of applications. The three created surrogates will

allow for further testing without constraints regarding the longevity of the mussels and will be evaluated regarding their comparability to the live-mussel data.

Chapter summary 3.1:

This chapter presents the conceptual design of additively manufactured surrogate models for mussel dropper lines based on a surface descriptor.

*Based on a comprehensive **3D-laser scan** of live mussels and a following treatment of the gathered 3D-point cloud data, a systematic approach employing the **Abbott–Firestone Curve** was developed. It allows an analysis regarding the material distribution as a function of the fluctuation in the material surface.*

*Based on this approach **three distinct surrogates** were developed for further testing. The first concept (SM 1) was based on single, uniform mussels, the second concept (SM 2) was based on the closest fitting 3D-point cloud section while the third concept (SM 3) was a reproduction of the material distribution through a much simpler geometry.*

3.2. Determination of drag and inertia coefficients of shellfish dropper lines under steady and oscillatory flow

Landmann, J., Fröhling, L., Gieschen, R., Buck, B.H., Heasman, K., Scott, N., Smeaton, M., Goseberg, N., Hildebrandt, A. (2021); Drag and inertia coefficients of live and surrogate shellfish dropper lines under steady and oscillatory flow. *Ocean Engineering*; 235:109377, <https://doi.org/10.1016/j.oceaneng.2021.109377>

3.2.1. Abstract

In this work, physical experiments with suspended bivalves provide new insights into their drag and inertia coefficients. Live bivalves and the manufactured surrogate models at a 1:1 scale (see Figure 11) were tested in a towing tank as well as under waves. The drag coefficient of live blue mussels (*Mytilus edulis*) was determined to be $C_D = 1.6$ for Reynolds numbers between 2.3×10^4 and 1.4×10^5 using towing experiments. The hydrodynamic coefficients obtained from wave tests were $C_D = 2.2$ and $C_M = 2.1$ for Keulegan-Carpenter numbers $KC < 10$. In a pursuit to better understand the differences between live mussels and surrogates in laboratory conditions, the analysis revealed that appropriate surrogates can be identified. Furthermore, a method to determine the characteristic diameter of mussel dropper lines is suggested.



Figure 11: Live mussel dropper line (LM) next to surrogate mussel dropper line 1 (SM 1), surrogate mussel dropper line 2 (SM 2) and surrogate mussel dropper lines 3 (SM 3).

3.2.2. Results

In the experiments reported herein, Reynolds numbers ranged between $Re = 2.3 \times 10^4$ and $Re = 1.4 \times 10^5$. This covers the sub-critical flow regime under steady currents and corresponds to the current velocities expected in marine environments. The wave towing tank alongside the measurement setup used in these experiments is shown in Figure 12.

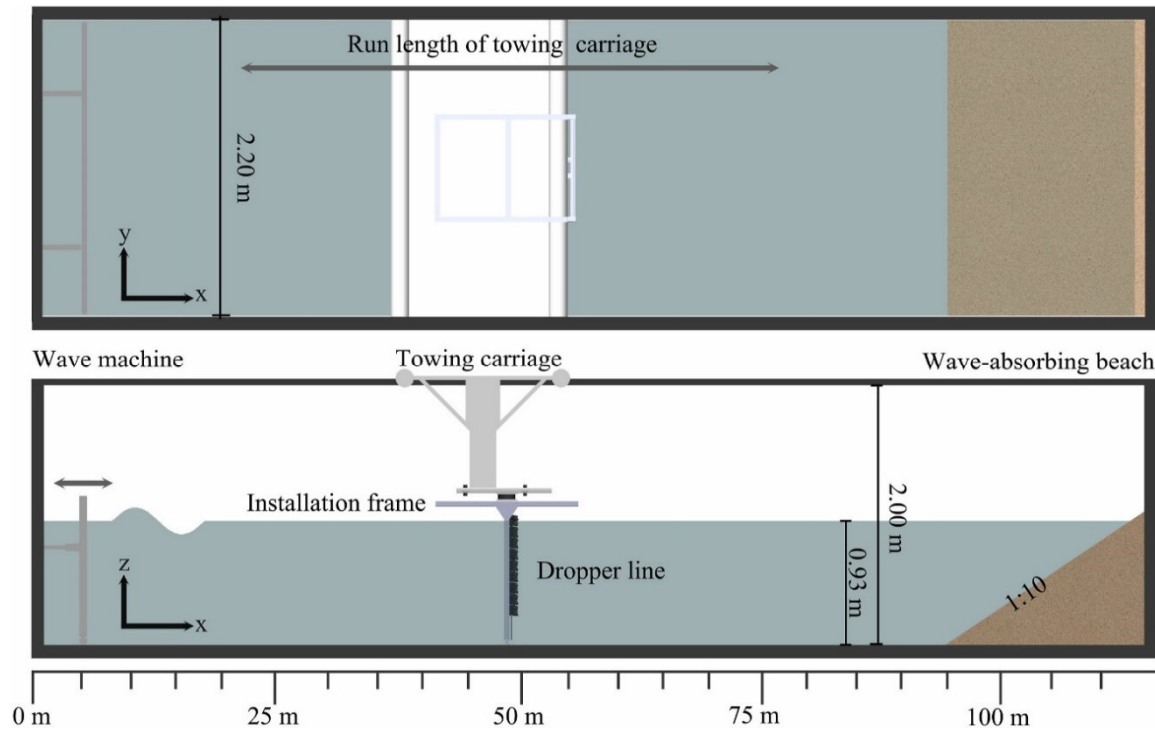


Figure 12: Sketch of the wave and towing tank in top and side view, highlighting the run length of the towing carriage as well as the position of the wave machine and dissipative beach.

The overall results regarding the steady flow experiments are shown as a scatter plot (see Figure 13). The drag coefficients are plotted as a function of the corresponding Reynolds numbers. Horizontal lines indicate the overall median values for all corresponding tests, for both live mussels and the tested surrogate models.

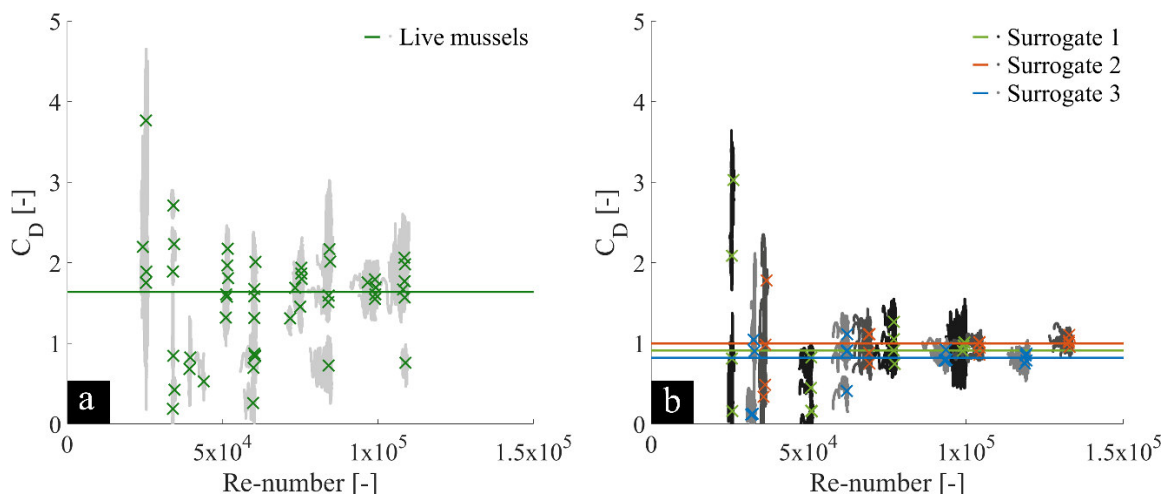


Figure 13: Drag coefficient C_D of mussel dropper lines (a) and surrogates 1–3 (b) with an indication of the median drag coefficients obtained from steady flow experiments as colored crosses.

As can be seen, the median drag coefficient of the live mussel dropper lines is $C_{D,LM} = 1.6$. The drag coefficients of the three surrogates were generally lower than the live mussel results, with median values of $C_{D,SM1} = 0.9$ for the first, $C_{D,SM2} = 1.0$ for the second, and $C_{D,SM3} = 0.8$ for the third surrogate type. The data points of each test are shown in grey scale and the median values of each test are depicted as colored cross symbols. The statistical median value was chosen as a descriptor as it is robust against outliers. Outliers present in the data contribute to the large spreading. The force contribution of the test frame was separated from the force contribution of the mussel dropper lines via a C_D -dependent mathematical adjustment of the measured forces. With the subtraction of the zero-test forces, the measured load level was reduced and this, in combination with vibrations in the velocity measurements from the rotary encoder, leads to the outlying low drag values especially for lower Reynolds numbers.

The use of three different lengths of dropper lines during testing explains the larger variance of the live mussels, in comparison to the surrogates. These live dropper lines varied in diameter and mass and exhibited natural variations in mussel density and marine growth, i.e. soft growth like algae, anemones or sponges, and secondary seeding. The inclusion of them in one dataset increases the amount of data available and the confidence in the results while slightly aggregating the variance. For Reynolds numbers larger than $Re = 6.5 \times 10^4$, a clustering of the drag coefficients is apparent as the mussel shells and the edges of the surrogate bodies promote flow separation. This behavior has been observed in the comparison of smooth and highly rough cylinders (see Chapter 2.2.1), where rough cylinders show near constant drag coefficients while the drag coefficients of smooth cylinders change significantly with Reynolds numbers (Allen and Henning, 2001). Therefore, constant values were used as an indication of the drag coefficient. Less outliers, or conversely, closely scattered data points, coincide with the increasing velocity. The relative error of the drag coefficients is largest where towing velocities are lowest, i.e. when the measured force is lowest. These current velocities around 0.1 m/s to 0.2 m/s are potentially influenced by the quality of the force measurements. Compared to realistic oceanic conditions, the range of small towing velocities is not as relevant for the design of marine aquaculture farms as the higher flow velocities; yet, for the sake of completeness are still reported here (Heasman et al., 1998). In regard to investigations pertaining to limiting biological

factors, e.g. seston concentration and initial mussel growth (Rosland et al., 2011), number of mussels in a cluster including attachment properties (Brenner and Buck, 2010), as well as hitchhiker/fouling organisms on the mussel shell (Telesca et al., 2018), further investigations for even smaller Reynolds numbers might be required.

An objective of these tests was to determine the hydrodynamic parameters under waves, i.e. oscillatory flow. With measured velocities and characteristic diameters based on the average diameter, Keulegan-Carpenter numbers ranged from $KC = 1.9$ to $KC = 8.8$. For small KC -numbers, results from steady-state flow experiments for the drag coefficient are not comparable to the results of the wave tests as the flow regime around marine cylinders is strongly inertia dominated (Denny, 1995). Drag coefficients become comparable when KC -numbers roughly larger than 30 are considered (Sumer and Fredsoe, 2006). Therefore, the use of separate coefficients for steady and oscillatory flow is recommended (Nath, 1987; Sarpkaya, 1987; Wolfram and Naghipour, 1999). To this end, Figure 14 provides an overview of the calculated drag and inertia coefficients based on the live dropper lines, and the surrogate dropper lines in oscillatory flow. These are given as a function of the KC number, along with the individual data as well as median values. The approximated median drag and inertia coefficients for the live mussels are $C_{D_{LM}} = 2.3$ and $C_{M_{LM}} = 2.1$. For the surrogates the hydrodynamic coefficients are $C_{D_{SM1}} = 2.4$, $C_{D_{SM2}} = 2.8$ and $C_{D_{SM3}} = 4.4$ and $C_{M_{SM1}} = 2.3$, $C_{M_{SM2}} = 2.9$ and $C_{M_{SM3}} = 4.9$. The mathematically best solution determined by a least-square optimization is strongly dependent on the inertia coefficient and less dependent on the drag coefficient. This results in explicit solutions for the inertia coefficient, while the solutions for the drag coefficient are prone to larger scattering. The mathematically lowest error was determined as correct. A weighted least square approximation of the Morison equation might provide more explicit results regarding the drag coefficient, but is not necessary for the small KC -numbers covered in this study due to the inertia dependence. A possible source of uncertainties in the determination of the inertia coefficient is the oscillatory movement of the dropper line under the waves as well as the movement of the live mussels themselves. In the study at hand rigid fastening as well as the short length of the dropper line prevents any major deflection which permits the use of the Morison equation. However, for tests on a larger scale a deflection of the dropper like can be expected

and needs to be considered. Similarly, the individual motion of live mussels will take a stronger effect on a larger scale. The similarity in the results between the rigid surrogates and the more flexible live mussels shows that the influence of movable mussels can be neglected for this setup.

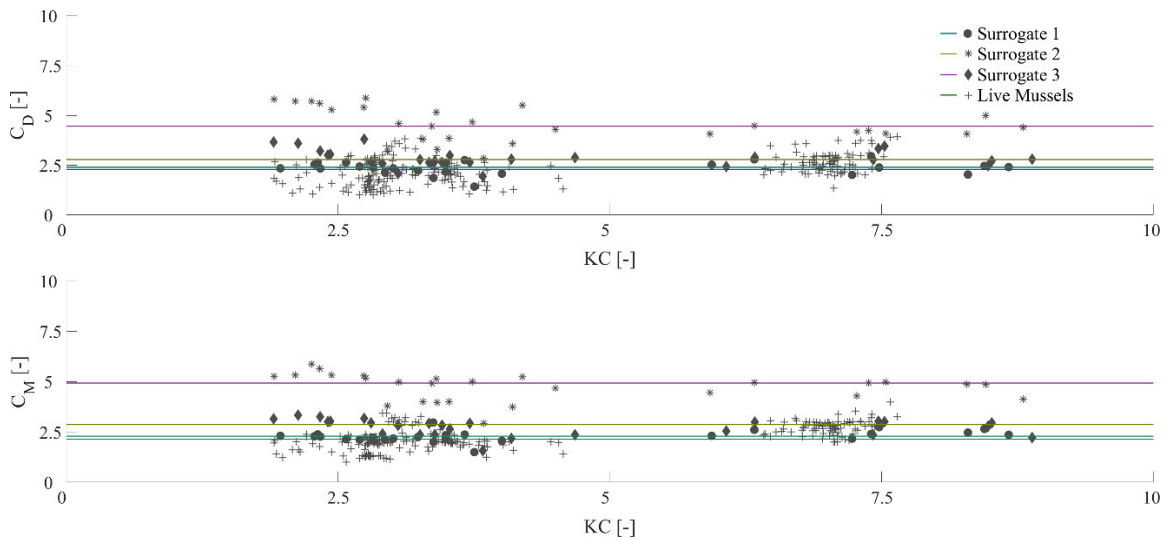


Figure 14: Drag C_D and inertia C_M values for live mussels and surrogates over Keulegan-Carpenter number KC with an indication (line) of the median value.

One of the objectives of this work was to better understand, how well live mussel specimen can be modelled hydrodynamically by developing geometrically similar surrogate models. By comparing the steady-state-, and oscillatory-based drag and inertia coefficients, a better understanding of the characteristics of the surrogates can be gained. Results show that the hydrodynamic coefficients of the surrogate bodies differ from those of the live mussel dropper lines. Specifically, the results regarding the drag coefficients of the surrogates for steady-state flow experiments are 77.8%, 60.0% and 100.0% lower for surrogate 1, 2 and 3 than the results of the live mussels, respectively. For oscillatory flow experiments, the results are 4.3%, 21.7% and 91.3% higher, respectively. The inertia coefficients of the surrogates exceed the results of the live mussels by 9.5%, 38.1% and 133.3%, respectively. Given the ranges of drag and inertia coefficients, surrogate 1 (SM 1) is proposed as the most similar and hydrodynamically suitable surrogate model of the live blue mussel dropper lines.

3.2.3. Conclusion

This work is related to the design and testing of new marine aquaculture concepts. During the planning and assessment of marine aquaculture projects, there is a need to determine the forces acting on the structural components for efficient designs. Mussel laden dropper lines form the bulk of the mass and surface area of a longline mussel farm. Therefore, comprehensive physical model tests were conducted to determine the hydrodynamic coefficients of live mussel dropper lines under laboratory conditions in the present study. This enables planners and researchers alike to quantify the influence and impact of a single dropper line and assess their combined effect in a farm. The main conclusions of this study can be summarized as follows:

- Drag tests with mussel dropper lines were conducted in a wave flume at varying velocities. Based on the results a drag coefficient of $C_D = 1.6$ is recommended for currents with subcritical flow regimes ($Re < 10^5$) and blue mussels (*Mytilus edulis*). Similarly, the mussel dropper lines were subjected to waves and a drag coefficient of $C_D = 2.3$ and an inertia coefficient of $C_M = 2.1$ are proposed for $KC < 10$.
- Simultaneously, tests with three surrogate models were carried out and their drag and inertia coefficients under steady and oscillatory flow were quantified. The aim was to obtain a simplified model, which can be used in both physical and numerical experiments without the need for keeping mussels alive or using geometrically divergent forms. The performance of the surrogates deviated from the live mussels under steady current while the performance under oscillatory flow showed a good fit. Surrogate 1, based on the average shell of the originally tested blue mussels (*Mytilus edulis*), was chosen for further testing as it showed the best fit. Likewise, to the live mussels, investigations of the surrogates with increasing Re - and KC -numbers are planned for future research.
- This study shows that the choice of the characteristic diameter has a large influence on the hydrodynamic coefficients and the findings suggest a larger characteristic diameter than former studies.
- A comparison to published studies reveals that experimental research regarding the hydrodynamic coefficients of mussel dropper lines is scarce,

since most studies focus on drag in steady flow. This study provides estimated inertia coefficients of mussel dropper lines and surrogates based on wave tests.

Applying the obtained knowledge to future research, this study provides a basis for the design and evaluation of new system designs for the cultivation of extractive species at exposed aquaculture sites. The insights gathered in this study facilitate the testing procedure for aquaculture systems and provide robust estimates for numerical approaches. This information can be used in the development of novel marine aquaculture systems in the light of the increasing demand for marine proteins.

Chapter summary 3.2:

This chapter presents an extensive investigation of the complex interdependent loads a mussel dropper is subjected to in open ocean environments.

*Drag C_D and inertia C_M coefficients of live and surrogate dropper lines under steady as well as oscillatory flow conditions, including surface gravity waves are created, evaluated, and assessed. Drag tests with mussel dropper lines were conducted in a wave flume at varying velocities. Based on the results a drag coefficient of $C_D = 1.6$ is recommended for currents with subcritical flow regimes ($Re < 10^5$) and blue mussels (*Mytilus edulis*). Similarly, the mussel dropper lines were subjected to waves and a drag coefficient of $C_D = 2.3$ and an inertia coefficient of $C_M = 2.1$ are proposed for $KC < 10$.*

*Simultaneously, tests with three surrogate models were carried out and their drag and inertia coefficients under steady and oscillatory flow were quantified. The aim was to obtain a simplified model, which can be used in both physical and numerical experiments without the need for keeping mussels alive or using geometrically divergent forms. The performance of the surrogates deviated from the live mussels under steady current while the performance under oscillatory flow showed a good fit. Surrogate 1, based on the average shell of the originally tested blue mussels (*Mytilus edulis*), was chosen for further testing as it showed the best fit.*

This study shows that the choice of the characteristic diameter has a large influence on the hydrodynamic coefficients and the findings suggest a larger characteristic diameter than former studies.

3.3. New system design for the cultivation of extractive species at exposed aquaculture sites

Landmann, J., Fröhling, L., Gieschen, R., Buck, B.H., Heasman, K., Scott, N., Smeaton, M., Goseberg, N., Hildebrandt, A. (2021); New system design for the cultivation of extractive species at exposed sites - Part 2: Experimental modelling in waves and currents. *Applied Ocean Research*; 113:102749, <https://doi.org/10.1016/j.apor.2021.102749>

3.3.1. Abstract

This work details physical laboratory tests of a new cultivation system for bivalve farming called “*Shellfish Tower*”. A side and top view of the final prototype system is provided in Figure 15. The tested 1:20 model depicted an earlier design step, consisting of a rectangular cage (2x2 m prototype scale) with a central buoyancy element and a height of 2 – 4 m. Experiments were conducted in both a current flume and a wave basin for current velocities between 0.4 – 2.2 m/s and wave heights of 1.6 to 5.0 m with periods between 5 to 14 s. The tests were conducted to prove the feasibility and functionality of this aquaculture system, which is usable for the collection and cultivation of mussel spat as well as for the grow-out of oysters, scallops, and seaweed in marine environments. Tests carried out in the current flume revealed that drag coefficients decrease with increasing current velocities and range between $C_D = 0.5 - 2.5$, while the mooring inclination increases from 12° to 84° with increasing flow velocity, which is highly dependent on the buoyancy related pretension. The examination of the mooring line tensions recorded in a wave basin showed that the largest values of snap-induced tension were up to 10 times that of the semi-static tension. The maximum-recorded tension on the system was 48 kN for a single and 89 kN for a double configuration, compared to non-snap tension values, which were in the range of 6 – 10 kN.

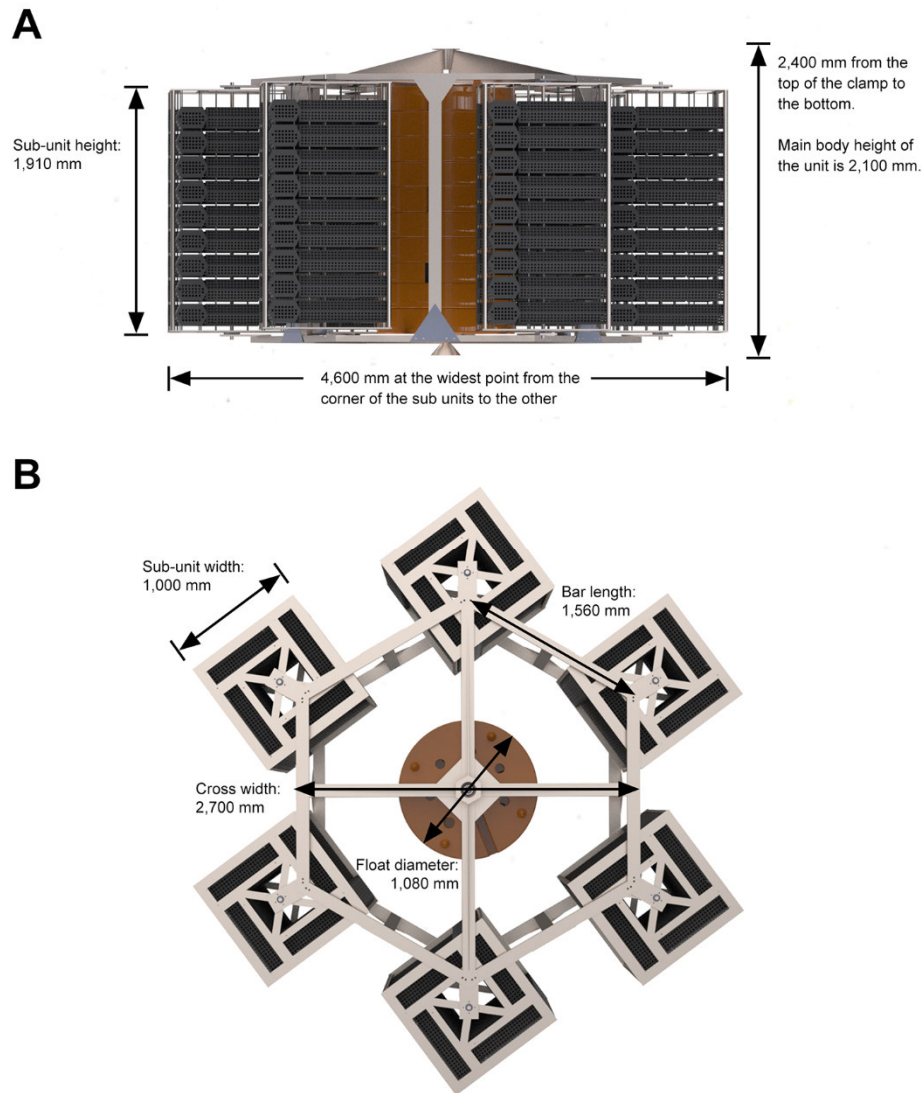


Figure 15: Side- (A) and top (B) view of a new cultivation system for bivalve farming called “Shellfish Tower” showing the prototype dimensions [©Heasman, K.].

3.3.1. Results

To measure the forces exerted on the system through current activity as well as the deflection of the cage system with a single mooring, experiments were conducted in a current flume. The experiments were carried out with a constant water depth of 0.4 m for the single cage size and 0.5m for the double cage size, respectively, which corresponds to 20 m and 25 m in prototype scale. The tested velocities were 0.1 m/s, 0.2 m/s, 0.3 m/s, 0.4 m/s, and 0.5 m/s measured at the water level where the model is situated. These current velocities correspond to velocities from 0.45 m/s to 2.24 m/s in prototype scale, which is slightly above the recorded current velocities at the prototype site. However, the larger range of velocities was chosen

as to inform the designers about the maximum deflection of the cage system. The maximum mooring forces for the single and double configuration are between 6.05 to 6.4 kN and 11.51 to 13.1 kN, respectively. Generally, the forces increase with the current velocity. With a constant model diameter across both height configurations, the current velocity is the only variable influencing the Reynolds number, which ranges from $Re = 0.8$ to $4.4 \cdot 10^6$ for the conducted tests. Figure 16 shows the drag coefficient over the Reynolds number. The determined drag coefficients range from $C_D = 0.5$ to 2.5 for $Re = 0.8$ to $4.4 \cdot 10^6$. The drag increase of the double configuration visible in Figure 16 is due to the larger surface area in comparison to the single configuration.

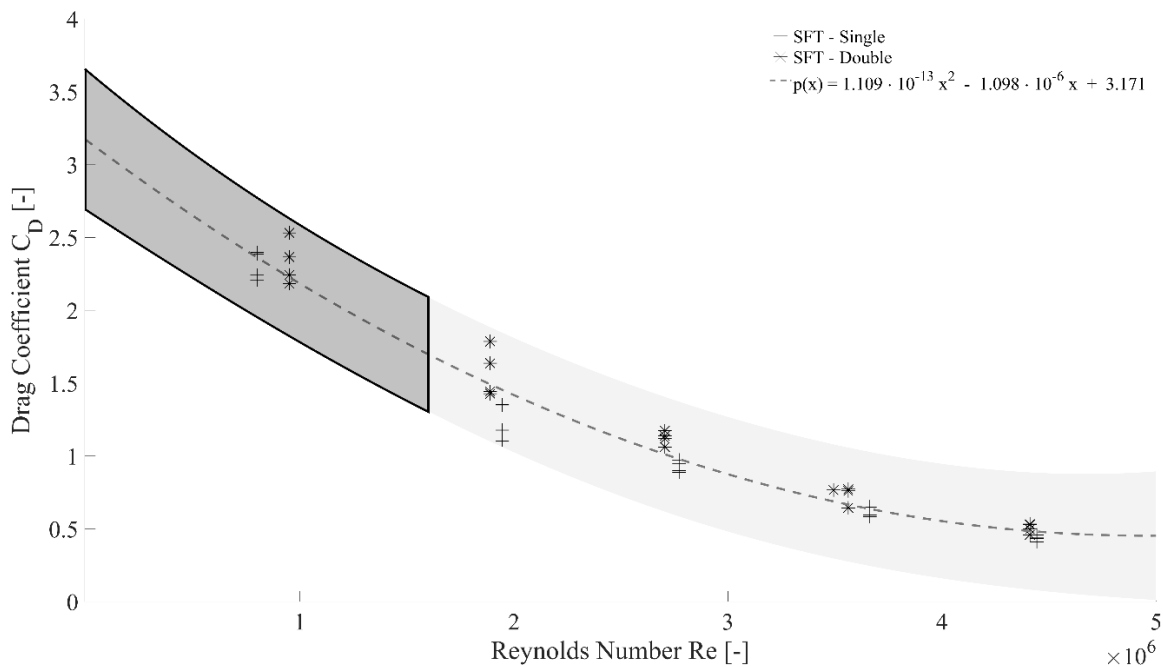


Figure 16: Current induced drag coefficient C_D over Reynolds number Re of all test cases for the single and double configuration of the *Shellfish Tower* with nonlinear fit and indication of expected Re -numbers in the Bay of Plenty (dark grey).

Experiments in the 3D-wave and current basin were carried out to quantify the forces exerted on the system by both waves and currents. By concentrating on the discrepancy between the high maximum and significantly lower median loads, a better understanding of the characteristics of the *Shellfish Tower* is gained. Figure

17 and Figure 18 show empirical cumulative distribution functions¹⁰ (ECDFs) for the single and double configurations, respectively. The ECDFs are displayed in twelve subpanels (a.1 – c.4) with differing wave parameters (columns) and current velocities (rows). The ECDFs of the varying wave directions are plotted together as the influence of wave direction was shown to be of minor relevance. Different characteristics of the ECDFs are identified for both the single and double configuration with the current as the influencing parameter. When there is no current (see a.1 – a.4 in Figure 17), the probability of occurrence for low to medium forces (2.4 – 11.9 kN) is about 70%, shown by the direct and sharp inclination of the curve. As the cumulative probability increases from 0 to 70% the normalized force only increases from the minimum of 0.08 to 0.18. These low to medium values represent the quasi-static tension within the mooring line. For cumulative probability >70%, the gradient changes drastically as the normalized force levels out towards the maximum value of one. High peak loads in the mooring system of the *Shellfish Tower* give reason for this sudden change in gradient. The steep gradient, visible for a cumulative probability higher than 95%, is especially indicative of these events. Snap loads cause these high-energy events, as the system falls slack after the previous higher wave load in the absence of a current. All varying waves without current show the same characteristic. However, an increase in wave height and wave period also leads to an increase in maximum forces and a steeper gradient is indicative of the snap loads. The highest maximum forces can thus be attributed to the snap load events. With a 1.5 m/s current present, the overall characteristics of the probability distribution differ, as the abrupt change in gradient is less prominent. With increasing periods as well as amplitudes, the shape of the ECDF changes to a more linear distribution (see b.3 and b.4 in Figure 17), which indicates a more cyclic force evolution and the absence of snap loads. These forces are representative of the dynamic loads acting on the system without the influence of snap loads. Another change in the characteristics can be observed for the single configuration and an increased current velocity of 2.2 m/s. The maximum forces are low with a small, normalized force range, which

¹⁰ The function describes the force distribution for the different test conditions over a cumulative probability and is normalized over the maximum occurring force of every test. This function is described as $\hat{E}_n(x) = \frac{1}{n} \sum_{i=1}^n \mathbf{1}(X_i \leq x)$ (Lawless, 2002) with n being the number of data points in the time series of the waves and x the value of the magnitude force.

indicates overall low forces. This is especially visible for waves with low periods (see c.1 in Figure 17). This distribution can be attributed to the submergence of the *Shellfish Tower* due to the increased current velocity. The small range of normalized forces covered is another indicator for the submergence, as the low forces are caused by the dynamic tension induced through small orbital motions.

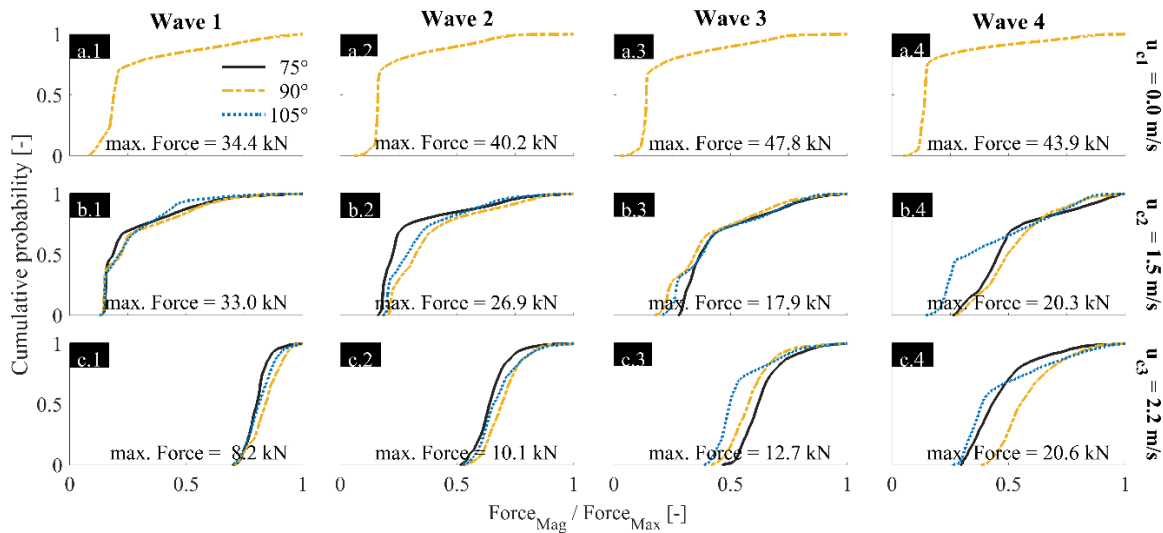


Figure 17: Empirical cumulative distribution functions of all test cases for the single configuration of the *Shellfish Tower* separated by the tested current velocity $u_{c1} = 0.0$ m/s, $u_{c2} = 1.5$ m/s and $u_{c3} = 2.2$ m/s as well as by wave 1 ($H = 1.6$ m, $T = 5$ s), wave 2 ($H = 3.0$ m, $T = 8.0$ s), wave 3 ($H = 4.0$ m, $T = 10.0$ s) and wave 4 ($H = 5.0$ m, $T = 14$ s).

The results for the double configuration (see Figure 18) differ regarding the maximum values but show similar characteristics for the probabilistic load distribution. When there is no current, the same observations as for the single configuration apply as the prominent snap loads lead to the highest maximum forces. For a current velocity of 1.5 m/s as well as 2.2 m/s the loads are reduced as the snap events are not as prominent due to pretension in the mooring line caused by the current, as well as a submergence of the structure. A near linear distribution of the ECDF can be found for all remaining cases (see b.1 – c.4 in Figure 18). The presented results in Figure 17 and Figure 18 allow for a probabilistic determination of the design load on the mooring system of the *Shellfish Tower*. Provided that the metocean conditions of a potential site are available, the data can be used for an initial approximation of the possible loads.

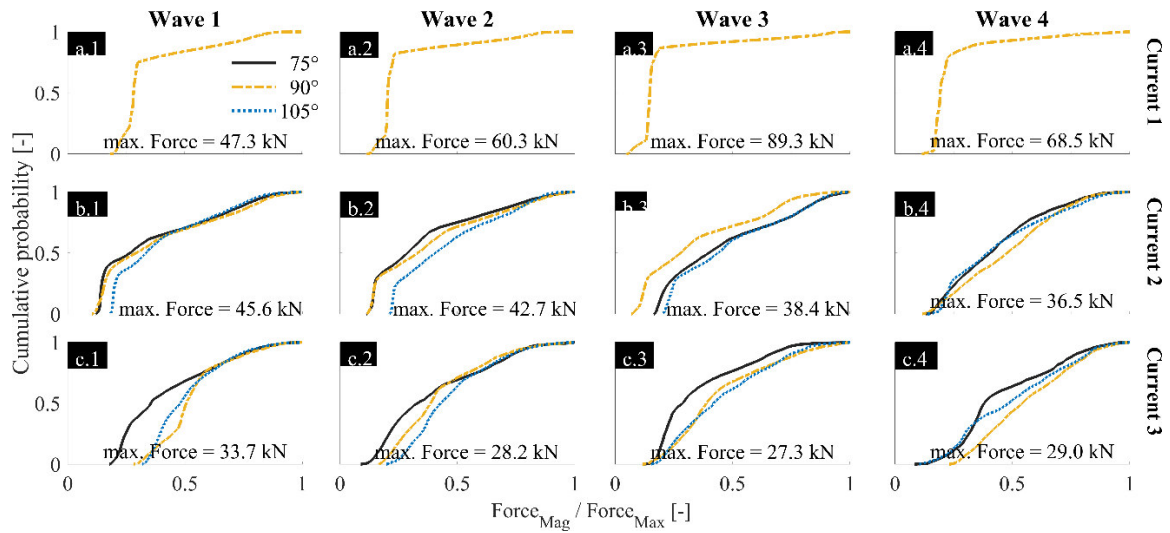


Figure 18: Empirical cumulative distribution functions of all test cases for the double configuration of the Shellfish Tower separated by the tested current velocity $u_{c1}=0.0$ m/s, $u_{c2}=1.5$ m/s and $u_{c3}=2.2$ m/s as well as by wave 1 ($H = 1.6$ m, $T = 5$ s), wave 2 ($H = 3.0$ m, $T = 8.0$ s), wave 3 ($H = 4.0$ m, $T = 10.0$ s) and wave 4 ($H = 5.0$ m, $T = 14$ s).

The high maximum loads visible in the results of the wave tests are attributed to snap loads. These are impact loads caused by the sudden tensioning of the mooring line after a state of zero tension, which mostly occurs when the mooring system is subjected to motions with large amplitudes. The duration of the snap load is instantaneous, but its amplitude can be many times greater than the maximum dynamic load as can be seen in Figure 19. Here, the force magnitude for a wave height of 4.0 m and a wave period of 10 s is displayed for two time-histories: (1) with a current velocity of $u_c=2.2$ m/s and, (2) without current. A tenfold difference between the force peaks can be observed. The main contributors are the z- and x- component of the force, whereas the y-components have a negligible influence. Without current nor waves present, the *Shellfish Tower* is floating upright, close to the water surface. During current activity, the *Shellfish Tower* is tilted, and the mooring line is pretensioned. Without the presence of waves, only the static tension needs to be considered. When the crest of the wave is at the model's center location, it is pulled upward, causing a peak in the resultant force shortly before the crest. This describes the normal, quasi-static tension for any moored system in a wave environment. During the following wave trough, the vertical forces of the orbital wave motion push the model downward. It cannot rise to its initial position and is submerged for the next wave and the mooring line falls slack. The next wave crest though causes a rapid re-tensioning and results in

the high snap load. Through the spring-like restoring force in the mooring line, the model is significantly submerged. Here, the exerted wave forces are significantly lower. Only when, as depicted in Figure 19, the third wave after the snap event propagates towards the model, has the model risen far enough up in the water column for the mooring to fall slack again due to the wave's amplitude. It instantaneously tightens again, resulting in the next snap load. These snap load events were observed for all wave heights and -periods as well as directions. Without the added pretension of the current, these events are especially dominated by high force levels, and this yields the highest maximum loads. For a current velocity of 1.5 m/s, single snap events could still be detected. No snap load events occurred for a current velocity of 2.2 m/s.

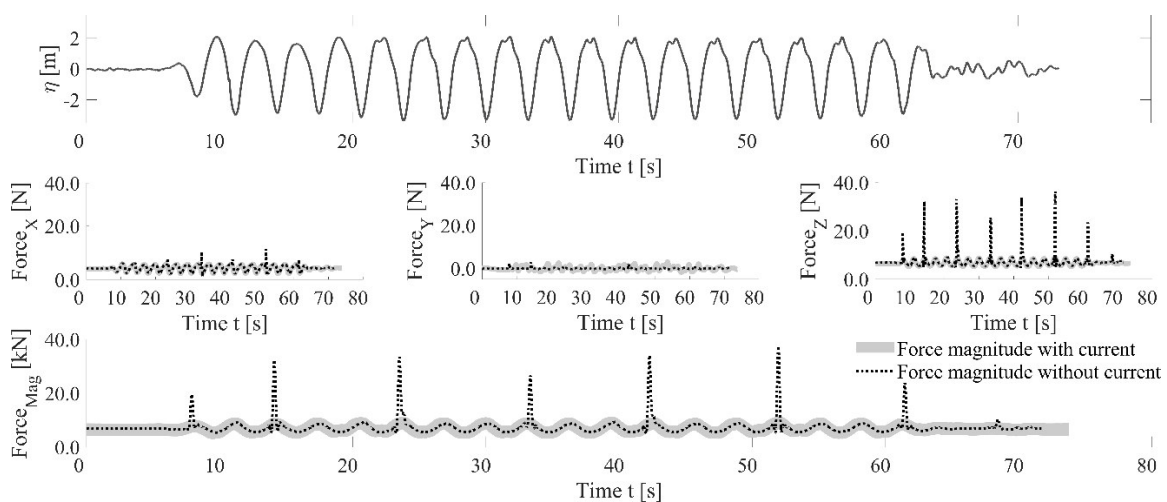


Figure 19: Comparison of force magnitude for an exemplary case (single configuration, $H = 4.0$ m, $T = 10$ s, $Dir = 90^\circ$) with ($u_c = 2.2$ m/s) in comparison to the no current case ($u_c = 0.0$ m/s) to exemplify occurring snap loads in the Shellfish Tower system. The x-, y- and z-force components forming the magnitude force are displayed.

3.3.2. Conclusion

This study assessed the feasibility and functionality of an aquaculture system usable for the collection and cultivation of mussel spat as well as grow out of oysters, scallops and seaweed in marine environments using comprehensive tests conducted under laboratory conditions. A submersible cage system was tested at a 1:20 scale at the Ludwig-Franzius-Institute 3D-wave and current basin and at the inclinable current flume of the Leichtweiß-Institute in open ocean conditions with wave heights up to 5.0 m, wave periods up to 14 s and current velocities up to 2.2 m/s in prototype scale. The main conclusions of this study are that:

- A detailed examination of the mooring line tensions, current velocities, and inclination angle from the experiments in the current flume revealed that the drag coefficients decrease with increasing current velocities from $C_D=2.5$ to 0.5 for $Re = 0.8$ to $4.4 * 10^6$, while the mooring inclination increases from 12° to 84° .
- The comprehensive examination of the mooring line tensions recorded in the wave basin showed that the largest values of snap-induced tension were up to 10 times that of the quasi-static tension. The maximum-recorded tension on the system was 47.8 kN for the single and 89.3 kN for the double configuration, compared to non-snap tension values, which were in the range of 6 – 10 kN.
- Without the added pretension of the current snap events are especially force intensive and result in maximum loads. For a current velocity of 1.5 m /s, single snap events could still be detected while no snap load events occurred for a current velocity of 2.2 m/s.
- To avoid an underestimation of the design loads, the authors recommend time-resolved, dynamic modelling of the coupled structure with the moorings to take snap loads and associated high accelerations into account during the design of open ocean aquaculture systems.

The insights gathered in this study, in conjunction with the results of (Heasman et al., 2021), provide an interdisciplinary approach to the design and evaluation of a novel aquaculture system usable in marine environments. In the light of the increasing demand for marine protein, the results of this study regarding the drag coefficient of the *Shellfish Tower* system and the probabilistic load distribution can be used as a robust estimate for the planning of future farm concepts.

Chapter summary 3.3:

This chapter presents an extensive investigation of the feasibility and functionality of an aquaculture system usable for the collection and cultivation of mussel spat as well as grow out of oysters, scallops, and seaweed in marine environments.

The comprehensive physical model study, involving current only as well as combined current-wave experiments, revealed that the drag coefficients decrease with increasing current velocities (0.4 - 2.2 m/s) from $C_D = 2.5$ to 0.5 for $Re = 0.8$ to $4.4 \cdot 10^6$, while the mooring inclination increases from 12° to 84° .

The tests showed that the largest values of snap-induced tension were up to 10 times that of the quasi-static tension. Without the added pretension of the current snap events are especially force intensive and result in maximum loads. For a current velocity of 1.5 m/s, single snap events could still be detected while no snap load events occurred for a current velocity of 2.2 m/s.

Based on these results, recommendations for the deployment, operation and maintenance of the structure are given.

3.4. Large-scale investigation of wave dampening characteristics of organic, artificial floating islands

Landmann, J., Hammer, T.C., Günther, H., Hildebrandt, A. (2022); Large-scale investigation of wave dampening characteristics of organic, artificial floating islands. *Ecological Engineering*; 181: 09258574, <https://doi.org/10.1016/j.ecoleng.2022.106691>

3.4.1. Abstract

The concept of floating vegetation-based islands (see Figure 20) for the bioremediation of aquatic ecosystems is well known. Less so, their hydrodynamic capabilities regarding the damping performance, positional stability, and water-structure interactions. To this end, physical model tests with fully organic, reed-based gabions were carried out in a large-scale facility (see Figure 21). The initial, reflected, and transmitted waves were recorded and analyzed regarding transmission and reflection coefficients. A motion tracking system was utilized to allow for an investigation regarding the motion of the artificial floating islands under waves. The results show that the artificial floating islands significantly dampen shorter waves with a wave period of $T \leq 2.25$ s. The transmission of the incident waves is reduced by 50% for the smallest wave periods ($T = 1.5$ s). The incident waves are reflected between 20 - 50% for the same wave period. The incident wave energy is dissipated by up to 85% for the smallest wave height and period ($H = 0.10$ m, $T = 1.5$ s). The comparable performance regarding more traditional floating breakwaters is discussed as well as the width of the structure as the key parameter for the layout of artificial floating islands in rivers and still waters regarding the damping performance.

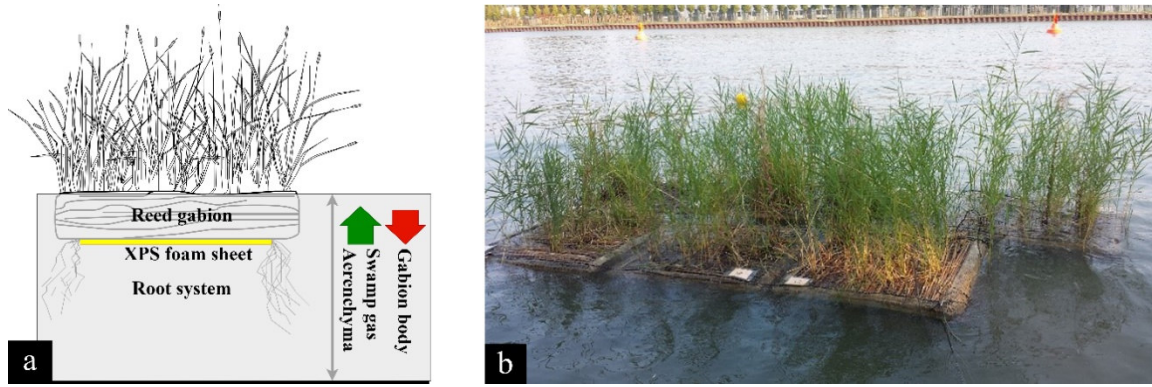


Figure 20: (a) Sketch of a single reed gabion with added XPS foam sheet as used in the experiments and the fundamental mechanisms responsible for buoyant behavior and (b) cultivated reed gabions floating in a canal.

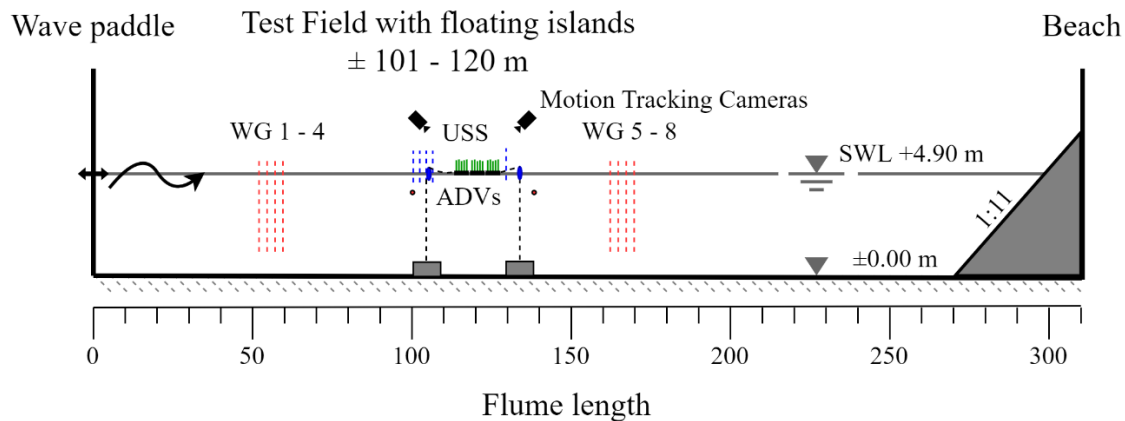


Figure 21: Large Wave Flume (GWK) with wave paddle to the right, test field with artificial floating islands in the middle and dissipative beach to the right (not to scale). The location of the wave gauges (WGs) needed for the determination of incident and transmitted wave heights is also indicated alongside the instrumentation in the test field consisting of ultrasonic sensors (USS), Acoustic Doppler Velocimeters (ADV), and motion tracking cameras.

3.4.2. Results

The identified transmission coefficients are plotted over the wave frequency since a clear dependency on the wave period is expected (see Figure 22). The results from two configurations differing in length and width ($3 \times 4 \text{ m} / 4 \times 3 \text{ m}$) are assembled, as the difference in width between both configurations (being 1.0 m) was too small to indicate significant changes in the results. Thus, the data sets of configurations 1 and 2 are merged. This can be seen in Figure 22 a. As one main result, Figure 22 show that waves with low frequencies $f < 0.35 \left[\frac{1}{s} \right]$ are transmitted almost unaffected. For waves with frequencies of $0.35 < f < 0.50 \left[\frac{1}{s} \right]$ a reduction of the transmitted wave height of around 10% is observed. For waves with frequencies

of $0.50 < f < 0.70 \left[\frac{1}{s} \right]$ a reduction of the transmitted wave height of up to 50% is observed and the scatter of C_T increases with increasing frequencies. Tests with short waves are less influenced by the reflection of the beach of the wave flume, which is why a higher number of waves was tested. The increasing number of test waves results in a higher statistical deviation. A minimal variation of wave periods caused a scatter of C_T . To reduce this scattering, C_T is plotted against the target wave period set for the test in Figure 22 b. This approach seems to be reasonable as the wave group with largest scattering (here $H = 0.1$), reveals that the ideal period is closely positioned to the density distribution of the corresponding data points (see Figure 22 c). Further, medians for all tests with same wave height and same period are calculated and sorted by their wave height along the y-axis for small wave frequencies. The statistical median value was chosen as a descriptor as it is robust against outliers. Outliers present in the data contribute to the large spreading. This is exemplified by the added boxplot for the data of the wave group of $H = 0.1$ with the largest scattering (see Figure 22 c).

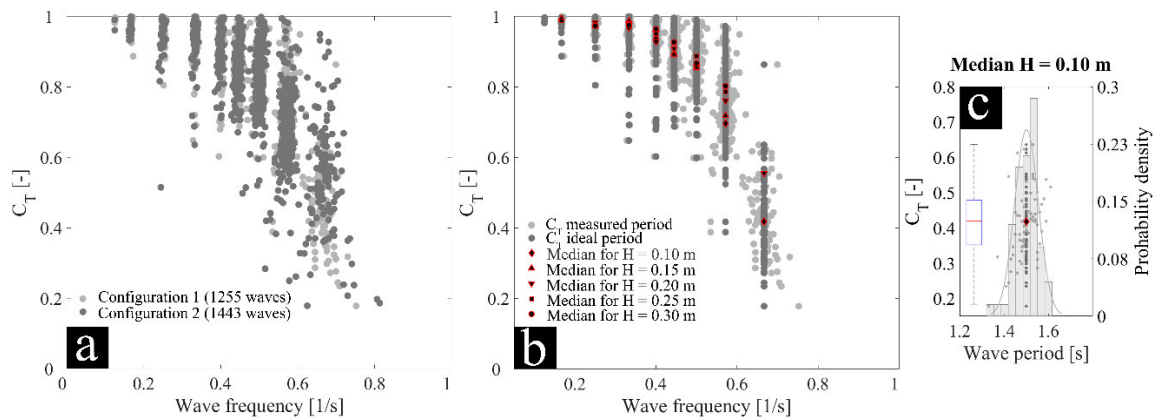


Figure 22: (a) The transmission coefficient is displayed as a scatter over wave frequency for a composite of configuration 1 (4x3 m AFIs) and configuration 2 (3x4 m AFIs). (b) The same data set with medians for tests with varying wave heights is displayed for the measured and ideal wave period. (c) A subpanel representation of the distribution for a single wave height, i.e., $H = 0.1$ m, is given together with the corresponding probability density distribution.

The results for the reflection coefficient C_R are plotted over the wave number k [1/m] in Figure 23. The wave number is defined as $k = \frac{2\pi}{L}$ [1/m] with L being the wavelength. The reflection coefficient C_R has an initial value of 0.1, as reflections in the flume are constantly present due to oblique wave reflections from the tested

structure. Waves with $k < 0.8$ [1/m] are not reflected by the structure ($C_R = 0.1$). For waves with $0.8 < k < 1.3$ [1/m] reflections increase to $C_R = 0.2$. For waves with $k > 1.3$ [1/m] a hyperbolic increase of the reflection to $C_R = 0.4$ is observed.

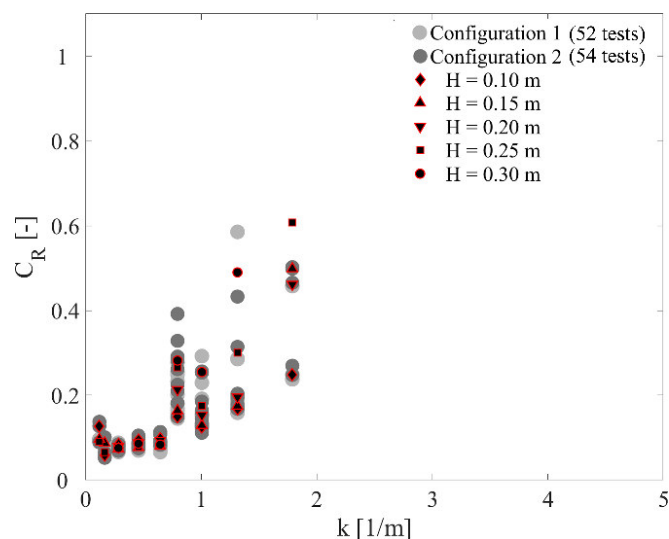


Figure 23: The reflection coefficient is displayed for a composite of configuration 1 (4x3 m AFIs) and configuration 2 (3x4 m AFIs) with the combined medians for tests with varying wave heights displayed for the ideal wave period.

These results are supported by the data from the motion tracking system as displayed in Figure 24. Here, the motion of a single reed gabion at the center is shown for all the tested wave periods and a wave height of 0.15 m. The variance in heave (z-direction) and surge (x-direction) over time for a single reed gabion at the center of the AFI system is displayed. A not-closed orbital motion for wave periods under 2.25 s is visible. The surge motion indicates a transport of the AFIs for short waves, caused by the waves reflecting of the front of the first gabions. This corresponds to the results regarding the reflection and transmission coefficients. For periods below 2.25 s, the surge motion over time increases with decreasing period to a maximum, overall deflection of over 6.0 m. The maximum is reached due to mooring-induced limitations, as the mooring is pulled back with the AFIs. The horizontal movement of the reed gabion is through-dominated for short waves as the high inertia of the AFIs leads to a not-closed orbital motion of the structure. The wave energy is lower than required to fully move the reed gabion with the wave peak. This range of wave periods matches the detected effective range regarding transmission and reflection coefficients. For longer waves with periods of 2.50 s and higher, a full orbital motion of the reed gabion is

detected. The wave energy is sufficient to lift and transport the reed gabions through the wave orbitals fully or partially. The elliptical motion for waves with periods of $T > 6.0$ s can be explained by the reflected waves of the beach, which are included in this plot. The reason for the different surge motions of the AFIs is the wave steepness, which is related to the nonlinearity of waves, too. The long wave periods are “intermediate waves”, which have a slightly increased (non-linear) wave crest and a longer extended trough than regular sinus waves. Therefore, the longer wave trough increases the time the AFIs are pulled backwards while the waves are passing the AFIs. The short waves below 2.25 s are in deep water conditions with the experimental water depth of 4.9 m. They have a more symmetric or sinusoidal profile but a much higher wave steepness. The higher the wave steepness the higher the loading on the AFI front and the higher the reflected contribution of the wave energy.

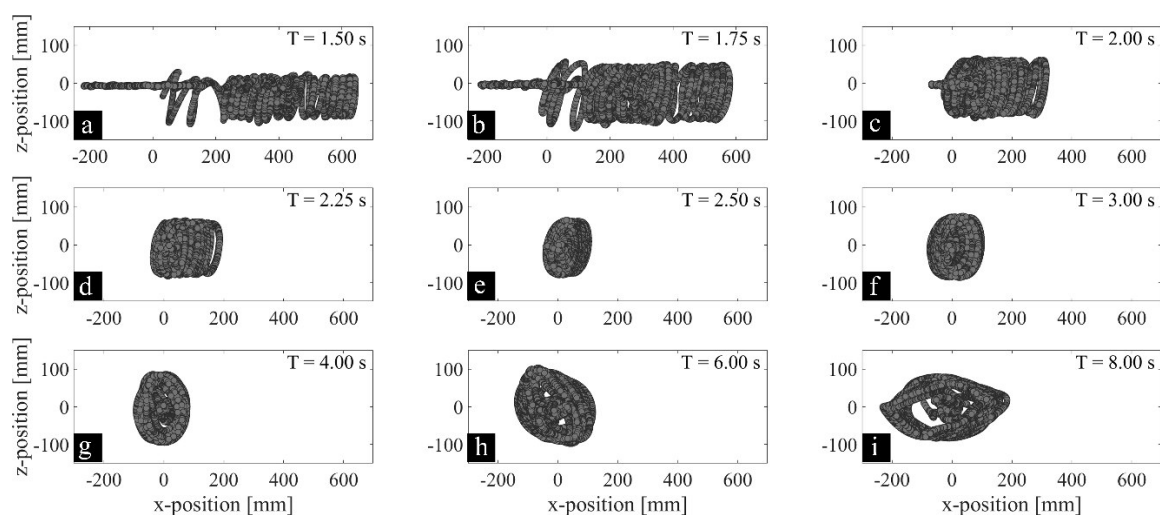


Figure 24: Motion behavior in heave (z-direction) and surge (x-direction) over time for a single reed gabion in the center of the AFIs. Every subplot (a - i) describes the motion under varying wave periods $T = 1.5$ s - 8.0 s and a constant wave height ($H = 0.15$ m) for the full test duration.

3.4.3. Conclusion

In the present study, the hydrodynamic interaction of regular waves and AFIs, which are based on the secondary wave system of vessels, are investigated. Physical model tests were conducted in a large-scale facility and following results are concluded:

- A comprehensive analysis of the hydrodynamic interaction of waves and AFIs shows a significant damping performance of the investigated AFIs for wave periods $T \leq 2.25$ s. The transmitted wave height of the incident waves is reduced by 50% for the smallest wave periods $T \leq 1.5$ s. The incident waves are reflected between 20 - 50% for these wave periods. The incident wave energy is dissipated by up to 85% for the smallest wave height and period ($H = 0.10$ m, $T = 1.5$ s). The damping performance of the structure depends mainly on the submerged depth, width, and mass of the AFIs.
- The results regarding transmission, reflection and dissipation need to be seen in connection with the hydrodynamic motion of the structure. It was shown that waves with long periods, comparable to the primary wave system of a passing vessel, lead to orbital motions of the AFIs and no significant damping. Waves with shorter periods, comparable to the secondary wave system of a passing vessel, describe not-closed orbital motions as the wave energy does not exceed the inertia of the structure and this in turn leads to wave damping. Overall, the performance of AFIs as floating breakwaters for vessel induced secondary wave systems can be seen as satisfactory.

This study takes a first step in predicting the effectiveness of AFIs as floating breakwaters. Based on these findings researchers, industry and government officials alike are enabled to better evaluate AFIs regarding their value for the protection of the shoreline and the ecosystem. AFIs are an appealing addition to existing revetment options, as they do not require additional land use and offer a variety of ecosystem services. In the context of the EU Water Framework Directive (2000), the AFIs could help to achieve a “*good ecological status*” of waterways as they are expected to lessen the morphological damage due to shipping, increase water quality and serve as an ecological stepping-stone. In the future, numerical or physical investigations are needed to determine the influence of the arrangement and configuration of the AFIs themselves, of the root system, of the wave scattering and energy redistribution due to wave-structure interaction, and of the mooring.

Chapter summary 3.4:

This chapter presents an extensive investigation of the hydrodynamics of artificial floating based islands used for the bioremediation of aquatic ecosystems.

*The comprehensive physical model study focused on **transmission, reflection, and dissipation coefficients**, as well as motion behavior of the gabion body. The results show that the artificial floating islands significantly dampen shorter waves ($T \leq 2.25$ s). The transmission of the incident waves is reduced by 50% for the smallest wave periods ($T = 1.5$ s). The incident waves are reflected between 20 and 50% for the same wave period.*

*The **motion of the system** in long periodic waves is orbital and no significant damping occurs. Short periodic waves describe not-closed orbital motions as the wave energy does not exceed the inertia of the system. Thereby, a motion-based indicator for the wave attenuation is identified.*

Based on a comparison to traditional, floating breakwaters the width of the structure is identified as the key parameter regarding the wave attenuation.



4. Discussion

This chapter utilizes the analysis and results presented above (see Chapter 3) and combines them with the gaps of knowledge identified in Chapter 2.4. The gaps of knowledge identified through the literature review show a:

- ❶ lack of information regarding the hydrodynamic coefficients of bivalve aquaculture components in steady and oscillatory flow
- ❷ lack of guidance as to how the complex surface of mussel dropper lines should be modelled
- ❸ lack of understanding regarding system motion and load evolution in bivalve aquaculture

This section summarizes the gathered insights and further encapsulates the limitations of the presented studies and the general applicability of the gathered insights to the real world. Additionally, new insights are complemented by a shortened and adapted version of the manuscripts' discussions.

4.1. Synopsis

Scarce information regarding the hydrodynamic coefficients of bivalve aquaculture components in steady and oscillatory flow identified in Chapter 2.1.3 is addressed by the results from the second manuscript (see Chapter 3.2).

Based on the experiments in steady flow, a C_d -coefficient ($C_d = 1.6$) for blue mussels (*Mytilus edulis*) for subcritical flow regimes ($Re < 10^5$) is recommended. The presented drag coefficient matches existing data (see Table 2) while it expands on the range of before assessed Reynolds numbers. Differences in results can mainly be attributed to the manner of data acquisition in the existing research. Raman-Nair and Colbourne (2003), Raman-Nair et al. (2008), Stevens et al. (2008) and Knysh et al. (2020) based their reported drag coefficients on assumptions in relation with ultra-rough cylinders. Xu et al. (2020) conducted numerical experiments with mussel dropper lines without a validation through physical tests. Plew et al. (2005), Plew et al. (2009), and Gagnon and Bergeron (2011) conducted physical experiments with dropper lines. In these experiments, a source for the differences are biological factors, e.g. stage of mussel growth, mussel density along the length of the dropper line, the number of hitchhiker/fouling organisms on the mussel shell. The results regarding the drag coefficient in steady flow presented here are the most exact results available to date and are recommended for future numerical studies and design approaches.

Regarding oscillatory flow, the hydrodynamic coefficients of mussel dropper lines have not been experimentally determined before; only now have these become available through the work reported herein. For $KC < 10$ a drag coefficient of $C_D = 2.3$ and an inertia coefficient of $C_M = 2.1$ are proposed for blue mussels (*Mytilus edulis*). While this only covers a very limited range, it has been demonstrated that an experimental determination of the hydrodynamic coefficients of mussel dropper lines in oscillatory flow is possible. A larger scale test in oscillatory flow has also been conducted in cooperation with Gieschen et al. (2021). Pending analysis of gathered data will provide hydrodynamic coefficients for a larger range of KC -numbers (10 - 380). This will greatly improve the parameter range into more relevant offshore regimes and will enable engineers to predict the forces on bivalve offshore aquaculture systems more accurately. Photographs relating the scale of the experiments in the Large Wave Flume in

Hannover, Germany are shown in Figure 25. They also show that the surrogates, of which the development was described in Chapter 3.1, were tested in in these large-scale experiments.



Figure 25: (a - f) Depiction of a single wave ($H = 0.8$ m, $T = 6$ s) passing two blue mussel (*Mytilus edulis*) specimen and the SM 1 surrogate. The wave peak (d) passes the live blue mussel dropper lines, and the surrogate, with a length of 2.0 m each, which were mounted to stainless steel wires connected to a concrete block at the bottom and a steel beam at the top of the flume (g) in a distance of approximately 97 m from the wave machine.

The manuscripts presented in Chapter 3.1 and 3.2 start to address the lack of guidance as to how the complex surfaces of mussel dropper lines should be modelled. They show that by using the Abbott-Firestone curve as a surface descriptor for an arbitrary natural structure surrogate structures can be created. Furthermore, by comparing the steady-, and oscillatory flow-based drag and inertia coefficients, a better understanding of the characteristics of the surrogates was obtained and SM 1 was proposed as the most similar and hydrodynamically suitable surrogate model of the live blue mussel dropper lines.

The analysis conducted in Chapter 3.2 showed that the characteristic diameter has a major influence on the force evolution of dropper lines. The determination of drag and inertia coefficients, on the other hand, is a challenging task since mussel dropper lines are natural structures with uneven growth, cavities, crevasses, and protrusions. They consist of hard growth composed of mussels of varying size

overgrown with soft growth consisting of different algae, anemones, sponges, and kelp species. To provide a better understanding of the importance of the chosen characteristic diameter, alternative approaches used in literature have been compared to the average diameter used in the manuscript. The use of 3D-scans and the average diameter for experiments under laboratory conditions as the most explicit representation of the characteristic diameter is recommended.

A schematic view of soft and hard growth on a dropper line is shown in Figure 26. This visualizes the inherent difficulties in determining the correct characteristic dimensions of any object exposed to nature. The combined influence of soft and hard growth on dropper lines could not experimentally be explored in this thesis. This would have required a more careful rearing of the specimen and the involvement of biologists, which was not foreseen at that early stage. With a mixture of soft and hard growth, the drag coefficient varies significantly from those with purely soft or hard growth. Through comparisons with research regarding marine growth (see Chapter 2.2.1) and biofouling some insights were gathered. The soft growth likely has a large influence on the boundary layer development as shown by Schoefs et al. (2022). Experiments by Theophanatos (1988) showed that the drag coefficient increased when soft growth was included. It was shown that it was about 1.4 times greater for fully kelp covered cylinders compared to cylinders fully covered with a single layer of mussels. The soft growth was not recreated during the modelling of the surrogates (see Chapter 3.1) which were made of smooth 3D-printing material. The live dropper lines, which were taken from in-situ cultures, had considerable soft growth (see Figure 11). Mussels, i.e. hard growth, form the main component of the dropper lines and are strongly affected to change as the mussels mature. The surface roughness increases as the outcropping mussels grow to a harvestable size, i.e. from 2.0 to 10.0 cm. The mass increases, which also results in a force increase. Simultaneously, the drag coefficient increases with the surface roughness and diameter and thus drag loads on the structure become more influential. This is another reason for the differences between the living mussels and the abiotic surrogates, as only a macroscopic roughness was incorporated in the models, e.g. the individual growth stages of single mussels were not considered. Therefore, with soft growth and natural variations, the surface roughness of the live mussel dropper lines was higher compared to the surrogate models. The increased roughness affects various aspects of the flow around the

mussel dropper lines such as hydrodynamic instabilities, i.e. vortex shedding, the interaction of vortices, the separation angle, the turbulence level as well as the vortex strength. Therefore, it can be assumed that the increased drag of the live mussels in the steady-state experiments is due to an increase in dropper diameter caused by the additional soft growth and a larger roughness. This is supported by the results of Wolfram and Theophanatos (1990) regarding the effects of marine growth on cylinders as well as more recent numerical studies by Xu et al. (2020). The fact that the lowest deviation from the resulting force coefficients of the live mussels can be seen by the second surrogate (SM 2), where soft growth was incorporated by the 3D-scanning further supports this assumption (see Figure 9).

In conclusion, it can be assumed that the differences regarding the hydrodynamic coefficients between the living mussels and abiotic surrogates are mostly due to natural growth on the living mussels, as well as and variations in surface roughness, flow regimes and referential frontal areas. While steady flow conditions are not adequately reproduced, a satisfactory representation of the live mussel dropper lines, considering oscillating flow conditions, is found.

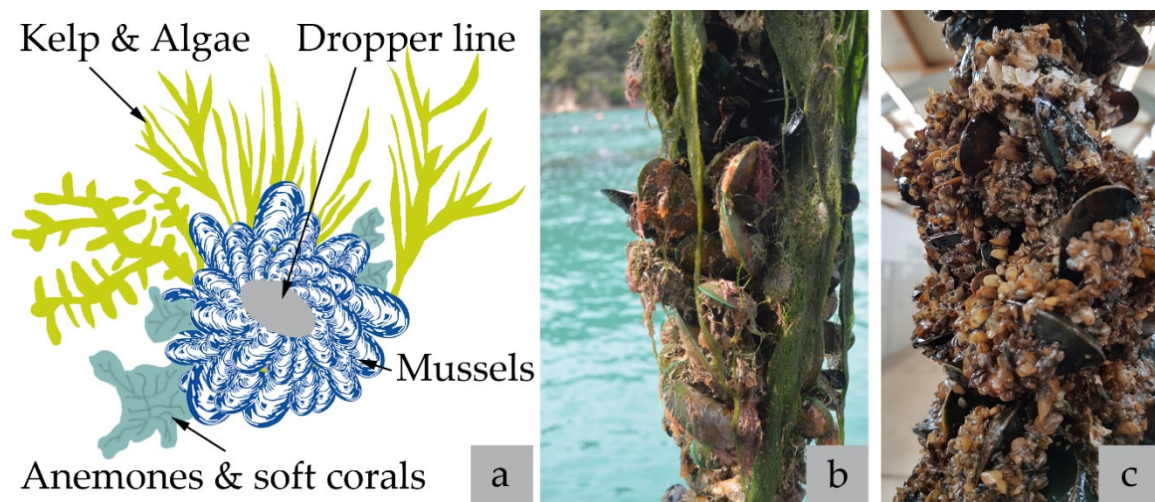


Figure 26: Schematic view of soft and hard biofouling on a dropper line (a) with real-life examples of green-lipped mussels (*Perna canaliculus*) [©Goseberg, N.] (b) and blue mussels (*Mytilus edulis*).

The lack of understanding of system motion and load evolution in bivalve aquaculture was addressed by the manuscripts presented in Chapters 3.3 and 3.4. Especially, the importance of snap loads observed in model tests, with snap-induced tension up to 10 times the quasi-static tension, was highlighted. Furthermore, the wave attenuation potential of floating structures with submerged

canopies was addressed and a comprehensive analysis of the hydrodynamic interaction with waves in a large-scale facility showed a significant damping performance of the investigated structures for wave periods $T \leq 2.25$ s.

A good understanding of the hydrodynamics and structure's response is crucially important for the design of any structure in open ocean environments. Snap loads are a known problem for the established oil and gas industry and pose a major challenge to robust mooring design for the growing aquaculture industry as was shown in Chapter 2.3. To mitigate the risk of snap loads on aquaculture systems such as the *Shellfish Tower* (see Chapter 3.3) an increased safety factor would minimize the risk of system failure and ensure longevity in high energy, open ocean conditions. A high flotation to mass ratio of a floating aquaculture system increases the resistance to the downward-oriented component of the orbital wave motion and increases the station-keeping capability. However, if a sufficiently large wave amplitude causes the mooring to slacken, then, as the orbital wave motion induces an upward force on the system, the additional flotation will combine with the water flow, increasing the speed of the system rising in the water column, resulting in higher snap forces. Conversely, a lower flotation to mass ratio (because of less flotation or higher shellfish biomass) will result in the mooring falling slack more easily as the system is driven down with the orbital wave motion. As the wave progresses and the downward motion changes to an upward motion, the speed of the system will be reduced as the combination of flotation force and water flow are not as great, reducing the snap force. The mooring system has a major influence on the load evolution and needs to be considered during the design stage to minimize stresses on the system.

For oyster farming, where periodic movement of the oysters within their basket prevents the oyster shells from growing and adhering together and increases the shell thickness and strength, the movement caused by the snap load event may prove to be disruptive to the grow-out of the product, with shell damage and loss of the oysters. In particular, the newly formed distal part of the shell could break off when the oysters are knocked together (Newkirk et al., 1995; Pogoda et al., 2011). The external appearance of the oyster shell plays an important role in the "half-shell-market" (Mueller Loose et al., 2013) for the consumer (Matthiessen, 2001), so any damage will reduce the value of the oyster. The same applies to the

culture of mussels as they could be shaken off their substrates. Although the choice of the longline in its surface condition could improve the adhesion of byssus plaques (Babarro and Carrington, 2013; Brenner and Buck, 2010), the risk of biomass reduction through snap events can have both ecological and economic consequences. With some macroalgae (e.g. family *Laminariales*) a tip loss occurs seasonally. This could be increased by snap events, which could lead to a lower biomass at harvest. To negate these snap loads aquaculture system should be repositioned deeper in the water column to avoid the damages caused by the snap event. By placing the system in deeper water, it may be positioning the system below the optimal availability of phytoplankton and organic particulate matter on which the shellfish feed. Prior to the deployment of any aquaculture system, the site-specific factors should always be examined. If the phytoplankton density and quality allow, the system can be installed deeper in the water column where the orbital wave is smaller leading to less forces and therefore to a low or non-existent snap load phenomenon. The importance to submerge the system during storm events has been highlighted by Kim et al. (2014). If this is not possible, technical improvements that prevent or greatly reduce snap load events should be considered. These could include the installation of shock absorbing elements, such as spring-like elements, rubber structures or other components that buffer the abrupt forces (Gordelier et al., 2015).

Alternatively, floating breakwaters could be installed. An investigation by Dong et al. (2008) showed that these may be adopted for aquaculture engineering in deep-water regions to provide effective protection for aquaculture systems. As identified in the study presented in Chapter 3.4, the breakwater width is a main parameter regarding wave attenuation. This has been shown in a variety of studies concerning wave dissipation. From offshore aquaculture (Plew et al., 2005; Zhu et al., 2021, 2020) over large floating structures and breakwaters (Zhang et al., 2020) to vegetation and natural phenomena (Lei and Nepf, 2019; Villanueva et al., 2021) it is shown that the width of any marine structure directly affects its ability to attenuate waves. The wider the breakwater systems are, the better their potential to dampen waves is, as the wave energy necessary to lift the structure is increased. This also becomes apparent from the results presented in Chapter 3.4, which similarly show that the wave attenuation is mainly a function of the breakwater width to incident wavelength ratio with a dependence on the relative depth and

the dissipation mechanism targeted by the individual system. Furthermore, the roots of the observed structure (see Figure 20) act as suspended canopies, i.e. porous obstacles that are suspended from the water surface with a gap between the canopy and the bottom of the water. These suspended canopies are known to increase the flow resistance while simultaneously reducing the flow speed within the root system as was shown in Chapter 2.3. As shown by a number of studies, suspended canopies alter the ambient flow and thus decrease current speeds and directions within and below the canopy (Blanco et al., 1996; Plew et al., 2005). The effect has especially been observed in regard to net-based and longline aquaculture (Bi et al., 2015; Zhao et al., 2015, 2013; Zhu et al., 2021) which present a promising option to attenuate waves while at the same time providing a sustainable source of nutrition. The effect of the canopies is also dependent on the density of the suspended system, as it increases the effective depth of immersion and the inertial force due to the enclosed water within the water column, which acts as added mass. Generally, the consideration of the suspended system further reduces the wave height due to increased drag forces and amplified wake formations around the structure, which affects the velocity profile. Similar to emergent canopies, wave attenuation is influenced by the vegetation. This indicates that the submerged canopies provide further wave dampening potential.

4.2. Limitations

Due to limitations of the experimental facilities, there are potential errors related to the model setup, equipment, and instrumentation used within this thesis. This section will address the potential measurement and analysis uncertainties that existed throughout the experiments.

Throughout the studies outlined in Chapters 3.1 and 3.2, only one species of mussels (blue mussels - *Mytilus edulis*) and the corresponding surrogate were used. It was chosen as blue mussels are a prime species used in aquaculture. Blue mussels have been proven to be reliable for industrial purposes due to their high economic value, a wide distributional pattern and their ability to withstand wide fluctuations in salinity, desiccation, temperature and oxygen levels (Favrel and Mathieu, 1996; Gosling, 2015; Gren et al., 2018; Jansen et al., 2016; Petersen et al., 2014; Schernewski et al., 2019, 2012). However, other species like the green-lipped mussel (*Perna canaliculus*) or the Mediterranean mussel (*Mytilus galloprovincialis*) are also harvested in aquaculture systems. While displaying similar characteristics, size differences are apparent. The shells of fully-grown blue mussels are on average 10 cm long, shells of fully-grown green-lipped mussels can reach a length of up to 24 cm and shells of fully-grown Mediterranean mussels a length of up to 12 cm (Gosling, 2015). Size differences heavily influence the choice of the characteristic diameter (see Chapter 3.2), which has a major influence on the determination of the forces acting on the dropper lines. Considering the lack of dedicated studies, the typical averaged diameter of fully grown mussel dropper lines can be assumed as approximately 0.15 – 0.2 m (Xu et al., 2020). Detailed work regarding species-specific force coefficients for mussel dropper lines used in aquaculture is missing.

It was shown that the AFC used in the creation of the surrogates (see Chapter 3.1) is applicable in 2D and 3D and additionally provides information on material-free and material-filled volumes. However, even though the AFC is appropriate for a non-ambiguous characterization of an existing surface, the reproduction of a certain surface based solely on the AFC is ambiguous. This can be seen in a comparison of the second and third surrogate concepts SM 2 and SM 3 (see Figure 11). SM 2 represents a close fit to the AFC, while SM 3 represents the most exact results and a direct fit to the AFC. This exemplifies that similar AFCs can be used

to generate a variety of surrogate structures. For this reason, additional characteristics of a surface that relate to a certain AFC need to be considered. This could be the number of break-off points along the structure or the solidity of the profile in flow. Eventually, energy dissipation and wake generation along the structure need to be better understood to find adequate additional surface descriptors. As a first step though, the developed surrogates are a promising starting point towards the creation of a mussel equivalent model. This can be used for research regarding the behavior of suspended long-lines in current and wave conditions.

During the experiments in the medium wave flume in Hannover, Germany, the live dropper lines, and surrogates were fastened at the top and bottom to the holding frame of the drag carriage (see Chapter 3.2). Under operational conditions, this is not the case. Dropper lines are suspended from the backbone without a support at the lowest point (see Figure 2). The fastening was methodically necessary to obtain the relevant data regarding the hydrodynamic coefficients without introducing further parameters such as the yaw angle. Load evasion by a reduction of the area in flow can be suspected. However, the author assumes that the forces on the 1 m long sections of mussel dropper line are accurately captured and can be used as a conservative estimate. This is because whole dropper lines, which are being suspended 15 m or more below the surface without a support at the lower end, have a significant mass which render them less mobile than the 1 m long sections of mussel dropper line investigated. Additionally, other aspects that would influence the loads on mussel dropper lines examined in this study, such as the density of fresh water vs. salt-water and temperature gradients, were also not accurately captured. Their effect is suspected to be marginal.

During the experiments in the 3D-wave and current flume in Hannover, Germany, as well as in the inclined current flume in Braunschweig, Germany, only one mooring system (single-point) was considered for the novel aquaculture system *Shellfish Tower* (see Chapter 3.3). As shown in several studies, the mooring system has a large influence on the forces and motion of floating aquaculture structures (Cheng et al., 2020; Feng et al., 2021; Zhao et al., 2019). While the forces were accurately captured for the chosen system and mooring configuration, different results can be expected for other mooring designs.

In the experiments with the floating, natural islands in the Large Wave Flume in Hannover, Germany, presented in Chapter 3.4 two configurations were used. The floating islands consisted of blocks of 3×4 reed gabions and as blocks of 4×3 gabions, i.e. the length of the structure facing the waves changed between 4 m and 3 m while the width changed between 3 m and 4 m. The width of the structure was identified as a main parameter for the wave attenuation capacity by literature (Dai et al., 2018; Sawaragi, 1995), but the tested width was not sufficient to reveal its effect. Due to the limited number of reed gabions available, 18 in total with 2-year growing periods, no alterations could be made. Thus, no insights in this regard could be obtained.

For the same experiments, the buoyancy for the reed gabions, naturally provided by swamp gas underneath each gabion, was simulated by panels of extruded polystyrene (XPS) hard foam to ensure floating stability throughout the experiments. The XPS-panels were chosen due to their robust, water-repellent characteristics and the comparable buoyancy of the trapped swamp gas. This allowed for replicable conditions during the experiments, but it leads to the neglect of the influence of the submerged root system due to coverage. As shown in Chapter 2.3, submerged canopies have an influence on the wave attenuation potential of any floating structure. The inclusion of the submerged root system would increase the wave attenuation.

Certain natural parameters were not fully accounted for in the same experiments. *Phragmites australis* (Common reed) was used during the experiments as it is a cosmopolitan grass and often the dominant species in whichever ecosystems it inhabits with high intraspecific diversity and phenotypic plasticity, an extensive ecological amplitude and a great capacity to acclimate to adverse environmental condition (Eller et al., 2017; Engloner, 2009; Marzec et al., 2018; Soukup et al., 2002). During the two-year growing period, the plants did not grow to their maximum natural heights and thus their parameters are not directly comparable to those of *P. australis* plants in their natural habitat. However, as no extraction of fully grown plants with root systems for the use in floating gabions is possible the author believes that the best efforts were undertaken to ensure realistic conditions for experiments with a focus on the hydrodynamics of reed gabions. Furthermore, the cultivation method, the gabion bodies as well as the cutting back of the above-

ground plant parts had an influence on the vegetation parameters. The above-ground parts had to be cut back for the experimental performance in the wave flume so that the motion could be recorded correctly. Thus, a fully grown vegetation piece was not the subject of the investigation. Rather overgrown gabion bodies were used. Modeling would still have to consider the seasonal aspect of vegetation development, because aquatic plants have a typical phenological sequence of the growing seasons. Before conducting the research in the wave flume, culm densities ($188 \text{ pcs} \pm 95$), height of above-ground culms ($87 \text{ cm} \pm 9$) with a cover ratio of 38%, and root lengths ($18 \text{ cm} \pm 5$) were recorded. This indicates a young, growing stock. In comparison, naturally, fully grown plants have smaller culm densities with fewer, larger plants reaching heights of up to 6.0 m and denser root systems.

4.3. Application

The application of the research presented within this thesis, with the long-term objective to help design safe and economic bivalve aquaculture systems, is possible to interested parties in research and industry alike.

The presented research can be applied to interdisciplinary concepts. As stated by the FAO (2020) (see Chapter 1.2), researchers and fish farmers are exploring alternative and innovative adaptation practices for increasing aquaculture production while avoiding adverse impact on sustainability. In this regard, the approach of integrated multitrophic aquaculture (IMTA) is seen as an environmentally friendly system for sustainable, future growth in aquaculture. IMTA describes the co-cultivation of foraged species with extractive species that can feed on the effluents of the former. By integrating multiple species from different trophic levels excess nutrients can be used and phenomena such as local eutrophication and algal blooms can be avoided (Anderson et al., 2008; Beman et al., 2005; Hu et al., 2010; Sorokin et al., 1996). Through the implementation of such a concept, the sustainability of aquaculture can be increased in the future (Buck et al., 2018; Chopin et al., 2001; Neori et al., 2004; Reid et al., 2020). Bivalves are seen as a major contributor to IMTA systems as they are filter feeders who extract organic matter from the water for their growth and therefore need no further feed. The production of mussels and other species is positively correlated. Co-cultivation of bivalves increase the yield and biomass of kelp (Hargrave et al., 2022). While in turn, the mussel production is higher in farms located less than 1000 m away from fish farms (Camelo-Guarín et al., 2021). The IMTA concept can be coupled with the multi-use of offshore areas where novel marine production systems can be envisioned. This multi-use is also described as “Blue Growth” and is related to the creation of economic activity offshore, while maximizing the efficient use of the available sea area by combining industries (Dalton et al., 2019). An integration of bivalve aquaculture into existing offshore structures, such as wind parks, is possible. There, the existing structures can act as a hub for the operation and maintenance of the other industries (Buck, 2004). To show that mussel aquaculture is an appealing commercial model for increased returns in offshore wind farms van den Burg et al. (2017) developed a business case for mussel aquaculture in the North Sea. They conclude that the economic

performance withstands considerable changes in cost and revenues and based on a risk assessment, formulate mitigation strategies which negate high risk scenarios. This is supported by Jansen et al. (2016), who based on macro-evaluation criteria conclude that offshore bivalve aquaculture is achievable both in single- and multi-use farm systems. Buck et al. (2010) note that the production of mussels using the longline technology in the German North Sea is profitable enough even assuming significant cost increases. However, if the existing vessels and equipment for operation and maintenance of the wind farms can be used, the risk is further reduced and profits increase. Di Tullio et al. (2018) also report on the sustainable use of marine resources through offshore wind and mussel farm co-location. They introduce an index for multi-use sustainability to do a first order selection of the most promising areas, which can be specifically studied in a second order approach based on local field data. The research presented in the first two manuscripts (see Chapters 3.1 and 3.2), which focuses on the hydrodynamic coefficients of mussel dropper lines and their surrogates, can directly be used by engineers to model and design the forces acting on bivalve aquaculture systems. Hydrodynamic coefficients as well as recommendations regarding the characteristic diameter needed to solve the Morison equation (1950) (see Chapter 2.1.1) are made available through the studies included in this thesis. The information can be incorporated into numerical models to estimate the forces acting on longline systems. This allows for the correct design and selection of system components, like buoys, mooring lines, connectors, and anchors. Furthermore, it facilitates the rapid development and testing of novel systems before physical or prototype experiments need to be conducted.

The experiments with the *Shellfish Tower* (see Chapter 3.3) led to a direct application as a number of prototype structures have been successfully deployed since 2019 (Heasman et al., 2021). The deployment process and underwater images at the Ōpōtiki site, New Zealand can be seen in Figure 27. The system, which has an intended lifespan of up to 20 years, can be positioned and operated at variety of depths to avoid highly energetic environments and maximize productivity. First results with the prototype indicate that the capture of spat and grow-out of oysters are economically viable uses for the *Shellfish Tower* (Heasman et al., 2021). The data gathered during the experiments (see Chapter 3.3) and prototype tests both show the occurrence of snap loads which suggests that more experience regarding the

mooring design and correct placement in the water column is necessary to avoid these load peaks in the future.

In conclusion, to achieve the SDGs set by the UN, future aquaculture operations require new, more holistic views regarding interdisciplinary problems, which combine hydrodynamic, ecological, and societal issues.

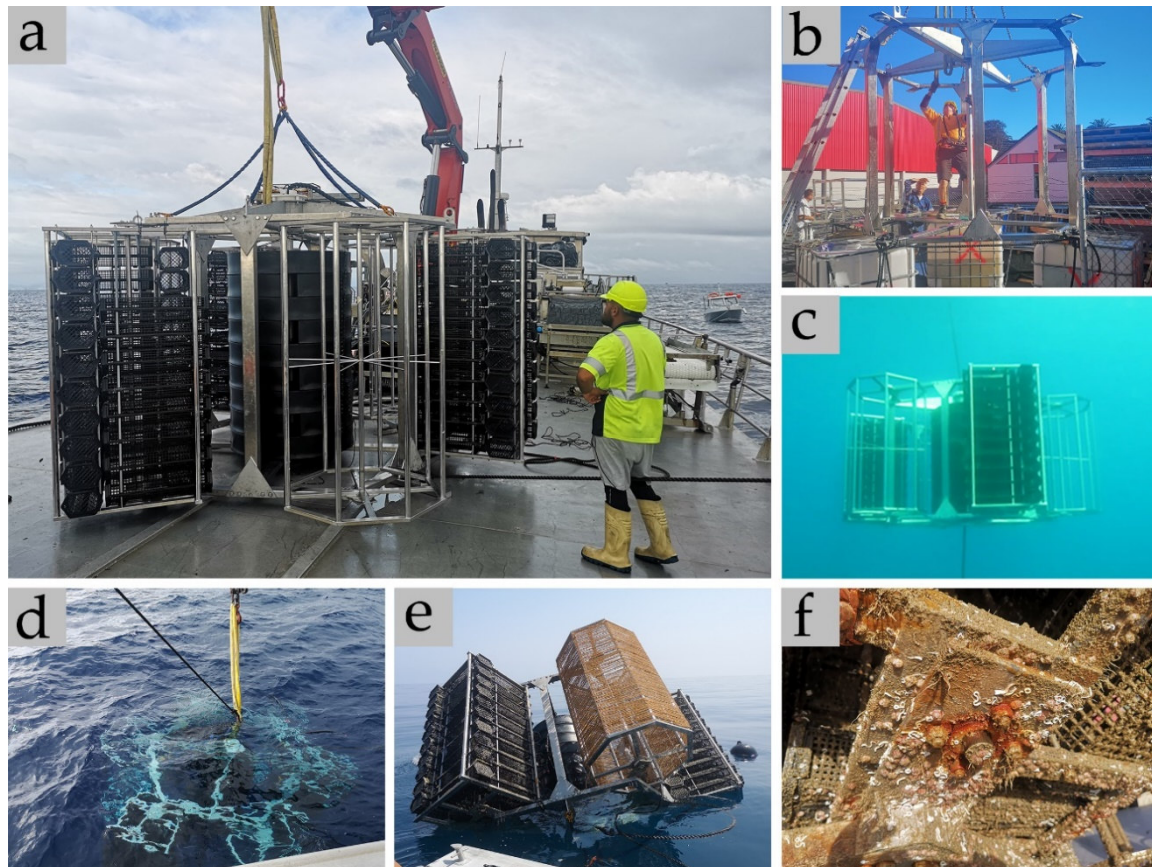


Figure 27: Images from the set-up, deployment, and operation of the *Shellfish Tower* at the Ōpōtiki site in New Zealand. (a) Shellfish Tower loaded on the service vessel just prior to deployment, (b) construction of the Shellfish Tower and conducting a weight test, (c) underwater image after deployment, (d) response test during deployment, (e) inspection after 4 months and horizontal test mode including a fouling inspection (f) [©Heasman. K.].

Chapter summary 4:

This chapter discusses the results made available through the published manuscripts considering the identified gaps of knowledge.

It is shown that the results regarding force coefficients provide engineers and researchers with more comprehensive data to use when designing bivalve aquaculture systems. Regarding the drag coefficient in steady flow the range of explored Reynolds numbers is expanded and a drag coefficient of $C_D = 1.6$ is recommended for subcritical flow regimes ($Re < 10^5$). Furthermore, it was shown for a limited range of Keulegan-Carpenter numbers, that an experimental determination of the hydrodynamic coefficients of mussel dropper lines in oscillatory flow is possible. A drag coefficient of $C_D = 2.3$ and an inertia coefficient of $C_M = 2.1$ are proposed for $KC < 10$.

It is demonstrated that the characteristic diameter has a major influence on the force evolution of dropper lines. The use of 3D-scans and the resulting average diameter for experiments under laboratory conditions as the most explicit representation of the characteristic diameter is recommended. The difficulties accounting for soft and hard growth are addressed. It is shown that the differences regarding the hydrodynamic coefficients between the live mussels and surrogates are mostly due to natural growth on the live mussels, as well as variations in surface roughness, flow regimes and referential frontal areas.

Recommendations to avoid snap loads in the ultimate design of the Shellfish Tower are given. The advantages and disadvantages of increasing or reducing the buoyancy as well as configurations to the mooring are discussed.

Potential errors related to the model setup, equipment, and instrumentation due to limitations of the experimental facilities are indicated. Especially the difficulties arising from biology related parameters, like the comparability of interspecies characteristics or influence of growth stages, are highlighted. The application of the research presented in this thesis is also possible. A use case is shown exemplary for alternative and innovative adaptation practices for increasing aquaculture production. Furthermore, the deployment of prototype structures directly based on the presented research is shown.



5. Conclusions and Outlook

5.1. Conclusions

The thesis presented here examines the impact of hydrodynamic influences on offshore bivalve aquaculture. Considering the rapid growth of human population in coastal areas, accentuated by issues of sustainability and environmental challenges, bivalve aquaculture can be a major contributor towards global food security. Furthermore, it could positively support economic and social developments, while also having far lower environmental costs and increased benefits in comparison to the current sources of animal protein available. Based on this background the general objective of this work is to separate, detail and discuss the governing hydromechanic drivers in bivalve offshore aquaculture systems to increase the predictability of motion and forces.

A comprehensive literature review was conducted regarding the parameters responsible for the interaction between steady and oscillatory flows and bivalve aquaculture systems. To this end, the basic formulations concerning fluid induced forces in high energy environments, studies on hydrodynamic loads to which submerged aquaculture components are subjected, and studies associated with hydrodynamic coefficients in bivalve aquaculture are presented. The fundamental and current research regarding the influence of roughness on the force evolution is shown, and studies on the influence of roughness on bivalve aquaculture components, including a method to accurately represent roughness of an arbitrary object are included. Finally, the current state of science regarding the influence of bivalve aquaculture systems on the flow and the motion of systems is presented.

The knowledge gaps identified through the literature review show:

- ❶ a lack of information regarding hydrodynamic coefficients for the safe determination of loads in offshore environments particularly for oscillatory flow.
- ❷ a lack of guidance as to how the complex surface of mussel dropper lines should be modelled and which factors are of importance for engineers.

- a lack of understanding regarding the motion and load evolution of whole systems.

Based on these shortcomings, several physical model tests were conducted. The model set-up, test program and covered parameter range were specifically developed to supplement the present knowledge gaps within the limitations of the available experimental facilities. The studies include 337 individual test sets with regular and irregular waves covering wave steepnesses from 0.002 to 0.11, and currents with velocities from 0.1 – 1.0 m/s. Reynolds numbers (Re) from 3.0×10^4 to 4.4×10^6 , and Keulegan-Carpenter numbers (KC) from 0.4 to 10 were covered. The analysis of the newly acquired data sets enables the quantification of hydrodynamic parameters for a wide range of hydraulic- and geometry-related boundary conditions. This allows for more holistic conclusions regarding the load evolution in dropper lines and bivalve aquaculture systems. Based on the results of these studies, the main findings are described below:

- Mussel dropper lines (blue mussel, *Mytilus edulis*) were tested against drag at varying velocities and under wave conditions. Based on the results a drag coefficient of $C_D = 1.6$ is recommended for subcritical flow regimes $Re < 10^5$ in steady flow conditions. Under oscillatory flow conditions, a drag coefficient of $C_D = 2.3$ and an inertia coefficient of $C_M = 2.1$ are proposed for $KC < 10$.
- A surrogate was created using 3D-scanning, a surface descriptor-based analysis and 3D-printing. A satisfactory performance of the surrogate was determined, which can be used in both physical and numerical experiments without the need for keeping mussels alive or using geometrically divergent forms.
- Wave and current tests with a novel aquaculture system were conducted for a variety of parameter ranges, which showed that the drag coefficients decrease with increasing current velocities from $C_D = 2.5 - 0.5$ for Reynolds numbers = 0.8×10^6 to 4.4×10^6 , while the mooring inclination increases from 12° to 84° . The comprehensive examination of the mooring line tensions shows that the largest values of snap-induced tension are up to 10 times that of the quasi-static tension.

- A comprehensive analysis of the hydrodynamic interaction of waves and floating natural islands in a large-scale facility shows a significant damping performance of the investigated islands for wave periods $T \leq 2.25$ s. The transmitted wave height of the incident waves is reduced by up to 50% for the smallest wave periods $T \leq 1.5$ s. The incident waves are reflected between 20 - 50% for these wave periods. The incident wave energy is dissipated by up to 85% for the smallest wave height and period ($H = 0.10$ m, $T = 1.5$ s). The damping performance of the structure depends mainly on the submerged depth, width, and mass of the islands.

The insights gained will help enable researchers, policy makers, and industry officials alike to design, operate, and maintain aquaculture systems to aid in the fulfillment of the SDGs set by the UN. Continuing population growth and urbanization of coastal areas alongside an increased need for sustainable alimentation show the need for action. The question how the research presented above can be best utilized to obtain the most efficient aquaculture farm designs and systems is multifaceted and spans a large range of scientific fields. From marine biologists determining the magnitude and spatial scales of changes to water column processes (e.g. stratification, nutrient intake, bio deposition and resuspension); to ecologists enhancing the understanding of offshore aquaculture-environment interactions and the overall footprint of bivalve aquaculture, to engineers who design and maintain the systems and its components. Ensuring a sustainable food supply for future generations remains an ongoing and interdisciplinary research topic, where the insights of offshore engineers are required to design, operate, and maintain critical systems in a highly energetic environment.

5.2. Outlook

The studies presented here examine hydrodynamic impacts on bivalve aquaculture systems and its components. However, further additions to the body of knowledge are necessary to accurately capture the influencing parameters and increase the applicability to larger parameter ranges. The methods applied here can be further developed in the following ways:

- Future testing of the proposed surrogate (SM 1) should include investigations regarding the scaling potential to enable physical investigations with increased accuracy. Additional tests with other commonly cultivated species, e.g. the green-lipped mussel (*Perna canaliculus*) or the Mediterranean mussel (*Mytilus galloprovincialis*), are also suggested to obtain species-specific hydrodynamic parameters and determine the general applicability of the surrogate.
- To provide more robust estimates of hydrodynamic coefficients relevant for shellfish-covered ropes in marine conditions, additional investigations on larger Re and KC -ranges are necessary. This is of special interest for the envisioned remote offshore aquaculture sites and could be achieved either by using large-scale facilities or by a downscaling of the surrogate structures.
- To allow for physical experiments with larger bivalve aquaculture structures, a research effort to scale and test the surrogates regarding their comparability with the live scale surrogates and mussels is necessary. Thereby, whole farms could be investigated and enhancements to the current configurations and new designs developed. Further studies may also include the research on fluid-structure-foundation interaction, and the capacity and failure mechanisms of mooring lines and anchors under snap loads or cyclic loads.
- The specific influence of soft growth and surface roughness on the hydrodynamic parameters of mussel dropper lines needs to be addressed. So far, research focuses on the hard growth of the mussels themselves, neglecting further growth that potentially could significantly alter the flow around the dropper lines and affect the hydrodynamic coefficients.

Addressing this need could lead to the creation of a reference cylinder or surrogate that represents soft and hard growth alike.

- ④ Detailed field studies using prototype structures and established systems are required to determine the magnitude and extent of the overall water flow modification and wake formation in the presence of bivalve aquaculture. This could also help to ascertain whether different system designs and orientations to the water flow significantly alter wave and current attenuation. More research in this regard is also required to determine the extent and importance of naturally occurring marine fouling which can change the drag of shellfish structures through soft growth and decreasing drag.
- ④ Calculating the load evolution of suspended aquaculture systems in marine environments is a challenging endeavor. Thus, future research should focus on the development and validation of numerical models capable of accurately predicting the loads, motions, and wave-structure interactions. This could include sensitivity studies exploring the influencing of varying hydrodynamic parameters and test a much wider range of scenarios of hydrodynamic loading otherwise difficult to test in the laboratory or in the field.

Bibliography

- Abbott, E.J., Firestone, F.A., 1933. Specifying Surface Quality - A Method Based on Accurate Measurement and Comparison. *J. Mech. Eng.* 55, 569–577.
- Airy, G.B., 1845. Tides and Waves, in: *Encyclopaedia Metropolitana*. pp. 241–396.
- Allen, D.W., Henning, D.L., 2001. Surface Roughness Effects on Vortex-Induced Vibration of Cylindrical Structures at Critical and Supercritical Reynolds Numbers, in: 13302, O. (Ed.), *Proceedings of Offshore Technology Conference*. Houston, TX. <https://doi.org/10.4043/13302-ms>
- Anderson, D.M., Burkholder, J.M., Cochlan, W.P., Glibert, P.M., Gobler, C.J., Heil, C.A., Kudela, R.M., Parsons, M.L., Rensel, J.E.J., Townsend, D.W., Trainer, V.L., Vargo, G.A., 2008. Harmful algal blooms and eutrophication: Examining linkages from selected coastal regions of the United States. *Harmful Algae* 8, 39–53. <https://doi.org/10.1016/J.HAL.2008.08.017>
- Babarro, J.M.F., Carrington, E., 2013. Attachment strength of the mussel *Mytilus galloprovincialis*: Effect of habitat and body size. *J. Exp. Mar. Bio. Ecol.* 443, 188–196. <https://doi.org/https://doi.org/10.1016/j.jembe.2013.02.035>
- Bardestani, M., Faltinsen, O.M., 2013. A Two-Dimensional Approximation of a Floating Fish Farm in Waves and Current With the Effect of Snap Loads, in: *Proceedings of the ASME 2013 32nd International Conference on Ocean, Offshore and Arctic Engineering*. American Society of Mechanical Engineers, pp. 1–10. <https://doi.org/10.1115/OMAE2013-10487>
- Beman, J.M., Arrigo, K.R., Matson, P.A., 2005. Agricultural runoff fuels large phytoplankton blooms in vulnerable areas of the ocean. *Nat.* 2005 4347030 434, 211–214. <https://doi.org/10.1038/nature03370>
- Bi, C.W., Zhao, Y.P., Dong, G.H., Cui, Y., Gui, F.K., 2015. Experimental and numerical investigation on the damping effect of net cages in waves. *J. Fluids Struct.* 55, 122–138. <https://doi.org/10.1016/j.jfluidstructs.2015.02.010>
- Bilkovic, D.M., Mitchell, M., Mason, P., Duhring, K., 2016. The Role of Living Shorelines as Estuarine Habitat Conservation Strategies. *Coast. Manag.* 44, 161–174. <https://doi.org/10.1080/08920753.2016.1160201>
- Blanco, J., Zapata, M., Morono, Á., 1996. Some aspects of the water flow through mussel rafts. *Sci. Mar.* 60, 275–282.
- Boyd, A.J., Heasman, K.G., 1998. Shellfish mariculture in the Benguela system: water flow patterns within a mussel farm in Saldanha Bay, South Africa. *J. Shellfish Res.* 17, 25–32.
- Brenner, M., Buck, B.H., 2010. Attachment properties of blue mussel (*Mytilus*

- edulis L.) byssus threads on culture-based artificial collector substrates. *Aquac. Eng.* 42, 128–139. <https://doi.org/10.1016/j.aquaeng.2010.02.001>
- Buck, B.H., 2004. Farming in a High Energy Environment: Potentials and Constraints of Sustainable Offshore Aquaculture in the German Bight (North Sea). Alfred Wegener Institute for Polar and Marine Research.
- Buck, B.H., Ebeling, M.W., Michler-Cieluch, T., 2010. Mussel cultivation as a co-use in offshore wind farms: potential and economic feasibility. <http://dx.doi.org/10.1080/13657305.2010.526018> 14, 255–281. <https://doi.org/10.1080/13657305.2010.526018>
- Buck, B.H., Langan, R., 2017. Aquaculture Perspective of Multi-Use Sites in the Open Ocean - The Untapped Potential for Marine Resources in the Anthropocene, Aquaculture Perspective of Multi-Use Sites in the Open Ocean: The Untapped Potential for Marine Resources in the Anthropocene. SpringerOpen. <https://doi.org/10.1007/978-3-319-51159-7>
- Buck, B.H., Troell, M.F., Krause, G., Angel, D.L., Grote, B., Chopin, T., 2018. State of the Art and Challenges for Offshore Integrated Multi-Trophic Aquaculture (IMTA). *Front. Mar. Sci.* 5, 165. <https://doi.org/10.3389/fmars.2018.00165>
- Camelo-Guarín, S., Molinet, C., Soto, D., 2021. Recommendations for implementing integrated multitrophic aquaculture in commercial farms at the landscape scale in southern Chile. *Aquaculture* 544, 737116. <https://doi.org/10.1016/j.aquaculture.2021.737116>
- Chakrabarti, S.K., 2005. Handbook of Offshore Engineering, Handbook of Offshore Engineering. <https://doi.org/10.1016/B978-0-08-044381-2.50022-9>
- Cheney, D., Langan, R., Heasman, K., Friedman, B., Davis, J., 2010. Shellfish Culture in the Open Ocean: Lessons Learned for Offshore Expansion. *Mar. Technol. Soc. J.* 44, 55–67.
- Cheng, W., Sun, Z., Liang, S., Liu, B., 2020. Numerical model of an aquaculture structure under oscillatory flow. *Aquac. Eng.* 89, 102054. <https://doi.org/10.1016/j.aquaeng.2020.102054>
- Chopin, T., Buschmann, A.H., Halling, C., Troell, M., Kautsky, N., Neori, A., Kraemer, G.P., Zertuche-González, J.A., Yarish, C., Neefus, C., 2001. Integrating seaweeds into marine aquaculture systems: A key toward sustainability. *J. Phycol.* 37, 975–986. <https://doi.org/10.1046/J.1529-8817.2001.01137.X>
- Clauss, G., Lehmann, E., Östergaard, C., 1994. Offshore Structures Volume II: Strength and Safety for Structural Design. Springer London, London. <https://doi.org/10.1007/978-1-4471-1998-2>

- Clauss, G., Lehmann, E., Östergaard, C., 1992. Offshore Structures Volume I: Conceptual Design and Hydromechanics, Meerestechnische Konstruktionen. <https://doi.org/10.1007/978-1-4471-3193-9>
- Cooksey, K.E., Wigglesworth-Cooksey, B., 1995. Adhesion of bacteria and diatoms to surfaces in the sea: A review. *Aquat. Microb. Ecol.* 9, 87–96. <https://doi.org/10.3354/ame009087>
- Costello, C., Cao, L., Gelcich, S., Cisneros-Mata, M.Á., Free, C.M., Froehlich, H.E., Golden, C.D., Ishimura, G., Maier, J., Macadam-Somer, I., Mangin, T., Melnychuk, M.C., Miyahara, M., de Moor, C.L., Naylor, R., Nøstbakken, L., Ojea, E., O'Reilly, E., Parma, A.M., Plantinga, A.J., Thilsted, S.H., Lubchenco, J., 2020. The future of food from the sea. *Nature* 588, 95–100. <https://doi.org/10.1038/s41586-020-2616-y>
- Cozzone, A.J., 2002. Proteins: Fundamental Chemical Properties, in: ELS. Wiley. <https://doi.org/10.1038/npg.els.0001330>
- Dai, J., Wang, C.M., Utsunomiya, T., Duan, W., 2018. Review of recent research and developments on floating breakwaters. *Ocean Eng.* 158, 132–151. <https://doi.org/10.1016/j.oceaneng.2018.03.083>
- Dalton, G., Bardócz, T., Blanch, M., Campbell, D., Johnson, K., Lawrence, G., Lilas, T., Friis-Madsen, E., Neumann, F., Nikitas, N., Ortega, S.T., Pletsas, D., Simal, P.D., Sørensen, H.C., Stefanakou, A., Masters, I., 2019. Feasibility of investment in Blue Growth multiple-use of space and multi-use platform projects; results of a novel assessment approach and case studies. *Renew. Sustain. Energy Rev.* 107, 338–359. <https://doi.org/10.1016/j.rser.2019.01.060>
- Davis, J.L., Currin, C.A., O'Brien, C., Raffenburg, C., Davis, A., 2015. Living Shorelines: Coastal Resilience with a Blue Carbon Benefit. *PLoS One* 10, e0142595. <https://doi.org/10.1371/journal.pone.0142595>
- de Sherbinin, A., Levy, M., Adamo, S., MacManus, K., Yetman, G., Mara, V., Razafindrazay, L., Goodrich, B., Srebotnjak, T., Aichele, C., Pistolesi, L., 2012. Migration and risk: net migration in marginal ecosystems and hazardous areas. *Environ. Res. Lett.* 7, 045602. <https://doi.org/10.1088/1748-9326/7/4/045602>
- Dean, R.G., Dalrymple, R.A., 1991. Water Wave Mechanics for Engineers and Scientists, Advanced Series on Ocean Engineering, Advanced Series on Ocean Engineering. WORLD SCIENTIFIC. <https://doi.org/10.1142/1232>
- Denny, M., 1995. Predicting Physical Disturbance: Mechanistic Approaches to the Study of Survivorship on Wave-Swept Shores. *Ecol. Monogr.* 65, 371–418. <https://doi.org/10.2307/2963496>
- Dewhurst, T., 2016. Dynamics of a Submersible Mussel Raft. Univ. New Hampsh.

University of New Hampshire.

- Di Tullio, G.R., Mariani, P., Benassai, G., Di Luccio, D., Grieco, L., 2018. Sustainable use of marine resources through offshore wind and mussel farm co-location. *Ecol. Modell.* 367, 34–41. <https://doi.org/10.1016/J.ECOLMODEL.2017.10.012>
- Díaz, C., Figueroa, Y., Sobenes, C., 2011. Effect of different longline farming designs over the growth of *Mytilus chilensis* (Hupé, 1854) at Llico Bay, VIII Región of Bio-Bio, Chile. *Aquac. Eng.* 45, 137–145. <https://doi.org/10.1016/j.aquaeng.2011.09.002>
- DIN-EN-ISO 19900:2019, 2019. Petroleum and natural gas industries – General requirements for offshore structures.
- DIN, 2012. DIN-EN-ISO-25178-3 (2012) ‘Geometrical product specifications (GPS) - Surface texture: Areal - Part 3: Specification operators (ISO 25178-3:2012); German version EN ISO 25178-3:2012’,.
- DIN, 1998. DIN-EN-ISO-13565-2 (1998) ‘Geometrical Product Specifications (GPS) - Surface texture: Profile method - Surfaces having stratified functional properties - Part 2: Height characterization using the linear material ratio curve.
- DNV, 2021. Oceans’ Future to 2050 - Marine Aquaculture Forecast.
- Donea, J., Huerta, A., 2003. Finite element methods for flow problems. *Int Assoc for Mathematics & Computers in Simulation.* <https://doi.org/10.1002/0470013826>
- Dong, G.H.H., Zheng, Y.N.N., Li, Y.C.C., Teng, B., Guan, C.T.T., Lin, D.F.F., 2008. Experiments on Wave Transmission Coefficients of Floating Breakwaters. *Ocean Eng.* 35, 931–938. <https://doi.org/10.1016/j.oceaneng.2008.01.010>
- Drapeau, A., Comeau, L.A., Landry, T., Stryhn, H., Davidson, J., 2006. Association between longline design and mussel productivity in Prince Edward Island, Canada. *Aquaculture* 261, 879–889. <https://doi.org/10.1016/j.aquaculture.2006.07.045>
- Duarte, P., Alvarez-Salgado, X.A., Fernández-Reiriz, M.J., Piedracoba, S., Labarta, U., 2014. A modeling study on the hydrodynamics of a coastal embayment occupied by mussel farms (Ria de Ares-Betanzos, NW Iberian Peninsula). *Estuar. Coast. Shelf Sci.* 147, 42–55. <https://doi.org/10.1016/j.ecss.2014.05.021>
- Dürr, S., Watson, D.I., 2009. Biofouling and Antifouling in Aquaculture, in: *Biofouling.* Wiley-Blackwell, Oxford, UK, pp. 267–287. <https://doi.org/10.1002/9781444315462.ch19>
- Dwarakish, G.S., Salim, A.M., 2015. Review on the Role of Ports in the Development of a Nation. *Aquat. Procedia* 4, 295–301.

<https://doi.org/10.1016/j.aqpro.2015.02.040>

- Eller, F., Skálová, H., Caplan, J.S., Bhattarai, G.P., Burger, M.K., Cronin, J.T., Guo, W.-Y., Guo, X., Hazelton, E.L.G., Kettenring, K.M., Lambertini, C., McCormick, M.K., Meyerson, L.A., Mozdzer, T.J., Pyšek, P., Sorrell, B.K., Whigham, D.F., Brix, H., 2017. Cosmopolitan Species As Models for Ecophysiological Responses to Global Change: The Common Reed *Phragmites australis*. *Front. Plant Sci.* 8. <https://doi.org/10.3389/fpls.2017.01833>
- Elmqvist, T., Andersson, E., Frantzeskaki, N., McPhearson, T., Olsson, P., Gaffney, O., Takeuchi, K., Folke, C., 2019. Sustainability and resilience for transformation in the urban century. *Nat. Sustain.* 2, 267–273. <https://doi.org/10.1038/s41893-019-0250-1>
- Engloner, A.I., 2009. Structure, growth dynamics and biomass of reed (*Phragmites australis*) – A review. *Flora - Morphol. Distrib. Funct. Ecol. Plants* 204, 331–346. <https://doi.org/10.1016/j.flora.2008.05.001>
- European Commission, 2021. The EU Aquaculture Sector – Economic report 2020 (STECF-20-12), Publications Office of the European Union, EUR 26336 EN, JRC 86671. <https://doi.org/https://data.europa.eu/doi/10.2760/441510>
- European Commission, 2000. Directive 2000/60/EC of the European Parliament and of the Council of 23 October 2000 establishing a framework for Community action in the field of water policy. *Off. J. Eur. Communities* 0001–0073.
- FAO, 2020. The State of World Fisheries and Aquaculture 2020. FAO, Rome. <https://doi.org/10.4060/ca9229en>
- Favrel, P., Mathieu, M., 1996. Cultured Aquatic Species Information Programme *Mytilus edulis* (Linnaeus, 1758) Fisheries [WWW Document]. Food Agric. Organ. United Nations a world without Hunger - Fish. Aquac. Dep.
- Feng, D., Meng, A., Wang, P., Yao, Y., Gui, F., 2021. Effect of design configuration on structural response of longline aquaculture in waves. *Appl. Ocean Res.* 107, 102489. <https://doi.org/10.1016/j.apor.2020.102489>
- Ferziger, J.H., Perić, M., 2002. Computational Methods for Fluid Dynamics. Springer Berlin Heidelberg, Berlin, Heidelberg. <https://doi.org/10.1007/978-3-642-56026-2>
- Fitridge, I., Dempster, T., Guenther, J., de Nys, R., 2012. The impact and control of biofouling in marine aquaculture: A review. *Biofouling* 28, 649–669. <https://doi.org/10.1080/08927014.2012.700478>
- Froehlich, H.E., Smith, A., Gentry, R.R., Halpern, B.S., 2017. Offshore Aquaculture:

- I Know It When I See It. *Front. Mar. Sci.* 4, 154.
<https://doi.org/10.3389/fmars.2017.00154>
- Gadelmawla, E.S., Koura, M.M., Maksoud, T.M.A., Elewa, I.M., Soliman, H.H., 2002. Roughness parameters. *J. Mater. Process. Technol.* 123, 133–145.
[https://doi.org/10.1016/S0924-0136\(02\)00060-2](https://doi.org/10.1016/S0924-0136(02)00060-2)
- Gagnon, M., 2019. Self-organization and mechanical properties of mussel culture suspensions: A critical review. *Aquac. Eng.* 87, 102024.
<https://doi.org/10.1016/j.aquaeng.2019.102024>
- Gagnon, M., Bergeron, P., 2017. Observations of the loading and motion of a submerged mussel longline at an open ocean site. *Aquac. Eng.* 78, 114–129.
<https://doi.org/10.1016/j.aquaeng.2017.05.004>
- Gagnon, M., Bergeron, P., 2011. Propriétés mécaniques des composantes des filières maricoles du Québec. Québec, Canada.
Title translation: Mechanical properties of Quebec mariculture components
- Gallup, J.L., Sachs, J.D., Mellinger, A.D., 1999. Geography and Economic Development. *Int. Reg. Sci. Rev.* 22, 179–232.
<https://doi.org/10.1177/016001799761012334>
- Garen, P., Robert, S., Bougrier, S., 2004. Comparison of growth of mussel, *Mytilus edulis*, on longline, pole and bottom culture sites in the Pertuis Breton, France. *Aquaculture* 232, 511–524. [https://doi.org/10.1016/S0044-8486\(03\)00535-0](https://doi.org/10.1016/S0044-8486(03)00535-0)
- Gentry, R.R., Froehlich, H.E., Grimm, D., Kareiva, P., Parke, M., Rust, M., Gaines, S.D., Halpern, B.S., 2017. Mapping the global potential for marine aquaculture. *Nat. Ecol. Evol.* 1, 1317–1324. <https://doi.org/10.1038/s41559-017-0257-9>
- Gibbs, M.M., James, M.R., Pickmere, S.E., Woods, P.H., Shakespeare, B.S., Hickman, R.W., Illingworth, J., 1991. Hydrodynamic and water column properties at six stations associated with mussel farming in pelorus sound, 1984–85. *New Zeal. J. Mar. Freshw. Res.* 25, 239–254.
<https://doi.org/10.1080/00288330.1991.9516476>
- Gieschen, R., Schwartpaul, C., Landmann, J., Fröhling, L., Hildebrandt, A., Goseberg, N., 2021. Large-Scale Laboratory Experiments on Mussel Dropper Lines in Ocean Surface Waves. *J. Mar. Sci. Eng.* 9, 29.
<https://doi.org/10.3390/jmse9010029>
- Gill, A.B., 2005. Offshore renewable energy: Ecological implications of generating electricity in the coastal zone. *J. Appl. Ecol.* 42, 605–615.
<https://doi.org/10.1111/j.1365-2664.2005.01060.x>
- Gittman, R.K., Peterson, C.H., Currin, C.A., Joel Fodrie, F., Piehler, M.F., Bruno, J.F., 2016. Living shorelines can enhance the nursery role of threatened

- estuarine habitats. *Ecol. Appl.* 26, 249–263. <https://doi.org/10.1890/14-0716>
- Goda, Y., 2010. *Random Seas and Design of Maritime Structures*, Advanced Series on Ocean Engineering. WORLD SCIENTIFIC. <https://doi.org/10.1142/7425>
- Gordelier, T., Parish, D., Thies, P.R., Johanning, L., 2015. A novel mooring tether for highly-dynamic offshore applications; mitigating peak and fatigue loads via selectable axial stiffness. *J. Mar. Sci. Eng.* 3, 1287–1310. <https://doi.org/10.3390/jmse3041287>
- Gosling, E., 2015. *Bivalve Molluscs: Biology, Ecology and Culture*, CEUR Workshop Proceedings. <https://doi.org/10.1017/CBO9781107415324.004>
- Gren, I.M., Säll, S., Aklilu, A.Z., Tirkaso, W., 2018. Does Mussel Farming Promote Cost Savings and Equity in Reaching Nutrient Targets for the Baltic Sea? *Water* 2018, Vol. 10, Page 1682 10, 1682. <https://doi.org/10.3390/W10111682>
- Hargrave, M.S., Nylund, G.M., Enge, S., Pavia, H., 2022. Co-cultivation with blue mussels increases yield and biomass quality of kelp. *Aquaculture* 550, 737832. <https://doi.org/10.1016/J.AQUACULTURE.2021.737832>
- He, P., Lu, S., Wang, Y., Li, R., Li, F., 2022. Analysis of the best roughness surface based on the bearing area curve theory. *Proc. Inst. Mech. Eng. Part J J. Eng. Tribol.* 236, 527–540. <https://doi.org/10.1177/13506501211018937>
- Heaf, N.J., 1979. The Effect Of Marine Growth On The Performance Of Fixed Offshore Platforms In The North Sea, in: *Offshore Technology Conference*. Offshore Technology Conference. <https://doi.org/10.4043/3386-MS>
- Heasman, K., Pitcher, G.C., McQuaid, C.D., Hecht, T., 1998. Shellfish mariculture in the benguela system: raft culture of *Mytilus Galloprovincialis* and the effect of rope spacing on food extraction, growth rate, production, and condition of mussels. *J. Shellfish Res.* 17, 33–39.
- Heasman, K.G., Scott, N., Smeaton, M., Goseberg, N., Hildebrandt, A., Vitasovich, P., Elliot, A., Mandeno, M., Buck, B.H., 2021. New system design for the cultivation of extractive species at exposed sites - Part 1: System design, deployment and first response to high-energy environments. *Appl. Ocean Res.* 110, 102603. <https://doi.org/10.1016/j.apor.2021.102603>
- Heideman, J.C., Johansson, P.I., Olsen, O.A., 1979. Local Wave Force Coefficients, in: *Civil Engineering in the Oceans IV*. American Society of Civil Engineers (ASCE), San Francisco, California, United States.
- Henry, P.-Y., Nedrebø, E.L., Myrhaug, D., 2016. Visualisation of the effect of different types of marine growth on cylinders' wake structure in low Re steady flows. *Ocean Eng.* 115, 182–188. <https://doi.org/10.1016/j.oceaneng.2016.02.023>
- Holthuijsen, L.H., 2007. *Waves in Oceanic and Coastal Waters*. Cambridge

- University Press, Cambridge. <https://doi.org/10.1017/CBO9780511618536>
- Houghton, D.R., 1978. Marine fouling and offshore structures. *Ocean Manag.* 4, 347–352. [https://doi.org/10.1016/0302-184X\(78\)90033-1](https://doi.org/10.1016/0302-184X(78)90033-1)
- Hsu, W.-T.T., Thiagarajan, K.P., Manuel, L., 2018. Snap load criteria for mooring lines of a floating offshore wind turbine, in: ASME 2018 1st International Offshore Wind Technical Conference, IOWTC 2018. pp. 1–9. <https://doi.org/10.1115/IOWTC2018-1047>
- Hsu, W., Thiagarajan, K.P., Manuel, L., 2017. Extreme mooring tensions due to snap loads on a floating offshore wind turbine system. *Mar. Struct.* 55, 182–199. <https://doi.org/10.1016/j.marstruc.2017.05.005>
- Hu, C., Li, D., Chen, C., Ge, J., Muller-Karger, F.E., Liu, J., Yu, F., He, M.X., 2010. On the recurrent *Ulva prolifera* blooms in the Yellow Sea and East China Sea. *J. Geophys. Res. Ocean.* 115. <https://doi.org/10.1029/2009JC005561>
- Hugo, G., 2011. Future demographic change and its interactions with migration and climate change. *Glob. Environ. Chang.* 21, S21–S33. <https://doi.org/10.1016/j.gloenvcha.2011.09.008>
- James, S.C., O'Donncha, F., 2019. Drag coefficient parameter estimation for aquaculture systems. *Environ. Fluid Mech.* 19, 989–1003. <https://doi.org/10.1007/s10652-019-09697-7>
- James, S.C., O'Donncha, F., Plew, D.R., 2016. Calibration of a 3D hydrodynamic aquaculture model, in: OCEANS 2016 MTS/IEEE Monterey, OCE 2016. IEEE, pp. 1–7. <https://doi.org/10.1109/OCEANS.2016.7761411>
- Jansen, H.M., Van Den Burg, S., Bolman, B., Jak, R.G., Kamermans, P., Poelman, M., Stuiver, M., 2016. The feasibility of offshore aquaculture and its potential for multi-use in the North Sea. *Aquac. Int.* 24, 735–756. <https://doi.org/10.1007/s10499-016-9987-y>
- Ji, C.-Y., Guo, Y.-C., Cui, J., Yuan, Z.-M., Ma, X.-J., 2016. 3D experimental study on a cylindrical floating breakwater system. *Ocean Eng.* 125, 38–50. <https://doi.org/10.1016/j.oceaneng.2016.07.051>
- Jonsson, P.R., Berntsson, K.M., Larsson, A.I., 2004. Linking larval supply to recruitment: flow-mediated control of initial adhesion of barnacle larvae. *Ecology* 85, 2850–2859. <https://doi.org/10.1890/03-0565>
- Keulegan, G.H., Carpenter, L.H., 1958. Forces on Cylinders and Plates in an Oscillating Fluid. *J. Res. Natl. Bur. Stand.* (1934). 60, 423–440.
- Kim, T., Lee, J., Fredriksson, D.W., DeCew, J., Drach, A., Moon, K., 2014. Engineering analysis of a submersible abalone aquaculture cage system for deployment in exposed marine environments. *Aquac. Eng.* 63, 72–88.

<https://doi.org/10.1016/j.aquaeng.2014.10.006>

- Knysh, A., Tsukrov, I., Chambers, M., Swift, M.R., Sullivan, C., Drach, A., 2020. Numerical modeling of submerged mussel longlines with protective sleeves. *Aquac. Eng.* 88, 102027. <https://doi.org/10.1016/j.aquaeng.2019.102027>
- Landmann, J., Fröhling, L., Gieschen, R., Buck, B.H., Heasman, K., Scott, N., Smeaton, M., Goseberg, N., Hildebrandt, A., 2021. Drag and inertia coefficients of live and surrogate shellfish dropper lines under steady and oscillatory flow. *Ocean Eng.* 235, 109377. <https://doi.org/10.1016/j.oceaneng.2021.109377>
- Landmann, J., Hammer, T.C., Günther, H., Hildebrandt, A., 2022. Large-scale investigation of wave dampening characteristics of organic, artificial floating islands. *Ecol. Eng.* 181, 106691. <https://doi.org/10.1016/j.ecoleng.2022.106691>
- Langhamer, O., Wilhelmsson, D., Engström, J., 2009. Artificial reef effect and fouling impacts on offshore wave power foundations and buoys - a pilot study. *Estuar. Coast. Shelf Sci.* 82, 426–432. <https://doi.org/10.1016/j.ecss.2009.02.009>
- Lawless, J.F., 2002. *Statistical Models and Methods for Lifetime Data*, Wiley Series in Probability and Statistics. John Wiley & Sons, Inc., Hoboken, NJ, USA. <https://doi.org/10.1002/9781118033005>
- Lei, J., Nepf, H., 2019. Wave damping by flexible vegetation: Connecting individual blade dynamics to the meadow scale. *Coast. Eng.* 147, 138–148. <https://doi.org/10.1016/j.coastaleng.2019.01.008>
- Lemke, H.W., Seewig, J., Bodschwinn, H., Brinkmann, S., 2003. Kenngrößen der Abbott-Kurve zur integralen Beurteilung dreidimensional gemessener Zylinderlaufbahn-Oberflächen 64, 438–444.
- Liu, Z., Huguenard, K., 2020. Hydrodynamic response of a floating aquaculture farm in a low inflow estuary. *J. Geophys. Res. Ocean.* 125. <https://doi.org/10.1029/2019JC015625>
- MacCamy, R.C., Fuchs, R.A., 1954. *Wave Forces on Piles: A Diffraction Theory*, United States, Beach Erosion Board Engineer Research and Development Center (U.S.).
- Malcherek, A., 2010. *Gezeiten und Wellen: die Hydromechanik der Küstengewässer*. Vieweg+Teubner Verlag / Springer Fachmedien Wiesbaden GmbH, Wiesbaden.
Title translation: Tides and waves : the hydromechanics of coastal waters.
- Mansard, E.P.D., Funke, E.R., 1980. The Measurement of Incident and Reflected Spectra Using a Least Squares Method, in: *Coastal Engineering 1980*.

- American Society of Civil Engineers, New York, NY, pp. 154–172.
<https://doi.org/10.1061/9780872622647.008>
- Marty, A., Schoefs, F., Soulard, T., Berhault, C., Facq, J.-V., Gaurier, B., Germain, G., 2021. Effect of Roughness of Mussels on Cylinder Forces from a Realistic Shape Modelling. *J. Mar. Sci. Eng.* 9, 598. <https://doi.org/10.3390/jmse9060598>
- Marzec, M., Józwiakowski, K., Dębska, A., Gizińska-Górna, M., Pytka-Woszczyło, A., Kowalczyk-Juško, A., Listosz, A., 2018. The Efficiency and Reliability of Pollutant Removal in a Hybrid Constructed Wetland with Common Reed, Manna Grass, and Virginia Mallow. *Water* 10, 1445. <https://doi.org/10.3390/w10101445>
- Mascorda Cabre, L., Hosegood, P., Attrill, M.J., Bridger, D., Sheehan, E. V., 2021. Offshore longline mussel farms: a review of oceanographic and ecological interactions to inform future research needs, policy and management. *Rev. Aquac.* 13, 1864–1887. <https://doi.org/10.1111/raq.12549>
- Matthiessen, G.C., 2001. Oyster culture. Wiley Online Library, London.
- Maul, G.A., Duedall, I.W., 2019. Demography of Coastal Populations, in: Finkl, C.W., Makowski, C. (Eds.), *Encyclopedia of Coastal Science*. Springer International Publishing, Cham, pp. 692–700. https://doi.org/10.1007/978-3-319-93806-6_115
- Méhauté, B., 1976. *An Introduction to Hydrodynamics and Water Waves*. Springer Berlin Heidelberg, Berlin, Heidelberg. <https://doi.org/10.1007/978-3-642-85567-2>
- Moosavi, S., 2017. Ecological Coastal Protection: Pathways to Living Shorelines, in: *Procedia Engineering*. Elsevier Ltd, pp. 930–938. <https://doi.org/10.1016/j.proeng.2017.08.027>
- Morison, J.R., O'Brien, M.P., Johnson, J.W., Schaaf, S.A., O'Brien, M.P., Johnson, J.W., Schaaf, S.A., 1950. The forces exerted by surface waves on piles. *Pet. Trans. AIME* 189, 149–157. <https://doi.org/10.2118/950149-G>
- Mueller Loose, S., Peschel, A., Grebitus, C., 2013. Quantifying effects of convenience and product packaging on consumer preferences and market share of seafood products: The case of oysters. *Food Qual. Prefer.* 28, 492–504. <https://doi.org/https://doi.org/10.1016/j.foodqual.2012.11.004>
- Nath, J.H., 1987. On Wave Force Coefficient Variability. *J. Offshore Mech. Arct. Eng.* 109, 295–306. <https://doi.org/10.1115/1.3257023>
- Nath, J.H., Hsu, M.-K., Hudspeth, R.T., Dummer, J., 1984. Laboratory wave forces on vertical cylinders, in: *Proceedings Ocean Structural Dynamics Symposium*. Oregon State University.

- Naylor, R., Burke, M., 2005. Aquaculture and ocean resources: Raising Tigers of the Sea. *Annu. Rev. Environ. Resour.* 30, 185–218. <https://doi.org/10.1146/annurev.energy.30.081804.121034>
- Naylor, R.L., Goldburg, R.J., Primavera, J.H., Kautsky, N., Beveridge, M.C.M., Clay, J., Folke, C., Lubchenco, J., Mooney, H., Troell, M., 2000. Effect of aquaculture on world fish supplies. *Nature* 405, 1017–1024. <https://doi.org/10.1038/35016500>
- Neori, A., Chopin, T., Troell, M., Buschmann, A.H., Kraemer, G.P., Halling, C., Shpigiel, M., Yarish, C., 2004. Integrated aquaculture: rationale, evolution and state of the art emphasizing seaweed biofiltration in modern mariculture. *Aquaculture* 231, 361–391. <https://doi.org/10.1016/J.AQUACULTURE.2003.11.015>
- Neumann, B., Vafeidis, A.T., Zimmermann, J., Nicholls, R.J., 2015. Future coastal population growth and exposure to sea-level rise and coastal flooding - A global assessment. *PLoS One* 10. <https://doi.org/10.1371/journal.pone.0118571>
- Newell, C.R., Richardson, J., 2014. The Effects of Ambient and Aquaculture Structure Hydrodynamics on the Food Supply and Demand of Mussel Rafts. *J. Shellfish Res.* 33, 257–272. <https://doi.org/10.2983/035.033.0125>
- Newkirk, G.F., Muise, B.C., Enright, C.E., 1995. Culture of the Belon oyster, *Ostrea edulis*, Cold-water aquaculture in Atlantic Canada. Moncton, Canada: Canadian Institute for Research on Regional Development.
- NOAA, 2011. MARINE AQUACULTURE POLICY. Washington D.C.
- Noakes, D.J., 2014. Overview of cage culture and its importance in the 21st century., in: *Diseases and Disorders of Finfish in Cage Culture*. CABI, UK, pp. 1–14. <https://doi.org/10.1079/9781780642079.0001>
- Oertel, H., Böhle, M., Reviol, T., 2015. *Strömungsmechanik für Ingenieure und Naturwissenschaftler*. Springer Fachmedien Wiesbaden, Wiesbaden, Germany. <https://doi.org/10.1007/978-3-658-07786-0>
Title translation: Fluid Mechanics for Engineers and Scientists
- Osmond, A.T.Y., Colombo, S.M., 2019. The future of genetic engineering to provide essential dietary nutrients and improve growth performance in aquaculture: Advantages and challenges. *J. World Aquac. Soc.* 50, 490–509. <https://doi.org/10.1111/JWAS.12595>
- Palinkas, C.M., Orton, P., Hummel, M.A., Nardin, W., Sutton-Grier, A.E., Harris, L., Gray, M., Li, M., Ball, D., Burks-Copes, K., Davlasheridze, M., De Schipper, M., George, D.A., Halsing, D., Maglio, C., Marrone, J., McKay, S.K., Nutters, H., Orff, K., Taal, M., Van Oudenhoven, A.P.E., Veatch, W., Williams, T., 2022. Innovations in Coastline Management With Natural and Nature-Based

- Features (NNBF): Lessons Learned From Three Case Studies. *Front. Built Environ.* 8, 62. <https://doi.org/10.3389/fbuil.2022.814180>
- Palm, J., Eskilsson, C., 2020. Influence of Bending Stiffness on Snap Loads in Marine Cables: A Study Using a High-Order Discontinuous Galerkin Method. *J. Mar. Sci. Eng.* 8, 795. <https://doi.org/10.3390/jmse8100795>
- Palm, J., Eskilsson, C., Bergdahl, L., 2017. An hp-adaptive discontinuous Galerkin method for modelling snap loads in mooring cables. *Ocean Eng.* 144, 266–276. <https://doi.org/10.1016/j.oceaneng.2017.08.041>
- Palm, J., Paredes, G.M., Pinto, F.T., Bergdahl, L., 2013. Simulation of Mooring Cable Dynamics Using a Discontinuous Galerkin Method. *Int. Conf. Comput. Methods Mar. Eng. - Mar.* 1–12.
- Petersen, J.K., Hasler, B., Timmermann, K., Nielsen, P., Tørring, D.B., Larsen, M.M., Holmer, M., 2014. Mussels as a tool for mitigation of nutrients in the marine environment. *Mar. Pollut. Bull.* 82, 137–143. <https://doi.org/10.1016/J.MARPOLBUL.2014.03.006>
- Pilditch, C.A., Grant, J., Bryan, K.R., 2001. Seston supply to sea scallops (*Placopecten magellanicus*) in suspended culture. *Can. J. Fish. Aquat. Sci.* 58, 241–253. <https://doi.org/10.1139/f00-242>
- Plew, D.R., 2011. Depth-averaged drag coefficient for modeling flow through suspended canopies. *J. Hydraul. Eng.* 137, 234–247. [https://doi.org/10.1061/\(ASCE\)HY.1943-7900.0000300](https://doi.org/10.1061/(ASCE)HY.1943-7900.0000300)
- Plew, D.R., Enright, M.P., Nokes, R.I., Dumas, J.K., 2009. Effect of mussel bio-pumping on the drag on and flow around a mussel crop rope. *Aquac. Eng.* 40, 55–61. <https://doi.org/10.1016/j.aquaeng.2008.12.003>
- Plew, D.R., Stevens, C.L., Spigel, R.H., Hartstein, N.D., 2005. Hydrodynamic implications of large offshore mussel farms. *IEEE J. Ocean. Eng.* 30, 95–108. <https://doi.org/10.1109/JOE.2004.841387>
- Pogoda, B., Buck, B.H., Hagen, W., 2011. Growth performance and condition of oysters (*Crassostrea gigas* and *Ostrea edulis*) farmed in an offshore environment (North Sea, Germany). *Aquaculture* 319, 484–492. <https://doi.org/https://doi.org/10.1016/j.aquaculture.2011.07.017>
- Qiao, D., Yan, J., Liang, H., Ning, D., Li, B., Ou, J., 2020. Analysis on snap load characteristics of mooring line in slack-taut process. *Ocean Eng.* 196, 106807. <https://doi.org/10.1016/j.oceaneng.2019.106807>
- Qiao, J.D., Delavan, S.K., Nokes, R.I., Plew, D.R., 2016. Flow structure and turbulence characteristics downstream of a spanwise suspended linear array. *Environ. Fluid Mech.* 16, 1021–1041. <https://doi.org/10.1007/s10652-016-9465->

- Railkin, A.I., 2003. Marine Biofouling. CRC Press. <https://doi.org/10.1201/9780203503232>
- Raman-Nair, W., Colbourne, B., 2003. Dynamics of a mussel longline system. *Aquac. Eng.* 27, 191–212. [https://doi.org/10.1016/S0144-8609\(02\)00083-3](https://doi.org/10.1016/S0144-8609(02)00083-3)
- Raman-Nair, W., Colbourne, B., Gagnon, M., Bergeron, P., 2008. Numerical model of a mussel longline system: Coupled dynamics. *Ocean Eng.* 35, 1372–1380. <https://doi.org/10.1016/j.oceaneng.2008.05.008>
- Reid, G.K., Lefebvre, S., Filgueira, R., Robinson, S.M.C., Broch, O.J., Dumas, A., Chopin, T.B.R., 2020. Performance measures and models for open-water integrated multi-trophic aquaculture. *Rev. Aquac.* 12, 47–75. <https://doi.org/10.1111/raq.12304>
- Reynolds, O., 1883. XXIX. An experimental investigation of the circumstances which determine whether the motion of water shall be direct or sinuous, and of the law of resistance in parallel channels, in: *Philosophical Transactions of the Royal Society of London.* pp. 935–982. <https://doi.org/10.1098/rstl.1883.0029>
- Röös, E., Bajželj, B., Smith, P., Patel, M., Little, D., Garnett, T., 2017. Protein futures for Western Europe: potential land use and climate impacts in 2050. *Reg. Environ. Chang.* 17, 367–377.
- Rosland, R., Bacher, C., Strand, Ø., Aure, J., Strohmeier, T., 2011. Modelling growth variability in longline mussel farms as a function of stocking density and farm design. *J. Sea Res.* 66, 318–330. <https://doi.org/10.1016/j.seares.2011.04.009>
- Saleh, F., Weinstein, M.P., 2016. The role of nature-based infrastructure (NBI) in coastal resiliency planning: A literature review. *J. Environ. Manage.* <https://doi.org/10.1016/j.jenvman.2016.09.077>
- Sarpkaya, T., 1990. On the Effect of Roughness on Cylinders. *J. Offshore Mech. Arct. Eng.* 112, 334–340. <https://doi.org/10.1115/1.2919875>
- Sarpkaya, T., 1987. Oscillating flow about smooth and rough cylinders. *Proc. ASME sixth int. Offshore Mech. Arct. Eng. Symp. II, J.S. C*, 307–313.
- Sarpkaya, T., 1976a. In-line and transverse forces on smooth and rough cylinders in oscillatory flow at high Reynolds numbers, *Offshore Technology Conference*. Monterey, California. <https://doi.org/10.4043/2533-MS>
- Sarpkaya, T., 1976b. Vortex Shedding and Resistance in Harmonic Flow about Smooth and Rough Circular Cylinders at High Reynolds Numbers. *Monterey, California*.

- Sarpkaya, T., 2010. *Wave Forces on Offshore Structures*. Cambridge University Press. <https://doi.org/10.1017/CBO9781139195898>
- Sawaragi, T., 1995. *Coastal engineering - waves, beaches, wave-structure interactions*, Coastal engineering - waves, beaches, wave-structure interactions. [https://doi.org/10.1016/0148-9062\(95\)99708-6](https://doi.org/10.1016/0148-9062(95)99708-6)
- Schernewski, G., Friedland, R., Buer, A.L., Dahlke, S., Drews, B., Höft, S., Klumpe, T., Schadach, M., Schumacher, J., Zaiko, A., 2019. Ecological-social-economic assessment of zebra-mussel cultivation scenarios for the Oder (Szczecin) Lagoon. *J. Coast. Conserv.* 23, 913–929. <https://doi.org/10.1007/S11852-018-0649-2/FIGURES/11>
- Schernewski, G., Stybel, N., Neumann, T., 2012. Zebra mussel farming in the Szczecin (Oder) Lagoon: Water-quality objectives and cost-effectiveness. *Ecol. Soc.* 17. <https://doi.org/10.5751/ES-04644-170204>
- Schoefs, F., Bakhtiari, A., Ameryoun, H., 2022. Evaluation of Hydrodynamic Force Coefficients in Presence of Biofouling on Marine/Offshore Structures, a Review and New Approach. *J. Mar. Sci. Eng.* 10. <https://doi.org/10.3390/jmse10050558>
- Schoefs, F., Tran, T.B., 2022. Reliability Updating of Offshore Structures Subjected to Marine Growth. *Energies* 15. <https://doi.org/10.3390/en15020414>
- Scyphers, S.B., Powers, S.P., Heck, K.L., Byron, D., 2011. Oyster Reefs as Natural Breakwaters Mitigate Shoreline Loss and Facilitate Fisheries. *PLoS One* 6, e22396. <https://doi.org/10.1371/journal.pone.0022396>
- Seelig, W.N., Ahrens, J.P., 1981. Estimation of wave reflection and energy dissipation coefficients for beaches, revetments, and breakwaters., U.S. Army Coastal Engineering Research Center, Technical Paper.
- Sekovski, I., Newton, A., Dennison, W.C., 2012. Megacities in the coastal zone: Using a driver-pressure-state-impact-response framework to address complex environmental problems. *Estuar. Coast. Shelf Sci.* 96, 48–59. <https://doi.org/10.1016/j.ecss.2011.07.011>
- Seto, K.C., 2011. Exploring the dynamics of migration to mega-delta cities in Asia and Africa: Contemporary drivers and future scenarios. *Glob. Environ. Chang.* 21, S94–S107. <https://doi.org/10.1016/j.gloenvcha.2011.08.005>
- Shi, J., Wei, H., Zhao, L., Yuan, Y., Fang, J., Zhang, J., 2011. A physical-biological coupled aquaculture model for a suspended aquaculture area of China. *Aquaculture* 318, 412–424. <https://doi.org/10.1016/j.aquaculture.2011.05.048>
- Shi, W., Park, H.C., Baek, J.H., Kim, C.W., Kim, Y.C., Shin, H.K., 2012. Study on the marine growth effect on the dynamic response of offshore wind turbines. *Int.*

- J. *Precis. Eng. Manuf.* 13, 1167–1176. <https://doi.org/10.1007/s12541-012-0155-7>
- Small, C., Nicholls, R.J., 2003. A global analysis of human settlement in coastal zones. *J. Coast. Res.* 19, 584–599.
- Soares, C.G., Garbatov, Y. (Eds.), 2017. *Progress in the Analysis and Design of Marine Structures*. CRC Press. <https://doi.org/10.1201/9781315157368>
- Sorokin, Y.I., Sorokin, P.Y., Ravagnan, G., 1996. On an extremely dense bloom of the dinoflagellate *Alexandrium tamarense* in lagoons of the PO river delta: Impact on the environment. *J. Sea Res.* 35, 251–255. [https://doi.org/10.1016/S1385-1101\(96\)90752-2](https://doi.org/10.1016/S1385-1101(96)90752-2)
- Soukup, A., Votrubova, O., Cizkova, H., 2002. Development of anatomical structure of roots of *Phragmites australis*. *New Phytol.* 153, 277–287. <https://doi.org/10.1046/j.0028-646X.2001.00317.x>
- Stevens, C.L., Petersen, J.K., 2011. Turbulent, stratified flow through a suspended shellfish canopy: Implications for mussel farm design. *Aquac. Environ. Interact.* 2, 87–104. <https://doi.org/10.3354/aei00033>
- Stevens, C.L., Plew, D.R., Hartstein, N.D., Fredriksson, D.W., 2008. The physics of open-water shellfish aquaculture. *Aquac. Eng.* 38, 145–160. <https://doi.org/10.1016/j.aquaeng.2008.01.006>
- Stevens, C.L., Plew, D.R., Smith, M.J., Fredriksson, D.W., Plew, ; D R, Smith, ; M J, Fredriksson, D.W., 2007. Hydrodynamic forcing of long-line mussel farms: Observations. *J. Waterw. Port, Coast. Ocean Eng.* 133, 192–199. [https://doi.org/10.1061/\(ASCE\)0733-950X\(2007\)133:3\(192\)](https://doi.org/10.1061/(ASCE)0733-950X(2007)133:3(192))
- Stokes, G.G., 1847. On the theory of oscillatory waves. *Transactions of the Cambridge Philosophical Society*, 8, 441-455.
- Sumer, B.M., Fredsoe, J., 2006. *Hydrodynamics around cylindrical structures*. World Scientific Publishing Co. Pte. Ltd.
- Tacon, A.G.J.J., 2020. Trends in Global Aquaculture and Aquafeed Production: 2000–2017. *Rev. Fish. Sci. Aquac.* 28, 43–56. <https://doi.org/10.1080/23308249.2019.1649634>
- Telesca, L., Michalek, K., Sanders, T., Peck, L.S., Thyrring, J., Harper, E.M., 2018. Blue mussel shell shape plasticity and natural environments: a quantitative approach. *Sci. Rep.* 1–15. <https://doi.org/10.1038/s41598-018-20122-9>
- Theophanatos, A., 1988. *Marine growth and the hydrodynamic loading of offshore structures*. University of Strathclyde.
- UN, 2019a. 2019 Revision of World Population Prospects [WWW Document]. Dep.

- Econ. Soc. Aff. Popul. Div. URL
<https://population.un.org/wpp/Download/Standard/Population/>
- UN, 2019b. World: Total population. <https://www.un.org/development/desa/publications/world-population-prospects-2019-highlights.html>
- van den Burg, S.W.K., Kamermans, P., Blanch, M., Pletsas, D., Poelman, M., Soma, K., Dalton, G., 2017. Business case for mussel aquaculture in offshore wind farms in the North Sea. *Mar. Policy* 85, 1–7. <https://doi.org/10.1016/J.MARPOL.2017.08.007>
- Villanueva, R., Thom, M., Visscher, J., Paul, M., Schlurmann, T., 2021. Wake length of an artificial seagrass meadow: a study of shelter and its feasibility for restoration. *J. Ecohydraulics* 1–15. <https://doi.org/10.1080/24705357.2021.1938256>
- Wang, H.Y., Sun, Z.C., 2010. Experimental Study of a Porous Floating Breakwater. *Ocean Eng.* 37, 520–527. <https://doi.org/10.1016/j.oceaneng.2009.12.005>
- Wolfram, J., Naghipour, M., 1999. On the estimation of Morison force coefficients and their predictive accuracy for very rough circular cylinders. *Appl. Ocean Res.* 21, 311–328. [https://doi.org/10.1016/S0141-1187\(99\)00018-8](https://doi.org/10.1016/S0141-1187(99)00018-8)
- Wolfram, J., Theophanatos, A., 1990. Marine Roughness And Fluid Loading. *Environ. Forces Offshore Struct. Their Predict. Proc. an Int. Conf.*
- Woods Hole Oceanographic Institution, 1952. Marine fouling and its prevention. United States Naval Institute.
- Wozniak, B., Dera, J., 2007. Light absorption in sea water, *Light Absorption in Sea Water*. <https://doi.org/10.1007/978-0-387-49560-6>
- Xu, Z., Qin, H., Li, P., Liu, R., 2020. Computational fluid dynamics approaches to drag and wake of a long-line mussel dropper under tidal current. *Sci. Prog.* 103, 003685041990123. <https://doi.org/10.1177/0036850419901235>
- Zhang, H., Zhou, B., Vogel, C., Willden, R., Zang, J., Zhang, L., 2020. Hydrodynamic performance of a floating breakwater as an oscillating-buoy type wave energy converter. *Appl. Energy* 257, 113996. <https://doi.org/10.1016/J.APENERGY.2019.113996>
- Zhao, Y.-P.P., Yang, H., Bi, C.W., Chen, Q.-P.P., Dong, G.-H.H., Cui, Y., 2019. Hydrodynamic responses of longline aquaculture facility with lantern nets in waves. *Aquac. Eng.* 86, 101996. <https://doi.org/10.1016/j.aquaeng.2019.101996>
- Zhao, Y.P., Bi, C.W., Chen, C.P., Li, Y.C., Dong, G.H., 2015. Experimental study on flow velocity and mooring loads for multiple net cages in steady current. *Aquac. Eng.* 67, 24–31. <https://doi.org/10.1016/j.aquaeng.2015.05.005>

- Zhao, Y.P., Bi, C.W., Dong, G.H., Gui, F.K., Cui, Y., Xu, T.J., 2013. Numerical simulation of the flow field inside and around gravity cages. *Aquac. Eng.* 52, 1–13. <https://doi.org/10.1016/j.aquaeng.2012.06.001>
- Zhong, W., Lin, J., Zou, Q., Wen, Y., 2022. Hydrodynamic effects of large- scale suspended mussel farms : Field observations and numerical simulations 1–18. <https://doi.org/10.3389/fmars.2022.973155>
- Zhu, L., Huguenard, K., Zou, Q., Fredriksson, D.W., Xie, D., 2020. Aquaculture farms as nature-based coastal protection: Random wave attenuation by suspended and submerged canopies. *Coast. Eng.* 160, 103737. <https://doi.org/10.1016/j.coastaleng.2020.103737>
- Zhu, L., Lei, J., Huguenard, K., Fredriksson, D.W., 2021. Wave attenuation by suspended canopies with cultivated kelp (*Saccharina latissima*). *Coast. Eng.* 168, 103947. <https://doi.org/10.1016/j.coastaleng.2021.103947>



Annex

Curriculum Vitae

Jannis Landmann

Personal data:

Date of Birth: 31.08.1989
Place of Birth: Recklinghausen, Germany
E-Mail: landmann@lufi.uni-hannover.de
Phone: +49 (0)511 762 2580

Experience:

2017 - today **Ludwig-Franzius-Institute for Hydraulic, Estuarine and Coastal Engineering**
Leibniz Universität Hannover, Germany;
Research Associate / PhD Student

2012 - 2014 **Department of Engineering, Specialization Geoinformatics and Surveying**
University of Applied Sciences Mainz, Germany;
Student Assistant / Tutor

2009 - 2010 **American Field Service – Intercultural Programs**
Mexico City, Mexico; *Assistant Hosting and Support Coordinator*

Education:

2017 - today **Doctorate Student**
Leibniz Universität Hannover, Germany;
Subject: *Coastal & Offshore Engineering*

2014 – 2017 **Master of Science**
Leibniz Universität Hannover, Germany;
Program: *Water, Environmental and Coastal Engineering*

2010 – 2014 **Bachelor of Engineering**
University of Applied Sciences Mainz, Germany;
Program: *Civil Engineering*

2007 - 2009 **Abitur (German qualification for higher education)**
Ernst-Barlach-Gymnasium, Castrop-Rauxel, Germany



Selbständigkeitserklärung

Ich erkläre gemäß § 5 des Verkündungsblattes der Gottfried Wilhelm Leibniz Universität Hannover vom 04.06.2020:

- ☞ die Regeln der geltenden Promotionsordnung zu kennen und eingehalten zu haben und mit einer Prüfung nach den Bestimmungen der Promotionsordnung einverstanden zu sein.
- ☞ die Dissertation selbst verfasst zu haben (Selbständigkeitserklärung), keine Textabschnitte von Dritten oder eigener Prüfungsarbeiten ohne Kennzeichnung übernommen und alle von ihr oder ihm benutzten Hilfsmittel und Quellen in seiner Arbeit angegeben zu haben.
- ☞ Dritten weder unmittelbar noch mittelbar geldwerte Leistungen für Vermittlungstätigkeiten oder für die inhaltliche Ausarbeitung der Dissertation erbracht zu haben (d.h. die wissenschaftliche Arbeit darf weder in Teilen noch in Gänze von Dritten gegen Entgelt oder sonstige Gegenleistung erworben oder vermittelt worden sein).
- ☞ die Dissertation noch nicht als Prüfungsarbeit für eine staatliche oder andere wissenschaftliche Prüfung eingereicht zu haben.
- ☞ die gleiche oder eine in wesentlichen Teilen ähnliche Arbeit bei einer anderen Hochschule als Dissertation eingereicht zu haben.

Ort, Datum

Unterschrift des Antragstellers

Bergisch Gladbach, 03.05.2023

Jannis Landmann



Paper 1:

Landmann J., Ongsiek T., Goseberg N., Heasman K., Buck B.H., Paffenholz J.-A., Hildebrandt A. (2019); Physical Modelling of Blue Mussel Dropper Lines for the Development of Surrogates and Hydrodynamic Coefficients. *Journal of Marine Science and Engineering*; 7(3):65. <https://doi.org/10.3390/jmse7030065>

Abstract:

In this work, laboratory tests with live bivalves as well as the conceptual design of additively manufactured surrogate models are presented. The overall task of this work is to develop a surrogate best fitting to the live mussels tested in accordance to the identified surface descriptor, i.e., the Abbott–Firestone Curve, and to the hydrodynamic behavior by means of drag and inertia coefficients. To date, very few investigations have focused on loads from currents as well as waves. Therefore, tests with a towing carriage were carried out in a wave flume. A custom-made rack using mounting clamps was built to facilitate carriage-run tests with minimal delays. Blue mussels (*Mytilus edulis*) extracted from a site in Germany, which were kept in aerated seawater to ensure their survival for the test duration, were used. A set of preliminary results showed drag and inertia coefficients C_D and C_M ranging from 1.16–3.03 and 0.25 to 1.25. To derive geometrical models of the mussel dropper lines, 3-D point clouds were prepared by means of 3-D laser scanning to obtain a realistic surface model. Centered on the 3-D point cloud, a suitable descriptor for the mass distribution over the surface was identified and three 3-D printed surrogates of the blue mussel were developed for further testing. These were evaluated regarding their fit to the original 3-D point cloud of the live blue mussels via the chosen surface descriptor.



Paper 2:

Landmann, J., Fröhling, L., Gieschen, R., Buck, B.H., Heasman, K., Scott, N., Smeaton, M., Goseberg, N., Hildebrandt, A. (2021); Drag and inertia coefficients of live and surrogate shellfish dropper lines under steady and oscillatory flow. *Ocean Engineering*; 235:109377, <https://doi.org/10.1016/j.oceaneng.2021.109377>

Abstract:

Against the background of a drastically increased demand of marine proteins, off-bottom, bivalve aquaculture, provides significant potential for production growth when moved into more energetic marine waters. Hence, research, industry and politics are currently proposing the development of new offshore sites. The highly energetic conditions at these sites present a challenging environment for bivalve aquaculture. In this work, physical experiments of suspended bivalves provide new knowledge on the commonly used design parameters: the drag and inertia coefficients. Live bivalves and manufactured surrogate models at a 1:1 scale were tested in a towing tank as well as under waves. The drag coefficient of live blue mussels was determined to be $C_D = 1.6$ for Reynolds numbers between 2.3×10^4 and 1.4×10^5 . The inertia coefficient obtained from the wave tests was $C_M = 2.1$ for Keulegan Carpenter numbers $KC < 10$. In a pursuit to better understand the differences between live mussels and surrogates in laboratory conditions, the analysis revealed that appropriate surrogates can be identified. A method to determine the characteristic diameter of mussel dropper lines is suggested. The results facilitate the future design of aquaculture systems in high-energy environments and allow for an integration into numerical models.



Paper 3:

Landmann, J., Fröhling, L., Gieschen, R., Buck, B.H., Heasman, K., Scott, N., Smeaton, M., Goseberg, N., Hildebrandt, A. (2021); New system design for the cultivation of extractive species at exposed sites - Part 2: Experimental modelling in waves and currents. *Applied Ocean Research*; 113:102749, <https://doi.org/10.1016/j.apor.2021.102749>

Abstract:

Aquaculture is projected to be a major supplier of marine proteins to large parts of the global population. This includes bivalves, which have a high potential to offset protein deficits, as they are highly adaptable to varying water temperature, salinity, desiccation, and oxygen conditions. This work is part of a two-piece contribution on novel marine aquaculture technology and details physical laboratory tests of a new cultivation system for bivalve farming called “Shellfish Tower”. The tested 1:20 model consists of a rectangular cage (2×2 m prototype scale) with a central buoyancy element and a height of 2 – 4 m. Testing was done in a current flume as well as a wave basin for current velocities between 0.4 – 2.2 m/s and wave heights of 1.6 to 5.0 m with periods between 5 to 14 s. The tests were conducted to prove the feasibility and functionality of this aquaculture system, which is usable for the collection and cultivation of mussel spat as well as for the grow-out of oysters, scallops, and seaweed in marine environments. Tests carried out in a current flume revealed that drag coefficients decrease with increasing current velocities, and range from $C_D = 0.5$ to 2.5, while the mooring inclination increases from 12° to 84° with increasing flow velocity, which is highly dependent on the buoyancy related pretension. The examination of the mooring line tensions recorded in a wave basin showed that the largest values of snap-induced tension were up to 10 times that of the semi-static tension. The maximum-recorded tension on the system was 48 kN for a single and 89 kN for a double configuration, compared to non-snap tension values, which were in the range of 6 – 10 kN. The insights gathered in this study will inform the future design of aquaculture systems in high-energy environments and allow for an integration into numerical models.



Paper 4:

Landmann, J., Hammer, T.C., Günther, H., Hildebrandt, A. (2022); Large-scale investigation of wave dampening characteristics of organic, artificial floating islands. *Ecological Engineering*; 181: 09258574, <https://doi.org/10.1016/j.ecoleng.2022.106691>

Abstract:

The concept of floating vegetation-based islands for the bioremediation of aquatic ecosystems is well known. Less so, their hydrodynamic capabilities regarding the damping performance, positional stability, and water-structure interactions. To this end, physical model tests with fully organic, reed-based gabions were carried out in a large-scale facility in this study. The initial, reflected, and transmitted waves were recorded and analysed regarding transmission and reflection coefficients. A motion tracking system was utilized to allow for an investigation regarding the motion of the artificial floating islands under waves. The results show that the artificial floating islands significantly dampen shorter waves with a wave period of $T \leq 2.25$ s. The transmission of the incident waves is reduced by 50% for the smallest wave periods ($T = 1.5$ s). The incident waves are reflected between 20 and 50% for the same wave period. The incident wave energy is dissipated by up to 85% for the smallest wave height and period ($H = 0.10$ m, $T = 1.5$ s). The comparable performance regarding more traditional floating breakwaters is discussed as well as the width of the structure as the key parameter for the layout of artificial floating islands in rivers and still waters regarding the damping performance.